Department of Material Physics
UNIVERSIDAD DEL PAIS VASCO
THE UNIVERSITY OF THE BASQUE COUNTRY

Light scattering from high refractive index nanostructures: Theory and applications

Thesis by
Jorge Olmos Trigo

Supervised by
Profs. Juan José Sáenz and **Eugene Chulkov**

Donostia - San Sebastián, Spain, October 2021

Tú no puedes volver atrás,
porque la vida ya te empuja,
como un aullido interminable,
interminable.

Te sentirás acorralada,
te sentirás perdida o sola,
tal vez querrás no haber nacido,
no haber nacido.

Pero tú siempre acuérdate
de lo que un día yo escribí
pensando en ti, pensando en ti,
como ahora pienso.

La vida es bella ya verás,
como a pesar de los pesares,
tendrás amigos, tendrás amor,
tendrás amigos.

Un hombre solo, una mujer,
así tomados de uno en uno,
son como polvo, no son nada,
no son nada.

Entonces siempre acuérdate,
de lo que un día yo escribí,
pensando en ti, pensando en ti,
como ahora pienso.

Nunca te entregues, ni te apartes,
junto al camino nunca digas
no puedo más y aquí me quedo,
y aquí me quedo.

Otros esperan que resistas,
que les ayude tu alegría,
que les ayude tu canción,
entre sus canciones.

Entonces siempre acuérdate
de lo que un día yo escribí,
pensando en tí, pensando en tí,
como ahora pienso.

La vida es bella ya verás,
como a pesar de los pesares,
tendrás amigos, tendrás amor,
tendrás amigos.

No sé decirte nada más,
pero tú debes comprender,
que yo aún estoy en el camino,
en el camino.

Pero tú siempre acuérdate
de lo que un día yo escribí,
pensando en tí, pensando en tí,
como ahora pienso.

Paco Ibáñez - José Agustín Goytisolo

Agradecimientos

"Esto que nos ha hecho el Mole no se lo voy a perdonar en la vida". Con esta frase resumía Txiki su sentir (y el de muchos) con la marcha temprana del Mole de nuestras vidas. Y es que... jamás se lo podremos perdonar.
Cualquiera que me conozca sabrá que Mole significa para mí mucho más que un director de Tesis. Su desbordante pasión, tanto por la vida como por la ciencia, me contagió como jamás podría haber imaginado y pensar que ya no le volveré a ver me persigue por las noches. Guardo como un tesoro todos los ratos que le robé para hablar de Física y le estaré eternamente agradecido por cuidarnos y querernos, tanto a Cris como a mí, en nuestra etapa en Donosti. De esto último también tiene mucha culpa la mencionada Txiki, su compañera de viaje. Ella siempre nos incluyó en todo tipo de socis con su posterior jarana de alcohol y cartas. Aunque ya lo sabrás, si el Mole tenía una pasión comparable a la Física, esa era su familia y todas las veces que salía zumbando del despacho cuando nos pasábamos de la hora era por ella. Un gusto haberla conocido al completo. Edurne y Carlos, conservad la alegría por la vida que vuestros padres os inculcaron. Yo intentaré hacer lo mismo.
Quiero seguir en Donosti para agradecer a las personas que, de una forma u otra, han participado en que esta Tesis vea la luz. Quiero empezar por Ion Mitxelena. Siempre estuvo pendiente de mi carrera por estar fit en vez de fot y a pesar de mi dejadez, quiero que sepas que te considero un buen amigo primo-txuti. Queda pendiente subir en un día el Monte Perdido. Sofía, mi compañera de cafés en el DIPC y una de las personas con las cuales más me he reído. Te llevo dentro. También quiero agradecer a mis profesoras de catalán, Mireia e Irene, que han soportado durante 4 años la misma broma de la pronunsiasió. Ojalá vernos pronto. No me quiero olvidar de gente que siempre estuvo dispuesta a tomarse una cerveza y reírse de los problemas de un estudiante de doctorado: Diego, Martín, Raúl, Antton, Alvaro, Cris, Carmen, Marina, Carlos, Fer, Miguel, María y Maru son buenos ejemplos de ello. En esta línea querría des-agradecer a algunos de sus directores de Tesis. Y es que, ser tan listo (y ni eso) para la ciencia, no debería ir ligado con ser un déspota con ínfulas. Querría por último destacar a Jon como a un compañero que representa punto por punto lo que yo hubiese querido tener cuando empecé mi doctorado.

Una de las mayores ventajas de haber sido estudiante del Mole es la gente que le rodea. Quiero agradecer a estudiante y director: Xavi y Gabriel, respectivamente, por haberme enseñado que un cacharro sin μ no es dual. Y punto. Situándonos en Madrid, querría agradecer a Manuel su paciencia conmigo en el Máster y su forma de ser. Cualquiera querría trabajar contigo. Por último, quiero agradecer a Nuno haber estado pendiente de Cris cuando más lo necesitaba.
Retrocediendo en el tiempo, pero siguiendo con personas a las cuales la Física no es ajena, querría destacar a Gentucilla Uni. Bueno, siendo sincero, no sé ni cómo se llama ahora el grupo por culpa de desamores. Sí, en Física existen. Ah, y antes de empezar a agradecer, el orden de las apariciones no altera el producto: os quiero mucho. Javi, quiero que sepas que tienes mucho que ver en que yo esté escribiendo esto, porque si no llega a ser por ti, habría dejado la Física en segundo. Espero que sigas siendo un titán y que volvamos a bebernos una botella y media para celebrarlo. ¿El qué? Lo que sea. Guille, por tu multipla, los Beatles y los partidos de pádel. Aún recuerdo cuando pasaste de ser Milans del Bosch, ojito con este, a Guille sin más en la agenda. Ojalá verte representando al Doctor amor y riéndote a pierna suelta en Galicia, Menorca, o donde podamos. Raquel, mi temida rival y profesora de Euskera. Quiero que sepas que estoy muy orgulloso de la tenacidad que demuestras y, a la vez, la dulzura con lo que lo cuentas. Espero que alguna vez me ganes al Pádel. No me pienso dejar. Álvaro, buena parte de culpa, si no toda, en despertar en mí la pasión por la Física. Aunque mis resultados académicos no lo reflejen. Guardo con infinito cariño el año de 4º de carrera y, en un porcentaje altísimo, se debe a ti. Gracias por estar pendiente de mí cuando más lo necesitaba y ser un amigo en mayúsculas. Mario, gracias a tu ingenio y sentido del humor la carrera se me hizo mucho más amena. Espero que tus alumnos lo valoren y que te aprueben, joder. Ah, y gracias también por incluir en nuestras quedadas a tus amigos. Son grandes. Sergio, muchas gracias por dejarte robar esas historias kafkianas en la biblioteca cuando tú querías estudiar. Has demostrado ser muy fuerte y volar siempre hacia arriba. Cuando quieras, unos pinitos. Pablo, mi profe de computación que me explicaba en pleno examen el por qué de su programa. No sé si te volveré a ganar al Starcraft, pero ya me vengaré con excursiones al monte donde te exprima como tú a C++ y a Papers Please. Melek, por tu sentido del humor y estar siempre dispuesta a gastarle bromas a quién sea. Ah, y si necesitas un coche, vete a Almería, los regalan. También querría mencionar a Gudín, Javi Sanz, Helena, Irene. Ojalá veros más.
Ahora quiero pasar a agradecer a mis amigos de toda la vida: los de Pozuelo-Aravacanoesmadrid y a los de Galicia. Voy a empezar por los primeros. Jaime, espero siempre tenerte cerca (nuestros padres lo han puesto sencillo) y que me sigas contando tus progresos y decepciones. Con suerte este verano en Galicia subimos el Mondigo y hacemos Sgamella por la noche. Para tí también va dedicada Palabras para Julia. Soti, mi compañero traidor de pupitre: “No lo

sabe usted bien". Por más alcohol, viajes y salvia de las ramas. No te separes nunca aunque sea en alemán, Mohnnnnoooo!. Dani, mi reciente compañero de atletismo por Garabitas. Eres un titán y estoy especialmente orgulloso de tenerte cerca Lombrizzzzzz. Lo de titán por lo personal, en lo físico te tengo a tiro. Lo veremos próximamente en la Behobia. Como me ganes no duermes en casa, tu verás, Pablo, espero que te vaya estupendo por NY. Cuando no haya nevadas, espero que me lo cuentes.
Viajando 500 km y pico rumbo norte está un sitio especial para mí: Galicia-Barreiros. Quiero empezar agradeciendo a Marta su dulzura y sus pedazos de praos. Si te oyese Merkel, te haría ministra. Hemos compartido más de 15 veranos y espero que sean muchos más, con ropa o con frío. Sigo con Adri, un amigo en mayúsculas. Aunque convaleciente todavía de nuestras conversaciones de política-economía-rajardeloquesea mientras a duras penas subo con la bici, quiero que sepas que te quiero mucho. Con o sin $\pm$14k, que a mí no me importa siempre que estés cerca. Emma y David, muchas gracias por ser como sois, por vuestras locuras y por haber demostrado ser unos grandes tipos (aunque chiquitos). Termino también esta sección gallega agradeciendo al grupo en su conjunto: Lisa, Ana, Alberto, Adri, Maria, Cristina, Miguel (ven más) y primas de Emma.
Quiero ahora referirme a mi familia más cercana. En especial a mis padres por apoyarme en todo momento. Siempre he sentido vuestro afecto y cariño y eso me ha dado especial estabilidad en los momentos que más lo he necesitado. Gracias. En particular quiero agradecer a mi madre su dulzura y entender a una temprana edad que su hijo era especial en algún sentido. Un auténtico desastre, pero un buen chico. También quiero agradecer a mi padre su pasión por los cantautores y el deporte. Esperemos que ganemos más partidos de pádel y alguna vez subamos la Fruseira sin esfuerzo. Ah, y con suerte cuando lea esto estés jubilado y con una furgo rumbo al norte. En esta línea, quiero agradecer a mi hermana Ana por su continuo esfuerzo a la hora de superar las vicisitudes que en la vida se presentan. Tú no puedes volver atrás porque la vida ya te empuja como un aullido interminable. Te sentirás acorralada, te sentirás perdida y sola, tal vez querrás no haber nacido. Pero tú siempre acuérdate de lo que un día yo escribí, pensando en ti, como ahora pienso. Por último, quiero agradecer a mis abuelos por sus comidas y partidas de cartas de todos los jueves de la carrera. Ojalá que las oportunidades que yo tuve para estudiar hubiesen sido las mismas para vosotros. Y por su puesto, a mi tío Paco, por su esfuerzo y su constante disposición a reírse de mis bromas. Ah, y a mi tío Xavier, por el ping-pong y el catán.

Finalmente, quiero agradecer a Cris, mi compañera de viaje, ser cómo es, ahora y siempre. Siento un tremendo orgullo de estar con mi persona favorita (a lo Kill Bill) y pensar que llevamos tanto tiempo con la misma ilusión que cuando empezamos. Bueno no, que al principio yo te quería dejar. Ojalá no te hubiera conocido nunca, Chelsea Hotel, So long Marianne, Suzanne, Le Partisien, Llorona, Y sin embargo, Ley innata, Standby, Heaven, Adromicfms, Forfri, Always on my mind, No sé por qué te quiero, Palabras para julia, y un largo etcetera han sido testigos de momentos únicos. Y aunque nos sobran los motivos, yo te sigo soñando. Por muchas más series, canciones y playas por descubrir. Quiero que sepas que a pesar de que te me vas de la ciencia, espero que estés dispuesta para ser mi co-autora en otras facetas. Por ello y al menos de momento, tú no te vayas muy lejos.

Will you surrender?
Restless in a war, war
We're sailling, farewell love
We praise our shared destiny
Be sure to embrace the dreams
I'm more than a dead and gone

Heaven, The Blaze

A la memoria del Mole

Toda buena historia comienza con una idea descabellada. En este caso, tratar de encontrar similitudes en las ecuaciones de Maxwell (a cargo el Mole y yo) y Schrödinger (a cargo Cris) utilizando el formalismo de las funciones de Green. Cabe preguntarse, ¿Con alguna inmediata aplicación?
Para responder a esta pregunta, es necesario traer a escena el famoso paper de Berger titulado "Side-Jump Mechanism for the Hall Effect of Ferromagnets" [1] que en castellano podría traducirse como "Salto lateral debido al efecto Hall de los ferromagnéticos". Traducciones aparte, en este artículo se demuestra que existe un desplazamiento lateral del paquete de ondas planas incidentes tras el impacto con un cacharro que presente la interacción de "spín y órbita". En el límite de partícula pequeña y usando la aproximación de Bohrn, Berger probó que la dirección del salto lateral depende drásticamente del spín incidente. Así pues, electrones con spin "up" y "down" se deflectan en sentidos opuestos tras el choque. Matemáticamente, la probabilidad de este salto lateral viene dado por la densidad de corriente electrónica tras el choque, que, como hemos comentado, alberga información del spin (up o down) del paquete de ondas planas incidente. Nuestra contribución llegó tras probar que este salto lateral es resonante, es decir, la magnitud del salto puede llegar a ser varios órdenes de magnitud mayor que la obtenida por Berger. Este descubrimiento no fue nunca publicado, quizás motivado por alguna exigencia experimental que se me escapa entre los dedos. Sin embargo, el hecho de encontrar que la corriente electrónica tras el choque es la responsable del salto lateral nos hizo preguntarnos al Mole y a mí si pudiese existir un análogo con el vector de Poynting en luz. En particular, tras descubrir el curro que se había pegado Arnoldus en esta dirección [2]. En este trabajo, se demuestra que, efectivamente, existe un desplazamiento aparente de una esfera dipolar eléctrica bajo iluminación de una onda plana circularmente polarizada. Es decir, con "spin" bien definido. Al igual que ocurre con el caso de Berger, este desplazamiento aparente tiene una dirección definida (o la contraria) con luz circularmente polarizada a derechas (o a izquierdas). El lector podrá notar que existe una clara analogía en los trabajos de Berger y Arnoldous y que aunque parezca mentira, nunca lo llegamos a escribir. No obstante, queda pendiente como un buen homenaje a cargo de Cris y un servidor.

De esto tenemos culpa todos y en particular, la curiosidad del Mole, que me hizo abandonar Berger y electrones y conducirme hacia el horizonte Kerker. Aún recuerdo cuando vino a verme al despacho y me dijo: "Tío, tenemos que entender como funciona la puta helicidad y su relación con las condiciones de Kerker". "En particular, como funcionan con las partículas de alto índice de refracción. Y bueno, si consiguiésemos unir todo esto con fuerzas... ya estoy viendo un PRL tío". "Que cojones, varios!". Ilusionado (él y yo), me encargó que me calculase el vector de Poynting dispersado por un dipolo eléctrico *y magnético* bajo iluminación de una onda plana circularmente polarizada. Este fue su primer y último encargo con respecto a la dirección de Tesis entendida como "Haz algo que se me ha ocurrido a mí", hecho por el cual estaré eternamente agradecido. Nostalgias a un lado, cuando lo calculé me di cuenta que si las polarizabilidades eléctricas y magnéticas eran iguales el vector de Poynting se anulaba en backscattering. El Mole me explicó que este hecho ya lo había publicado él anteriormente y que esa condición se llamaba "primera condición de Kerker". Por otro lado, me contó que existía una explicación fundamental de este fenómeno dada por parte de Gabriel, Zambrana y Corbatón (como los llamábamos entonces) a través de la helicidad y las simetrías del sistema [3,4]. Que, por favor, se lo explicase. Cuando terminé de contarle lo que buenamente entendí, volvimos al cálculo del vector de Poynting y nos dimos cuenta de algo genial: el desplazamiento aparente, sí, el de Arnoldous con dipolo magnético, que llamamos a posteriori espejismo óptico, petaba en backscattering!. Tras casi un año escribiendo el artículo conseguimos por fin subir publicarlo [5], no sin dificultades. Consejo: no enseñéis resultados en un congreso si no los tenéis subidos al ARXIV. Consejos aparte, entendí el efecto de la primera condición de Kerker en la dispersión, algo clave para el desarrollo de esta Tesis. Por otro lado y gracias a la respuesta de uno de los Referees, nos montamos otro artículo con el objetivo de distinguir el spin y la helicidad magnitud [6]. Sugerido por el Mole, también incluimos efectos de absorción y de forma completamente fortuita, encontramos que la helicidad no se conserva en este escenario. Por tanto y siempre en el régimen dipolar eléctrico y magnético bajo onda plana, el vector de Poynting no se anula en backscattering. En un artículo de invitación, incluimos este "descubrimiento" donde escribimos que la primera condición de Kerker no se conseguía en presencia de efectos disipativos [7]. Sin embargo, no encontramos una demostración formal para este fenómeno.

Intrigado por las condiciones de Kerker y con el objetivo de probarle al Mole que alguno de sus artículos no eran correctos (siempre he sido un poco puñetero), me puse a investigar las propiedades de la segunda condición de Kerker. Esta condición, también denominada Generalized second Kerker condition (GSKC) para esferas dieléctricas, era entendida (no sé si aún) como la condición a partir de la cual el cacharro no dispersa prácticamente nada de luz en la dirección forward. Sin embargo, y a pesar de la cantidad inmensa de artículos que lo dan por sentado, me di cuenta que este fenómeno simplemente no se sostenía de

forma general [8]. Únicamente cuando el cacharro dispersa relativamente poca luz. De hecho, en la GSCK y con un régimen alto de dispersión, el patrón de luz dispersado puede ser idéntico al de la primera condición de Kerker. Cuando fui a ver a mi añorado Mole, supe de la importancia de este hecho tras su: "Y una mierda, no me lo creo, eres un cabrón con pintas eh". "Escríbelo en un Latex y me lo mandas hoy por favor". Escribí este artículo junto con Cris y mis principales colaboradores (y amigos), entre los cuales destaca Diego Romero Abujetas. En una de sus infinitas estancias en Donostia y recordando que la absorción "mata a Kerker", el Mole quiso que Diego lo probará, ya que yo estaba disperso en otras vainas. La idea del Mole: demostrar que la parte electrostática de polarizabilidad dipolar eléctrica no podía ser igual que la estática de la magnética. Viendo cómo Diego se puso a hacer estos cálculos infinitos y tras haber quemado una parte no desdeñable del Amazonas, desistió. Sin embargo, en vista del interés y para probarme a mí mismo, decidí atacar este problema mediante una vía alternativa. Sin duda uno de los libros que más me ha ayudado a entender las condiciones de Kerker es el Hulst [9]. En este libro, las condiciones de Kerker (no llamadas así en el mismo) se presentan en una notación tremendamente simplificada. Así pues, demostrar que la absorción "mata a Kerker" resultó brutalmente sencilla. Superorgulloso, fui con mi demostración completa allá por septiembre de 2019 al despacho del Mole en el DIPC: "Esto está bien, pero, ¿Para qué sirve?". Aunque pueda resultar duro, este tipo de comentarios siempre fueron superútiles para mí, pues siempre me incitaban (tras pasar unos días odiando al Mole) a seguir trabajando. En particular, siempre intenté demostrarle a él y a mí mismo que valía para currar en esto. En esta línea y gracias tanto a la notación del Hulst, como a unas relaciones de las funciones de Bessel del año de la tana, probé que la helicidad no se conserva de forma general para esferas dieléctricas. Es decir, que si tienes un par de coeficientes cumpliendo "Kerker", los demás no pueden cumplir Kerker para la misma frecuencia. Concerté una reunión con Gabriel y el Mole para contárselo y su respuesta fue contundente: "No le encuentro una aplicación inmediata, mira a ver si esto funciona para los whispery gallery modes". ¿Entendéis la Física de estos modos? Yo tampoco. Así pues, me volví con mi demostración convencido de que podía sacarle partido a estas pruebas matemáticas. En efecto, conseguí demostrar a raíz de esto que existen regiones dipolares para partículas gordas más allá de las resonancias cuadrupolares y octupolares. Por otro lado y colaborando con Diego y Cris, vimos que en estas regiones dipolares se cumplía el "optimum forward light-scattering condition". Y más interesante aún, esta condición de optimización no depende de un material particular sino del ratio entre el tamaño del cacharro y la longitud de onda incidente (en oposición a la visión de la Russian Task Force). Ya sí, volví a enseñárselo al Mole y me dijo algo que jamás olvidaré: "Tío, eres la persona que conozco que más sabe de las condiciones de Kerker". "No te rías, te lo digo sinceramente, eres un cabrón".

Ya sin el Mole entre nosotros y en un confinamiento tremendamente doloroso, me refugié en the abovementioned trabajos. Tras hacer un "curro de jefe", que ojalá nunca hubiese sido necesario, conseguimos publicar un PRL (siempre fue mi sueño con el Mole) que por supuesto le dediqué [10]. Posteriormente, nos publicaron el artículo del cual más orgulloso estoy, quizás, porque también era la idea preferida del Mole [11]. Hoy en día el Mole sigue persiguiéndome en sueños. Quiero pensar que guardaba un buen recuerdo de mí y de los infinitos ratos que le robaba al día para hablar de Física. Cada vez que escribo "However, we..." o "in striking contrast to..", te recuerdo riéndote con un cigarro cortado entre los labios.

As he came, he disappeared
Left, just a shadow, in your eyes
But his love always on your mind
And his smile haunting you at night

Heal, Racoon Racoon

Resumen

La presente Tesis se enmarca dentro del campo de la Nanofotónica, es decir, del estudio de la interacción de la luz con la materia en la nanoescala. En particular, de la forma en que una onda plana interacciona con el objeto más simétrico existente en la naturaleza: una esfera homogénea.
El problema de cómo una esfera homogénea iluminada con una onda plana dispersa la luz se remonta a comienzos del siglo XX.. Concretamente, al año 1908, en el cual Gustav Mie resolvió analíticamente este problema en el límite semiclásico, apoyado en las ecuaciones de Maxwell y en la correcta visión de la luz como una onda electromagnética [12]. Con el paso de las décadas y a pesar de que en sus comienzos el trabajo de Mie pasó casi inadvertido, el interés por lo que hoy en día se conoce como Teoría de Mie ha crecido enormemente. En particular, tras el auge de los materiales con un índice de refracción alto [13–16]. Estos presentan, en la región espectral del visible, resonancias eléctricas y magnéticas con relativamente pocas pérdidas óhmicas, en fuerte oposición a los metales en los cuales se basa la Plasmónica [17–21]. Además, en el caso en el cual el tamaño de los objetos sea considerablemente menor que la longitud de onda incidente, la respuesta óptica es dipolar. Este hecho posibilita la existencia de soluciones analíticas que simplifican brutalmente el entendimiento de los problemas bajo consideración. En esta línea se han desarrollado importantes trabajos tanto sobre fuerzas ópticas [22–25], presión de radiación, o en la física emergente de fuentes no radiativas como los anapolos [26–28]. Sin embargo, quizás una de las mayores ventajas de los materiales con índice de refracción alto reside en el grado óptimo de control de la luz dispersada por los mismos. Gracias a que presentan una respuesta eléctrica y magnética (sin la necesidad de tener magnetización en el objeto) se pueden recuperar las condiciones anómalas de dispersión de luz predices por Milton, Wand y Kerker en los años 90 [29]. Esencialmente, estos autores auguraron que si las respuestas eléctrica y magnética de una esfera homogénea con magnetización permanente eran idénticas, no existía luz en retrodispersión, es decir, en el sentido opuesto a la dirección de la onda incidente. Por otro lado, vaticinaron justo el efecto contrario bajo otro ratio más complicado de la respuesta eléctrica y magnética. En este último escenario, no debía existir luz en el sentido de la dirección de la onda plana incidente.

Sin embargo, sendas predicciones, actualmente denominadas "condiciones de Kerker", no se pudieron corroborar debido a la ausencia de materiales magnéticos a frecuencias ópticas. Como hemos adelantado previamente, estas mediciones experimentales llegaron de la mano de los materiales de índice de refracción alto. En particular, cuando la respuesta eléctrica y magnética (sin magnetización permanente) del objeto es, en valor absoluto, idéntica. En este caso y dependiendo del signo de las polarizabilidades eléctricas y magnéticas en el límite dipolar, podemos tener tanto la primera condición de Kerker (polarizabilidades en fase) como la segunda condición de Kerker (polarizabilidades en antifase).

El objeto de esta Tesis es ahondar tanto en los fundamentos matemáticos como en posibles aplicaciones de las condiciones de Kerker en materiales de alto índice de refracción. En esta línea, demostramos en el Capítulo 3 que existe un error importante a la hora de localizar la posición de una nanoesfera de Silicio en la primera condición de Kerker bajo iluminación de onda plana. De hecho, si se coloca el detector en campo lejano en las inmediaciones de retrodispersión, la nanoesfera parece estar dispersando luz desde una posición tremendamente lejana a su localización real. Este intrigante efecto, denominado comúnmente como espejismo óptico, se discute tanto tanto desde la interacción del spín y órbita en luz como de la conservación de helicidad y momento angular en la dirección de propagación de la onda incidente.

En el Capítulo 4, se demuestra que no es necesario medir la dispersión de luz en retrodispersión para inferir el espejismo óptico de la esfera de Silicio. En particular, se muestra que con una sola medida de la polarización en la dirección perpendicular de la onda incidente se puede inferir, de manera indirecta, la magnitud del espejismo óptico en cualquier dirección de medida. Curiosamente y a través de esta única medida de polarización, se puede colegir la redistribución de spín y órbita de la luz y la asimetría de la misma. Gracias a ello, en este Capítulo se establece una clara distinción entre helicidad y spín tras la dispersión. En vista de la literatura vigente hasta la fecha [30, 31], esta aclaración es necesaria pues, en una onda plana, estos dos conceptos se entremezclan y su interpretación puede conducir a error. En este capítulo, también se discute el rol de la absorción. En este escenario, comprobamos numéricamente que la primera condición de Kerker no se puede conseguir. Como consecuencia, la helicidad no se conserva tras la dispersión. Del mismo modo, demostramos que la asimetría en la dispersión de la luz no es máxima debido a la absorción. Motivado por este hecho, en el Capítulo 5 se demuestra analíticamente que la absorción (y hasta una eventual ganancia óptica) "matan" la primera condición de Kerker. Para ilustrar este resultado, se muestra gráficamente cómo se va desvaneciendo el cero de dispersión de luz predicho por Kerker, Wang y Miles a medida que se incrementa la absorción. En esta línea, demostramos que la helicidad tras la dispersión no se conserva. Este descubrimiento revela una importante conexión entre la simetría de du-

alidad y la conservación de energía. En otras palabras, si hay absorción, no se recupera dualidad.
Siguiendo con la investigación sobre la naturaleza de las condiciones de Kerker, demostramos en el Capítulo 6 que la segunda condición de Kerker para esferas dieléctricas ha sido completamente malentendida en numerosos trabajos previos. Hasta ahora, se daba por hecho que el efecto de la segunda condición de Kerker en la luz dispersada era que esta caía enteramente en el semiplano de retrodispersión. Sin embargo, en este Capítulo demostramos que la luz dispersada puede ser totalmente simétrica con respecto al anterior plano y, para un régimen de dispersión fuerte, puede caer en la dirección de incidencia, mimetizando el efecto de la primera condición de Kerker. Discutimos estos efectos mediante el parámetro de asimetría, cuyo signo controla el patrón de radiación de la luz dispersada. Para terminar, mostramos en el Capítulo 7 que el régimen dipolar eléctrico y magnético no es excluyente de las partículas pequeñas si estas se comparan con la longitud de onda incidente. En estos nuevos regímenes dipolares, que aún no han sido explorados con profundidad, mostramos que la mejor condición de retrodispersión, es decir, donde la transmisión de luz es más eficiente, se da para un ratio entre la longitud de onda y el tamaño de la esfera. Este hecho supone un avance con respecto al entendimiento de este fenómeno de optimización, ya que anteriormente fue predicho erróneamente para un particular índice de refracción (diamante en visible).
En resumen, en esta Tesis se discute el efecto de las condiciones de Kerker sobre esferas dieléctricas. Sorprendentemente, y a pesar de la simplicidad de los cálculos aquí obtenidos, podremos extraer bastante información que, o no ha sido explorada, o ha sido malinterpretada. Los resultados de esta Tesis aspiran a servir como inspiración de futura investigación teórica y experimental adicional sobre los fenómenos en ella descritos.

Contents

CHAPTER 1

Introduction

Light-matter interactions date back to the origin of the universe with the Big Bang explosion and the forming of galaxies, stars, planets, and moons. Hence, scattering and absorption of light, which is the central problem of study in this Thesis, is present in nature long before life's existence and humankind. Two illustrative examples of the abovementioned were the observation of the cosmic microwave background (relic radiation) in 1965 by Arno Penzias and Robert Wilson [32] and more recently, the experimental corroboration of the existence of gravitational waves in 2016 by the LIGO collaboration [33]. Both achievements corroborate the validity of the general relativity, introduced by Albert Einstein. The previous examples are invisible to our naked eye since they occur out of the visible spectral range. Examples of these phenomena can be found, for instance, in low-energy electromagnetic radio waves in which long-distance communications are based, microwaves that heat our coffee in the mornings, X-rays that helps cancer diagnoses, or high-energy gamma rays that arise from the radioactive decay of atomic nuclei. Hence, phenomena associated with light-matter transitions have been crucial along with the history in diverse branches of science, such as engineering, medicine, and astrophysics. In recent years and with the emergence of Nanophotonics, the branch of physics devoted to studying light-matter interaction at the nanoscale, scattering, and absorption of light in the ultraviolet, visible, and near-infrared spectral range has received a great deal of interest. We can describe the electromagnetic radiation by the wave picture at these dimensions, and the use of Maxwell's equations is suitable.

1.1 A brief history of the origin of Maxwell equations

These equations were first formulated in 1865 by James Clerk Maxwell in his paper "A Dynamical Theory of the Electromagnetic Field" [34]. In this work, Maxwell summarized, organized, and decisively contributed to the understanding of electromagnetics until the date. These contained, among others, the Gauss's law for both electric and magnetic fields, stating that only static electric fields can be related to a source, whereas no magnetic monopoles exist, or the Coulomb's law (1970), which quantifies the force between two stationary, electrically charged particles. Moreover, in these equations, we can find an extension of Ampère's law (1825) that relates the integrated magnetic field around a closed loop to the electric current passing through the loop, or Michael Faraday's induction, namely, the production of an electromotive force across an electrical conductor in a changing magnetic field. Later, Oliver Heaviside synthesized Maxwell's over 20 equations into the four recognizable ones modern physicists use. Remarkably, Maxwell's equations also inspired Albert Einstein to develop the theory of special and general relativity. Hence, both the observation of the relic radiation and gravitational waves' detection also owe Maxwell's work.

Maxwell's equations successfully unified the concepts of light and electromagnetism, one of physics's grand unification. These equations depict the dynamics of macroscopic electromagnetic fields in materials described by their dielectric response. However, Maxwell's equations' exact solution is generally arduous, depending on the ratio between the incident wavelength and the object. Moreover, both object's shape and the nature of the incoming wave play an important role. Several approximations have been employed along history to get some insight into the scattering and absorption of light. For instance, for objects much smaller than the incident wavelength, the so-called Rayleigh scattering, named after the nineteenth-century British physicist John William Strutt (3rd Baron Rayleigh), accurately describes the elastic electromagnetic interaction between an incoming wave and a small single scatter described by just its electric dipolar polarizability. In that scenario, Rayleigh showed that the scattering cross-section of the particle scales with the incident wavelength as λ^{-4}. This strong wavelength dependence of the scattering means that shorter (blue) wavelengths are scattered more strongly than longer (red) wavelengths. This phenomenon results in the indirect blue light coming from all-sky regions when viewed from earth. More examples of Rayleigh scattering can be found, for instance, in amorphous solids such as glass, in the scattering of optical signals in optical Silica fibers, or nanoporous materials. On the other hand, for objects much bigger than the incident wavelength, the so-called geometrical optics or ray optics, based on describing light propagation after scattering in terms of optical rays, is an optimal approximation. This

model assumes that light propagates in straight paths in homogeneous mediums and may split in two at the interface between two different but constant media. Snell's law follows this principle, and hence, it does the phenomena associated with reflection and refraction. The techniques in which ray optics accurately describes light propagation are particularly useful in describing geometrical aspects of imaging, including optical aberrations. However, they fail when considering interference or/and diffraction effects as the wave's picture is absent in this physical scenario.
The previous approximations, namely, Rayleigh scattering and geometric optics, are tremendously helpful in getting some insight into the scattering and absorption properties of light in each of the cases mentioned above. However, an exact analytical solution to Maxwell's equations is missing in both optical models. In this vein and for objects with dimensions similar to the wavelength, it is customary to consider the formal solution of Maxwell's equations with appropriate boundary conditions. This approach is handy due to exact solutions, particularly for cylindrically symmetric objects such as disks, cylinders, or spheres. As a vast part of this Thesis is dedicated to understanding the scattering of arbitrarily sized spheres under plane wave illumination, let us briefly comment on the origin of this problem.

1.2 Mie theory and Kerker conditions

The electromagnetic scattering by a homogeneous and isotropic sphere embedded in a nondispersive medium under plane wave illumination is often referred to as Mie scattering. However, Gustav Mie was not the first to formulate this electromagnetic scattering problem (1908). Before him, Ludvig Lorenz solved this problem independently in 1890. The scientific community did not pay too much attention to this contribution because it was written in Danish. It remained hardly known even after it had been translated to French. Also, Lorenz did not connect his derivation with the Maxwell's theory of electromagnetics. Moreover and independently, Peter Debye considered the very related radiation pressure problem on a spherical particle using two scalar potential functions. Accordingly, the scattering by a homogeneous isotropic sphere embedded in a nondispersive host medium under plane wave illumination has also been referred to as Lorenz-Mie theory, or even Lorenz-Mie-Debye theory. However, Mie's name has predominantly stuck in the most recent literature. This recognition did not certainly arrive just after publishing his work, titled "Beiträge zur Optik trüber Medien, speziell kolloidaler Metallösungen" (Contributions to the optics of turbid media, particularly colloidal metal suspensions) [12]. This paper aim at a fundamental theoretical explanation of the beautiful coloration of metals, specifically gold, in a colloidal state. At that time, Mie, and the

optical community, considered his treatise to be a relatively trivial application of Maxwell's electromagnetics. Moreover and importantly, Mie's theory could not be numerically corroborated at that time due to the absence of computers. Due to these facts, Mie's work remained almost unnoticed for over 50 years. As a result, the paper is often referred to as "Sleeping Beauty" because of its late recognition considering both the increased interest in the field and the actual increasing number of citations.

This late recognition doubtless arrived after the book of Stratton (1941) [35]. In the latter, the Mie theory was reformulated in terms of the vector spherical harmonics (VSWFs), making the Mie theory more accessible and understandable for a broad scientific audience. Besides Stratton's book, a crucial role in the Mie theory dissemination and popularization has been played by the monographs by Born and Wolf (1959) [36], Kerker (1969) [37], and Bohren and Huffman (1983) [38]. However, the monograph by van de Hulst (1957) [9] has had by far the most significant impact on the dissemination of Mie's work. As a result, the Mie theory's physical picture, which was initially restricted to the scattering of a homogeneous sphere embedded in a nonabsorbing host medium under plane wave illumination, extended to more complex scattering systems. Examples of these can be found, for instance, in the seminal work done by Mundy et al. in 1974 [39], in which an absorbing host medium can be included in the scattering system, or in work done by Aden and Kerker [40], in which the typical homogeneous Mie sphere can be replaced by a coated sphere made of two different materials. With growing interest in magnetic nanostructures, these works, among others, motivated Kerker, Wand, and Miles to extend the physical picture of the Mie theory, initially derived for spheres with $\mu = 1$, to magnetic spheres with $\mu \neq 1$ [29]. In this seminal work, the authors predicted an anomalous zero optical backscattering condition regardless of the sphere's size when the magnetic sphere's optical response satisfies $\epsilon = \mu$, ϵ is the electrical permittivity of the sphere. In this scenario, they also showed that the state of polarization of the scattered wave is preserved. On the other hand, the authors also predicted, in the limit of the small particle (Rayleigh scattering), a zero light scattering condition in the forward direction when the condition $\epsilon = (4 - \mu)/(2\mu + 1)$ is met. At this optical response, the state of polarization was predicted to flipping its incoming handedness. Nevertheless, as occurred with the Mie theory in its early ages, these predictions remained almost unnoticed due to the lack of magnetic materials at optical frequencies. Moreover, a fundamental theoretical explanation of these "anomalous light scattering phenomena" associated with the so-called first and second Kerker conditions was somehow missing. Before proceeding to explain these "anomalous Kerker conditions," let us briefly discuss the concepts of both angular momentum (AM) and polarization of light since they are needed for this task.

1.3 Spin-orbit interactions of light

Like all phenomena involving waves, light has mechanical properties such as energy and linear and AM. The first to suggest that light carries linear momentum was Johannes Kepler in 1619[1]. By observing the sky at night, he postulated the existence of radiation pressure to explain why comet tails always point away from the Sun. Later, in 1909, John Poynting suggested that polarized light has AM, associated with circular polarization [41]. He linked this AM to the spin angular momentum (SAM) of light. A single-photon has a value of $\pm\hbar$ and, thus, is quantized. The first experimental demonstration of the transfer of SAM from a light beam was carried out in 1936 by Richard Beth at Princeton University [42]. In this work, Beth showed that a suspended quarter-wave plate took AM from a circularly polarized beam, confirming Poynting's physical insight a few decades before [41]. However, it is nowadays well-accepted that AM of light not only contains spin but an orbital contribution. The first work in this direction was done by Humblet [43]. In this paper, he decomposed the AM of a classical electromagnetic field as a sum of two terms[2]: the spin and the orbital angular momentum (OAM). However, the interest in this work was not much noticed at that time. In fact, it has not been appropriately taken into account even nowadays considering the current research activity on the topic.

The interest in the AM doubtless arrived in 1992 by the hand of a group in the Netherlands [44]. In this work, they demonstrated that light beams with an azimuthal phase dependence of $e^{i\ell\varphi}$ carry a net AM regardless of the polarization state it cannot be associated with the SAM. The angle φ denotes the azimuthal coordinate in the beam's transverse cross-section, and ℓ can take any integer value, positive or negative. This OAM has then a value of $L = \hbar\ell$ per photon[3]. Just as with circularly polarized light, the sign of the orbital angular moment indicates its handedness concerning the beam direction. The first experiment of a transfer of OAM to an object was performed in 1995 by Halina Rubinsztein-Dunlop and coworkers at the University of Queensland in Brisbane, Australia [45]. Indeed, they used an unpolarized, helically phased laser beam to impart OAM to a small ceramic particle held by optical tweezers. Two years later, the Brisbane group repeated the experiment, this time transferring SAM from a polarized beam to a birefringent particle which encored Beth's experiment [46].

[1] It is worth noticing that Kepler did not name it linear momentum as this concept was introduced by Isaac Newton in 1687.

[2] The AM contains a more unfamiliar surface AM. Humblet showed that the time-averaged flux of AM through a spherical surface, this surface term does not contribute. As a result, it is usually neglected in most discussions regarding this AM separation.

[3] We refer to as "per photon" when we define a EM density, just as it is done in quantum mechanics, $\ell_z = E_i^* L_z E_i / |E|^2$.

Besides these abovementioned seminal works, there has been an increasing interest in the so-called spin-orbit interactions (SOI) of light [47]. In other others, in the interchange between the SAM and OAM in different scenarios. These include spin-Hall effects in inhomogeneous media and at optical interfaces [48–50], in single homogeneous dielectric spheres [2, 30, 51], spin-dependent effects in nonparaxial (focused or scattered) fields [31,52], and spin-controlled shaping of light using anisotropic structured interfaces [53].
Rigorously speaking, though, the separation from the total AM into its SAM and OAM contributions cannot be made on firm physical grounds out of the paraxial approximation [54]. This incompatibility is motivated since both SAM and OAM operators break the transversality requirement and throw vectors out of the Hilbert space of transverse Maxwell fields [54]. Consequently, an effective transfer between the two quantities is not an entirely satisfactory explanation for physical phenomena. Moreover, in the previous work, it is demonstrated that a field's polarization is not a contributor to its AM, in striking contrast to the current state-of-the-art. These facts motivated Gabriel Molina-Terriza and his group to use an alternative theoretical framework for the general and rigorous treatment of the AM of light and its role in light-matter interactions. As we will shortly see, this is especially interesting in the fundamental understanding of the first and second Kerker conditions.

1.4 Duality symmetry and high refractive index particles

The fundamental explanation of the origin of the anomalous light scattering patterns arising at the first and second Kerker conditions arrived through the seminal work done by Gabriel Molina-Terriza et al. titled "Electromagnetic Duality Symmetry and Helicity Conservation for the Macroscopic Maxwell's Equations " [3]. They proved that when $\epsilon = \mu$ is satisfied, a non-geometrical symmetry, namely, the electromagnetic duality symmetry, broken in the microscopic Maxwell's equations by the presence of charges, can be restored for the macroscopic Maxwell's equations. This duality restoration leads the system to preserve the helicity of the electromagnetic field interacting with it, which Calkin previously showed for the electromagnetic fields in vacuum 1965 [55]. The helicity, defined as the normalized projection of the total AM onto the linear momentum of the wave, $\Lambda = (\mathbf{J} \cdot \mathbf{p})/|\mathbf{p}|$, describes the state of polarization in the frame of reference of the wave. A useful interpretation of helicity can be obtained by considering the electromagnetic field's expansion as a superposition of plane waves. In that representation, we can link helicity with the handedness of each plane wave. The scattering of an object will present a well-defined helicity if all plane waves are circularly polarized and have the same handedness to the direction of the wave's momentum, as can be inferred

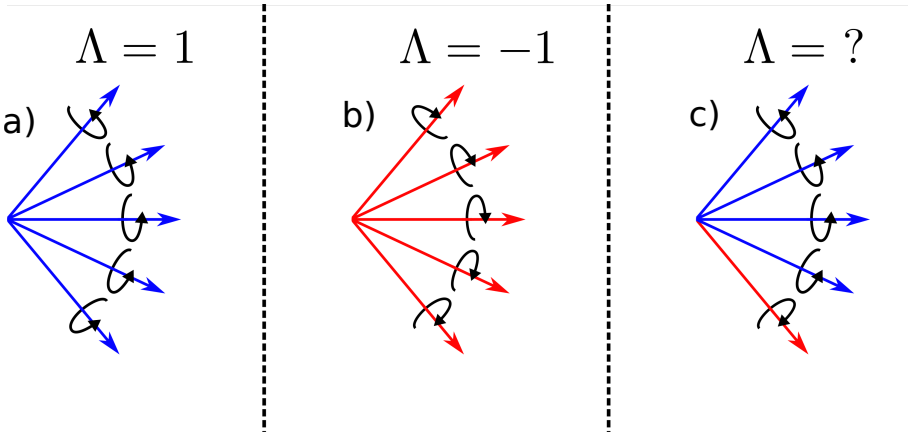

Figure 1.1 – Electromagnetic fields decomposed in left and right circularly polarized plane waves. (a) Well-defined helicity $\Lambda = +1$. (b) Well-defined helicity $\Lambda = -1$. (c) Undefined helicity since both left and right circularly polarized plane waves appear in the decomposition.

from Fig. 1.1. This explanation provides a fundamental explanation of the state of polarization's invariance, first introduced by Kerker, Wang, and Miles in 1983 [56]. Notably, the zero optical backscattering condition can also be understood through both the preservation of helicity (duality symmetry) and the conservation of the total AM in the incident direction of the wave (rotational symmetry) in the following way [4]. From the definition of the helicity and at backscattering we have $\mathbf{p} = -|\mathbf{p}|$, and hence, $\Lambda = -J_z$. However, if the electromagnetic duality is restored (dual material), the helicity must be preserved, identical to the AM of the incident PW per photon, i.e., $\Lambda = J_z$. Both relations cannot be fulfilled simultaneously, and consequently, the only solution is that no backscattered plane wave can exist. Although rigorously demonstrated by Molina-Terriza and his former group in Sidney, the restoration of duality leads to the conservation of the state of polarization, and the zero optical backscattering condition requires the existence of magnetic materials ($\mu \neq 1$). However, these do not exist at optical frequencies, and hence, they could not be experimentally corroborated.

Almost simultaneously, another group led by Prof. Juan Jose Saenz brought to the physical scene the so-called high refractive index (HRI) materials [14], which present at optical frequencies resonant electric and magnetic modes with reduced dissipative losses, in contrast to plasmonic particles [17,57]. Until that date, the vast majority of the efforts were devoted to metallic nanoparticles that present well-defined resonances due to the electrons' collective excitation [58–60]. Plasmon resonances are strongly dependent on the material,

shape, and size of the supporting elements, allowing for manipulating and tuning light at the subwavelength scale [61–63]. For these reasons, it was presumed to open the door to the control of light behavior [64]. However, due to the high losses, heating, and incompatibility with complementary metal-oxide-semiconductor fabrication processes at working frequencies, a relatively small number of applications have been realized in practice. Moreover, the absence of magnetic response at optical frequencies limited their widespread use.

In contrast, dielectric and semiconductor nanoparticles with a HRI, such as silicon or germanium in the visible and telecom spectral range, present themselves as a real alternative to plasmonic particles [13–16]. For small HRI nanoparticles under plane wave illumination, the optical response of these objects can be fully described by just electric and magnetic dipolar modes with a negligible contribution from higher orders multipolar modes [13–16]. In this scenario, and when the electric and magnetic dipolar polarizabilities oscillate in-phase and with equal amplitude, the first Kerker condition is satisifed [23], and then, the zero optical backscattering condition is met [65–67]. This absence of backscattered light prediction was experimentally demonstrated first for millimeter-scale ceramic spheres in the microwave regime [65] and shortly after for nanometer-scale HRI Si [67] and GaAs [66] nanospheres. Since then, the study of Kerker conditions has been significantly expanded and generalized, becoming ubiquitous in Nano-Optics and Photonics [68,69]. New Kerker phenomena have been shown to emerge from the interplay between dipolar and higher-order multipolar responses [70–73], from non-spherical particle's shapes [74, 75] or from near-field [76, 77], and structured beam illumination [78–81].

In contrast with the first Kerker condition, the zero-forward condition, which arises when the second Kerker condition is satisfied in the dipolar regime, is strictly inhibited by the optical theorem [82–86]. As an alternative definition, we can consider the *generalized second Kerker condition* (GSKC) [23], corresponding to crossed electric and magnetic dipoles of equal amplitude oscillating in *anti-phase*. Strong suppression of forwarding scattering was as well experimentally observed in the microwave regime [65] at this condition, in agreement with the near-zero-forward intensity condition for Rayleigh particles [23, 84]. Strong suppression of forwarding scattering is an important issue in light transport and scattering in nanostructured complex media [87–95]. Significant efforts have been made in this direction to find novel efficient ways to control the directionality of light propagation in a broader sense, not just optimizing the scattering of light in the forward and backward directions, but also introducing the steering or switching of light [96, 97].

Another interesting regime that has been actively exploited within HRI nanostructures is nonlinear optics, in particular, for second and third harmonic generation[4] [98, 99]. The latter plays a key role in the excitation of the so-

[4]Harmonic generation denotes a nonlinear optical process in which n photons with the same frequency interact with a nonlinear material, are "combined," and generate a new

called non-radiating anapole[5] [100]. In short, a non-radiating anapole refers to as the physical scenario in which the total scattering is identical to zero, yet the electromagnetic energy is enhanced inside the particle[6]. As a result, the target under illumination feels the incoming radiation's presence, yet light propagates without an effective change in its linear momentum. Indeed, the tunability of the electric and magnetic modes of HRI nanostructures has been widely employed to reach the anapole state [101]. The electric anapole has been observed for HRI nanodisks [26, 28, 102–104], nanowires [105–108], or core-shells [109, 110] under PW illumination. Further, tightly focused radially polarized beams, which do not excite the magnetic multipole components, have been presented as a possible approach to unveil anapoles in HRI spheres in the limit of small particle [111, 112]. However, the simultaneous suppression of the electric and magnetic dipolar scattering efficiencies for larger spheres under plane wave illumination, at the so-called hybrid anapole [27], is still a matter of research.

HRI dielectric nanoantennas can also be extended to more complex systems, such as the so-called metasurfaces [113]. These structures are just flat ultrathin optical components consisting of arrays of subwavelength optical particles [114]. The optical properties of metasurfaces are determined by the electric and magnetic resonant properties of the constituting HRI nanostructures. One example of this phenomena is the enhanced transmission efficiency that a metasurface supports when its unit cell acts as Huygens' sources [115]. Namely, when its constituting HRI nanostructures maximize the optical transmission with zero reflection. On the other hand, perfect flat reflectors have also been reported using metasurfaces by tunning the two electric and magnetic dipolar resonances' spectral separation [116, 117].

Having now introduced the most relevant fields in which HRI nanostructures are employed, namely, control of the directionality of light through Kerker conditions, optical invisibility given by the anapole state, or optical metasurfaces, let us move on to the main structure of the Thesis.

1.5 Thesis structure

The structure of this Thesis is organized as follows: In Chapter 2, we present the fundamental tools used in the Thesis. After the introductory Chapter, we

photon with n times the energy of the initial photons.

[5] The term anapole, meaning "without poles" in Greek, was introduced in the physics of elementary particles by Yakov Zel'dovich.

[6] Notice that this definition does not need of the traditional Cartesian decomposition, in which the anapole state is explained by means of the destructive interference between the electric dipole and electric toroidal dipole. For a rigorous explanation, check Ref. [100].

present the main research results in five Chapters. Their respective highlights are summarized in the following items:

- In Chapter 3, we show that a Si nanosphere satisfying the first Kerker condition can give rise to a divergent apparent-shift in the backscattering direction. We analyze this optical localization error, commonly referred to as *optical mirage*, from two frameworks: SOI of light and helicity conservation. Our results go beyond previous studies that only consider apparent displacements from Rayleigh spheres.

- In Chapter 4, we demonstrate that the SOI of light expressions, optical mirage, and g-parameter are linked and entirely determined by a measurement of helicity at the perpendicular direction to the incoming plane wave. From this finding, we reveal that SAM and helicity are not equivalent. Moreover, we demonstrate that the maximum optical mirage does not correspond to the SAM's zeros, in contrast to what occurs when only considering a pure electric dipole. We also analyze how absorptive effects may modify the abovementioned magnitudes.

- In Chapter 5, we demonstrate that either losses or optical gain inhibit the restoration of the EM duality for the scattering by a single homogeneous dielectric sphere. This phenomenon precludes the conservation of helicity and the zero optical backscattering condition for pure-multipolar regimes. Finally, we demonstrate that optical gain is a compulsory requirement to achieve zero forward light scattering.

- In Chapter 6, we analyze the physics behind the GSKC for subwavelength electric and magnetic dipolar particles. At this optical condition, we find that the scattered light does not always lie in the backward semi-sphere, in striking contrast to the current state-of-art.

- In Chapter 7, we show that helicity conservation can be used as a probe of pure-multipolar spectral regions. Under PW illumination, we show that the dipolar behavior is not necessarily limited to small particles, contrary to what could be expected. In these unexplored dipolar regimes, we demonstrate that the optimum forward light scattering condition does not (only) appear for a given refractive index but to a given size parameter.

CHAPTER 2

Methods

Light is in the range of the electromagnetic spectrum where the wave-particle duality is most significant. This region is where low energy radiation, described like waves, and high energy radiation, related like particles, come together. Its interaction with matter is a complex phenomenon that can be addressed in different ways. Although the most precise description is given by quantum electrodynamics, in nano-optics, a large number of problems can be tackled by considering a semi-classical approach. Usually, it is primarily sufficient to adopt a wave picture to describe the optical radiation, allowing the use of classical field theory based on Maxwell equations.
In this Chapter, we start by introducing in Section 2.1 Maxwell's and Helmholtz equations together with the transversal continuity of the EM fields between two different media. In Section 2.2, we show that the incident, internal, and scattered EM fields can be expressed on a suitable multipolar basis. In Section 2.3, we explicitly write down the electric and magnetic Mie coefficients to show a new way to express the first Kerker condition. In Section 2.4, we present the scattering, extinction, and absorption efficiencies. Finally, we show in Section 2.5 that the g-parameter may be used as a signature of duality restoration in pure-multipolar spectral regimes.

2.1 Maxwell equations

The underlying dynamics of interacting charged particles and EM fields are described by Maxwell's equations [34]. These equations are formulated as macroscopic equations that describe the dynamics of EM fields in materials that can be described by their dielectric response,

$$\nabla \cdot \mathbf{B} = 0, \tag{1}$$
$$\nabla \cdot \mathbf{D} = \frac{\rho_{\text{ext}}}{\epsilon_0}, \tag{2}$$
$$\nabla \times \mathbf{E} = -\frac{\partial \mathbf{B}}{\partial t} \tag{3}$$
$$\nabla \times \mathbf{H} = \frac{\partial \mathbf{D}}{\partial t} + \mathbf{J}_{\text{ext}}. \tag{4}$$

Here $\mathbf{E}$ and $\mathbf{H}$ are the electric and magnetic fields, respectively, $\mathbf{D}$ is the electric displacement, and $\mathbf{B}$ the magnetic induction. Moreover, ρ_{ext} and $\mathbf{J}_{\text{ext}}$ denote the free density charge and density current, respectively. For further convenience, we use here Maxwell's equations in the Fourier domain [38], where the harmonic time-dependence of the EM fields is assumed, $e^{-\mathrm{i}wt}$, with w being the frequency of light. Then, any field can be expressed as $\mathbf{A}(\mathbf{r},t) = \text{Re}\{\mathbf{A}(\mathbf{r})e^{-\mathrm{i}wt}\}$, where $\mathbf{A}(\mathbf{r})$ represents a complex-amplitude vector and Re{} denote the real part.
In this description, Maxwell equation's can be re-written as,

$$\nabla \cdot \mathbf{B} = 0, \tag{5}$$
$$\nabla \cdot \mathbf{D} = \frac{\rho_{\text{ext}}}{\epsilon_0}, \tag{6}$$
$$\nabla \times \mathbf{E} = \mathrm{i}w\mathbf{B}, \tag{7}$$
$$\nabla \times \mathbf{H} = -\mathrm{i}w\mathbf{D} + \mathbf{J}_{\text{ext}}. \tag{8}$$

At this point, it is useful to make use of the constitutive relations,

$$\mathbf{D} = \epsilon_0\mathbf{E} + \mathbf{P}, \tag{9}$$
$$\mathbf{B} = \mu_0\mathbf{H} + \mathbf{M}, \tag{10}$$

with ϵ_0 and μ_0 being the electric permittivity and magnetic permeability in vacuum. $\mathbf{P}$ denotes the polarization density, namely, the density of molecular dipole moments induced by the electric field [38]. Similarly, $\mathbf{M}$, defined as the magnetization density, is the density of molecular magnetic dipole moments induced by the magnetic field. Since we will be dealing with an isotropic, non-dispersive, homogeneous, and linear media, the constitutive relations reduce to $\mathbf{D} = \epsilon\mathbf{E}$ and $\mathbf{B} = \mu\mathbf{H}$. Here ϵ and μ are scalars that define the electric

and magnetic properties of the medium, respectively. In this scenario, the macroscopic Maxwell's equations can be written only as functions of $\mathbf{E}$ and $\mathbf{H}$,

$$\begin{aligned} \nabla \cdot \mathbf{H} &= 0, && (11)\\ \nabla \cdot \mathbf{E} &= \frac{\rho_{\text{ext}}}{\epsilon}, && (12)\\ \nabla \times \mathbf{E} &= \mathrm{i}w\mu\mathbf{H}, && (13)\\ \nabla \times \mathbf{H} &= -\mathrm{i}w\epsilon\mathbf{E} + \mathbf{J}_{\text{ext}}. && (14) \end{aligned}$$

One interesting feature of Maxwell's equations is that in the absence of free charges and currents ($\rho_{\text{ext}} = \mathbf{J}_{\text{ext}} = 0$), it is possible to obtain a non-trivial solution. In this scenario, by applying the curl operator and taking into account the vector calculus identity, $\nabla \times \nabla \times \mathbf{A} = \nabla(\nabla \cdot A) - \nabla^2\mathbf{A}$, we arrive to

$$\nabla^2\mathbf{E} + k^2\mathbf{E}^2 = 0 \qquad \text{and} \qquad \nabla^2\mathbf{H} + k^2\mathbf{H}^2 = 0, \tag{15}$$

where $k = w\sqrt{\epsilon\mu}$ is the wave-number in the medium. Equation (15) is commonly referred to as Helmholtz equation for the vectorial EM fields. As above-mentioned, it has a non-trivial solution even in the absence of free charges and currents. However, its solution crucially depends on the boundary conditions (BC). Firstly, the EM fields must vanish at infinity and be finite everywhere else. Secondly, the following relation must be satisfied between two different media, denoted by $\{\mathbf{E}_1, \mathbf{H}_1\}$ and $\{\mathbf{E}_2, \mathbf{H}_2\}$, respectively,

$$\begin{aligned} (\epsilon_2\mathbf{E}_2 - \epsilon_1\mathbf{E}_1) \cdot \hat{\boldsymbol{n}} &= \sigma_{\text{surf}}, & (\epsilon_2\mathbf{H}_2 - \epsilon_1\mathbf{H}_1) \cdot \hat{\boldsymbol{n}} &= 0,\\ \hat{\boldsymbol{n}} \times (\mathbf{E}_2 - \mathbf{E}_1) &= 0, & \hat{\boldsymbol{n}} \times (\mathbf{H}_2 - \mathbf{H}_1) &= j_{\text{surf}}. \end{aligned} \tag{16}$$

Here σ_{surf} denotes the surface charge density at the surface, j_{surf} is the surface current density; $\hat{\boldsymbol{n}}$ is the unitary normal vector to the interface between 1 and 2. From these expressions, it is noticeable that the tangential components of $\mathbf{E}$ and $\mathbf{H}$ must be continuous, while the normal components of $\mathbf{D} = \epsilon\mathbf{E}$ and $\mathbf{B} = \mu\mathbf{H}$ can be discontinuous depending on the properties of the interface.

2.2 Multipolar expansion of the electromagnetic fields

Before applying the BC conditions mentioned above to obtain the internal and scattering Mie coefficients, let us briefly introduce the electromagnetic fields' multipolar expansion. This expansion is beneficial to describe EM interactions with spherical symmetry and has been widely used in different branches of physics ranging from nanoantennas to nuclear physics. Perhaps this is the reason that explains why there is not an unified notation for them. Throughout

this Thesis, we will make use of a convenient linear combination of the vector spherical wavefunctions (VSWFs),

$$\boldsymbol{\Xi}_{lm}^{\sigma} = \frac{1}{\sqrt{2}}\left[\frac{\boldsymbol{\nabla}\times g_l(kr)\mathbf{X}_{lm}}{k} + \sigma g_l(kr)\mathbf{X}_{lm}\right], \tag{17}$$

$$g_l(kr) = A_l^{(1)} h_l^{(1)}(kr) + A_l^{(2)} h_l^{(2)}(kr), \tag{18}$$

$$\mathbf{X}_{lm} = \frac{1}{\sqrt{l(l+1)}}\mathbf{L}Y_l^m(\theta,\varphi), \tag{19}$$

Following Jackson's notation [118], $\mathbf{X}_{lm}$ denote the vector spherical harmonics, with $\mathbf{X}_{00}=0$, $g_l(kr)$ is a linear combination of the spherical Hankel functions, $Y_l^m(\theta,\varphi)$ are the scalar spherical harmonics, and $\mathbf{L}=-\mathrm{i}\,(\mathbf{r}\times\boldsymbol{\nabla})$ is the OAM operator. The quantum numbers l, m, and $\sigma=\pm1$ denote the eigenvalues of the square of the total AM [119], J^2, the AM in the incident direction [119], J_z, and helicity [54], $\boldsymbol{\Lambda}$, respectively. The multipoles $\boldsymbol{\Xi}_{lm}^{\sigma}$ can be built following the standard rules of AM addition [119,120] as simultaneous eigenvectors of J^2, J_z, with $\mathbf{J}=\mathbf{L}+\overleftrightarrow{\mathbf{S}}$ given by the sum of the OAM, $\mathbf{L}$, and SAM, $\overleftrightarrow{\mathbf{S}}$, operators:

$$\overleftrightarrow{\mathbf{S}} \equiv \mathrm{i}\mathbf{I}\times \quad , \quad \mathbf{L}\equiv\{-\mathrm{i}\mathbf{r}\times\boldsymbol{\nabla}\} \tag{20}$$

$$\overleftrightarrow{\mathbf{S}}_i = \hat{\boldsymbol{e}}_i\cdot\overleftrightarrow{\mathbf{S}} = \mathrm{i}\hat{\boldsymbol{e}}_i\times\,. \tag{21}$$

Here $\hat{\boldsymbol{e}}_{i=x,y,z}$ indicates unitary Cartesian vectors and $\mathbf{I}$ is the unit dyadic. Moreover, these multipoles are as well eigenvectors of the helicity operator for monochromatic fields, which can be expressed without loss of generality as $\boldsymbol{\Lambda}=(\mathbf{J}\cdot\mathbf{p})/|\mathbf{p}|=(1/k)\nabla\times$ [54].
Therefore, the multipoles $\boldsymbol{\Xi}_{lm}^{\sigma}$ are then simultaneous eigenvectors of J^2, J_z, and $\boldsymbol{\Lambda}$, i.e. :

$$\mathbf{J}^2\boldsymbol{\Xi}_{lm}^{\sigma} = l(l+1)\boldsymbol{\Xi}_{lm}^{\sigma} \tag{22}$$

$$J_z\boldsymbol{\Xi}_{lm}^{\sigma} = m\boldsymbol{\Xi}_{lm}^{\sigma} \tag{23}$$

$$\boldsymbol{\Lambda}\boldsymbol{\Xi}_{lm}^{\sigma} \equiv \frac{1}{k}\boldsymbol{\nabla}\times\boldsymbol{\Xi}_{lm}^{\sigma} = \sigma\boldsymbol{\Xi}_{lm}^{\sigma} \tag{24}$$

Depending on the domain in which the EM fields are defined, we shall write $\boldsymbol{\Xi}_{lm}^{\sigma}=\boldsymbol{\Psi}_{lm}^{\sigma}$ if $g_l(kr)=j_l(kr)=j_l$ (incident and internal EM fields) while $\boldsymbol{\Xi}_{lm}^{\sigma}=\boldsymbol{\Phi}_{lm}^{\sigma}$ if $g_l(kr)=h_l(kr)=h_l$ (scattered EM fields). In this notation, j_l and h_l denote the spherical Bessel and Hankel functions, respectively [118]. The orthonormalization relation for $\boldsymbol{\Xi}_{lm}^{\sigma}$ is given by

$$\int_{\Omega}\boldsymbol{\Xi}_{lm}^{\sigma\,*}\cdot\boldsymbol{\Xi}_{l'm'}^{\sigma'}\,d\Omega = \frac{1}{2}\left(|g_l|^2\left(1+\frac{l(l+1)}{(kr)^2}\right)+\frac{1}{(kr)^2}\left|\frac{\partial\,(rg_l)}{\partial_r}\right|^2\right)\delta_{\sigma\sigma'}\delta_{ll'}\delta_{mm'} \tag{25}$$

where $d\Omega=\sin\theta d\varphi d\theta$ and, again, $g_l=j_l$ accounts for internal and external EM fields and $g_l=h_l$ for the EM scattered field.

An explicit expression of the VSWFs in spherical polar coordinates (with unitary vectors $\hat{\boldsymbol{e}}_{r,\theta,\varphi}$) is given by

$$\begin{aligned}\boldsymbol{\Xi}_{lm}^{\sigma} &= \hat{\boldsymbol{e}}_r\, \mathrm{i}\sqrt{\frac{l(l+1)}{2}}\frac{g_l(kr)}{kr}Y_l^m \\ &+ \hat{\boldsymbol{e}}_\theta \frac{1}{\sqrt{2l(l+1)}}\left\{-g_l(kr)\left(\frac{\sigma m}{\sin\theta}Y_l^m\right)+\mathrm{i}\tilde{g}_l(kr)\left(\frac{\partial Y_l^m}{\partial\theta}\right)\right\} \\ &+ \hat{\boldsymbol{e}}_\varphi \frac{1}{\sqrt{2l(l+1)}}\left\{-\tilde{g}_l(kr)\left(\frac{m}{\sin\theta}Y_l^m\right)-\mathrm{i}\sigma g_l(kr)\left(\frac{\partial Y_l^m}{\partial\theta}\right)\right\},\end{aligned}$$

with

$$\tilde{g}_l(kr) \equiv g_{l-1}(kr) - l\frac{g_l(kr)}{kr} = (l+1)\frac{g_l(kr)}{kr} - g_{l+1}(kr). \tag{26}$$

2.3 Mie theory: Scattering and internal coefficients

The solution to the Mie theory arises by imposing Eq. (16) to the EM fields evaluated at the surface of the sphere in the absence of free currents,

$$\hat{\mathbf{r}}\times(\mathbf{E}_2-\mathbf{E}_1)=0, \qquad \hat{\mathbf{r}}\times(\mathbf{H}_2-\mathbf{H}_1)=0. \tag{27}$$

where $\hat{\boldsymbol{n}}=\hat{\mathbf{r}}$ is the radial unit vector.
The EM fields outside of the sphere are given by the sum of both incident and scattered EM fields, $\{\mathbf{E}_2,\mathbf{H}_2\}=\{\mathbf{E}_\mathrm{i}+\mathbf{E}_\mathrm{sca},\mathbf{H}_\mathrm{i}+\mathbf{H}_\mathrm{sca}\}$ while in the inside of the sphere are given by the internal fields, $\{\mathbf{E}_1,\mathbf{H}_1\}=\{\mathbf{E}_\mathrm{int},\mathbf{H}_\mathrm{int}\}$. As a result, Eq. (27) becomes

$$\hat{\mathbf{r}}\times(\mathbf{E}_\mathrm{sca}+\mathbf{E}_\mathrm{i}-\mathbf{E}_\mathrm{int})=0, \qquad \hat{\mathbf{r}}\times(\mathbf{H}_\mathrm{sca}+\mathbf{H}_\mathrm{i}-\mathbf{H}_\mathrm{int})\,. \tag{28}$$

Under circularly polarized PW illumination , these electric fields are given by

$$\mathbf{E}_\mathrm{i}^{\sigma} = \sum_{l=0}^{\infty}\sum_{m=-l}^{+l}\sum_{\sigma'=\pm1} C_{lm}^{\sigma\sigma'}\boldsymbol{\Psi}_{lm}^{\sigma'}, \tag{29}$$

$$\mathbf{E}_\mathrm{int}^{\sigma} = \sum_{l=0}^{\infty}\sum_{m=-l}^{+l}\sum_{\sigma'=\pm1} F_{lm}^{\sigma\sigma'}\boldsymbol{\Phi}_{lm}^{\sigma'}, \tag{30}$$

$$\mathbf{E}_\mathrm{sca}^{\sigma} = \sum_{l=0}^{\infty}\sum_{m=-l}^{+l}\sum_{\sigma'=\pm1} D_{lm}^{\sigma\sigma'}\boldsymbol{\Phi}_{lm}^{\sigma'}, \tag{31}$$

where

$$C_{lm}^{\sigma\sigma'} = \sigma \mathrm{i}^l \sqrt{4\pi(2l+1)}\delta_{m\sigma}\delta_{\sigma\sigma'}, \tag{32}$$

$$F_{lm}^{\sigma\sigma'} = -\mathrm{i}^l \sqrt{4\pi(2l+1)}\frac{\sigma c_l + \sigma' d_l}{2}\delta_{m\sigma}, \tag{33}$$

$$D_{lm}^{\sigma\sigma'} = -\mathrm{i}^l \sqrt{4\pi(2l+1)}\frac{\sigma a_l + \sigma' b_l}{2}\delta_{m\sigma}. \tag{34}$$

Here $\{a_l, b_l\}$ are the electric and magnetic scattering Mie coefficients while $\{c_l, d_l\}$ denote the electric and magnetic internal Mie coefficients. The magnetic field is given by $Z\mathbf{H} = -\mathrm{i}\mathbf{\Lambda E}$, where $Z = \sqrt{\mu/\epsilon}$ is the medium impedance. The steps needed to solve Mie theory under PW illumination are explicitly shown in many light-scattering books such as Bohren and Huffman [38] (with the e^{-iwt} convention) or van der Hulst [9] (with the e^{iwt} convention). As a result, we will not repeat here its tedious yet elegant calculation. Instead, we will comment on some overlooked aspects of the physics behind these results. So, by inserting Eqs. (29)-(31) into the BC shown in Eq. (28) and after some cumbersome algebra, we arrive to the explicit expressions of the scattered and internal Mie coefficients,

$$a_l = \frac{\mathrm{m}S_l(\mathrm{m}x)S_l'(x) - S_l(x)S_l'(\mathrm{m}x)}{\mathrm{m}S_l(\mathrm{m}x)C_l'(x) - C_l(x)S_l'(\mathrm{m}x)}, \tag{35a}$$

$$b_l = \frac{S_l(\mathrm{m}x)S_l'(x) - \mathrm{m}S_l(x)S_l'(\mathrm{m}x)}{S_l(\mathrm{m}x)C_l'(x) - \mathrm{m}C_l(x)S_l'(\mathrm{m}x)}, \tag{35b}$$

$$c_l = \frac{S_l(x)C_l'(x) - S_l'(x)C_l(x)}{\mathrm{m}S_l(\mathrm{m}x)C_l'(x) - C_l(x)S_l'(\mathrm{m}x)}, \tag{35c}$$

$$d_l = \frac{S_l(x)C_l'(x) - S_l'(x)C_l(x)}{S_l(\mathrm{m}x)C_l'(x) - \mathrm{m}C_l(x)S_l'(\mathrm{m}x)}. \tag{35d}$$

Here, the scatterer (and the host medium) is assumed to be non-magnetic, so the permeability contrast is $\mu = \mu_\mathrm{p}/\mu_\mathrm{h} = 1$, where the sub-indices p and h refer to particle and host medium. The refractive index contrast is denoted by $\mathrm{m} = \mathrm{m}_\mathrm{p}/\mathrm{m}_\mathrm{h}$, $S_l(z) = zj_l(z)$ and $C_l(z) = zh_l^{(1)}(z)$ are the Riccati-Bessel functions, and the argument $x = ka = \mathrm{m}_\mathrm{h}k_0 a = 2\pi\mathrm{m}_\mathrm{h}(a/\lambda_0)$ is the *size parameter*. Here a denotes the radius of the sphere and λ_0 the incident wavelength in vacuum. As introduced in Sec 1.2, The first Kerker condition, at which both the incoming helicity is preserved and the zero optical condition is satisfied, is given by setting $a_1 = b_1$ in the dipolar regime. An interesting feature that had not been explored until the publication of some of our works [10, 11] is how the scattering Mie coefficients behave when the first Kerker condition is satisfied. Generally and out of the dipolar regime, this is given by $a_l = b_l$. As a matter of fact and by exploring the mathematical nature of both Eq. (35a) and Eq. (35b), it is straightforward to notice that $a_l = b_l$ arises

for either $S_l(\mathrm{m}x) = 0$ (node of first kind) or $S_l'(\mathrm{m}x) = 0$ (node of second kind) [9]. The beauty of this representation lies in the extreme simplification of the first Kerker condition. As we discuss in Chapters 5 throughout the nodes notation, the first Kerker condition cannot be obtained for lossy spheres. This phenomenon precludes the conservation of the EM helicity after scattering, and hence, the restoration of the EM duality. Moreover, by using some helpful mathematical proofs concerning Bessel functions, we also demonstrate that, for lossless spheres, the scattering cannot preserve EM helicity in general terms. It is only conserved in the physical scenario in which a pure-multipolar order l contributes to the optical response. This finding allowed us to get some insight into unexplored dipolar regimes that arise well beyond the electric and magnetic quadrupolar resonances for HRI under plane wave illumination, contrary to what was assumed by the broad optical community [13–16]. This precise result can be found, for instance, in Chapter 7.
Summarizing, the reader will note that although the Mie coefficients were calculated over 100 years ago, there still new physics behind them. However, to fully understand the physics of the following Chapters, we need to introduce measurable quantities in a laboratory, such as the extinction, scattering, and absorption cross-sections.

2.4 Optical theorem and cross-sections

In the previous section, we have shown the EM field's expressions under a circularly polarized plane wave. Nonetheless, it is not easy to measure the EM field in experiments at optical frequencies. Hence, we need to derive some physical magnitudes that could be experimentally determined. An example of this quantity is the radiation's EM power in its geometrical representation (cross-sections), as we will shortly see. In order to do that, we first need to define the time-averaged Poynting vector [118].

$$\langle \mathbf{S}_{\mathrm{t}} \rangle = \frac{1}{2}\mathrm{Re}\{\mathbf{E}_{\mathrm{t}} \times \mathbf{H}_{\mathrm{t}}^{*}\} = \langle \mathbf{S}_{\mathrm{i}} \rangle + \langle \mathbf{S}_{\mathrm{sca}} \rangle + \langle \mathbf{S}_{\mathrm{ext}} \rangle, \tag{36}$$

where

$$\langle \mathbf{S}_{\mathrm{i}} \rangle = \frac{1}{2}\mathrm{Re}\{\mathbf{E}_{\mathrm{i}} \times \mathbf{H}_{\mathrm{i}}^{*}\}, \tag{37}$$

$$\langle \mathbf{S}_{\mathrm{sca}} \rangle = \frac{1}{2}\mathrm{Re}\{\mathbf{E}_{\mathrm{sca}} \times \mathbf{H}_{\mathrm{sca}}^{*}\}, \tag{38}$$

$$\langle \mathbf{S}_{\mathrm{ext}} \rangle = \frac{1}{2}\mathrm{Re}\{\mathbf{E}_{\mathrm{i}} \times \mathbf{H}_{\mathrm{sca}}^{*} + \mathbf{E}_{\mathrm{sca}} \times \mathbf{H}_{\mathrm{i}}^{*}\}. \tag{39}$$

The flux of the Poynting vector across a closed surface containing the scatterer is defined by the energy flux per unit of area and time, accounting for the loss

or gain of energy inside the surface. This magnitude, accounting for energy conservation, and hence, the optical theorem [38]. This is defined as follows,

$$W_{\text{abs}} = -\int_A \langle \mathbf{S}_{\text{t}} \rangle \cdot \hat{\mathbf{r}}\, dA = \cancelto{0}{\int_A \langle \mathbf{S}_{\text{i}} \rangle \cdot \hat{\mathbf{r}}\, dA} + \underbrace{\int_A \langle \mathbf{S}_{\text{sca}} \rangle \cdot \hat{\mathbf{r}}\, dA}_{W_{\text{sca}}} - \underbrace{\int_A \langle \mathbf{S}_{\text{ext}} \rangle \cdot \hat{\mathbf{r}}\, dA}_{W_{\text{ext}}}, \tag{40}$$

where $dA = r^2 \sin\theta d\theta d\varphi$. In Eq. (40), we have used that the power carried by the incident EM wave is strictly zero for a non-absorbing host medium. In other words, the flux entering this imaginary surface surrounding the scatterer is identical to the one that is coming out. Moreover, it is clear that if the scatterer does not absorb some of the incident radiation, Eq. (40) is identical to zero[7]. Nevertheless, this plausible phenomenon does not imply that the W_{sca} and W_{ext} vanish. As a matter of fact and as briefly introduced in Sec 1.4, this physical scenario would correspond to the excitation of the anapole state [26], in which the particle under illumination does not scatter, and light propagates without a change of its linear momentum. However, in general terms, $W_{\text{sca}} \neq 0$ and $W_{\text{ext}} \neq 0$, and then, both scattering and extinctions contributions are accessible in a laboratory. W_{ext} accounts for the total amount of energy (scattering plus absorption) removed from the incident wave due to the presence of a particle. As a result, it is convenient to express W_{ext} in terms of the incoming wave's irradiance. This is nothing but the concept of the extinction cross section [38]. The explicit extinction and scattering cross-sections's calculations can be found again in Bohren's [38] and Hulst's [9] books. In those books, they show that these scattering cross-sections do not depend on the incoming PW's polarization [8] and read as

$$\sigma_{\text{sca}} = \frac{W_{\text{sca}}}{I_{\text{i}}} = \frac{2\pi}{k^2} \sum_{l=1}^{\infty} (2l+1) \left(|a_l|^2 + |b_l|^2 \right), \tag{41}$$

$$\sigma_{\text{ext}} = \frac{W_{\text{ext}}}{I_{\text{i}}} = \frac{2\pi}{k^2} \sum_{l=1}^{\infty} (2l+1)\, \Re\{a_l + b_l\}, \tag{42}$$

where $\sigma_{\text{abs}} = \sigma_{\text{ext}} - \sigma_{\text{sca}}$. Here, it is used the incoming radiance of a PW. The calculation of the incoming irradiance is straightforward and does not depend on polarization. Indeed and by taking into account the most generic expression of a PW, $\mathbf{E} = E_0 e^{\mathrm{i}(\mathbf{k}\cdot\mathbf{r})} \hat{\boldsymbol{u}}$, $\hat{\boldsymbol{u}}$ being any polarization unit vector, we arrive to $I_{\text{i}} = |\langle \mathbf{S}_{\text{i}} \rangle| = Z E_0^2$. Equations (41)-(42) represents the extinction and scattering cross-sections for a homogeneous sphere under PW illumination.

[7] Besides absorptive effects, another case for $W_{\text{abs}} \neq 0$ occurs in the presence of gain, i.e., when energy is pumped onto the system. This scenario will be discussed in Chapter 5.

[8] Notice that the polarization of the incoming wave cannot play any role in the energy conservation as it is decoupled from Mie coefficients.

However, it is convenient to introduce efficiencies (or efficiencies factors) for these cross-sections.

$$Q_{\text{sca}} = \frac{\sigma_{\text{sca}}}{G}, \qquad \sigma_{\text{ext}} = \frac{\sigma_{\text{ext}}}{G}, \tag{43}$$

where G is the cross-sectional particle area projected onto a plane perpendicular to the incident beam (e.g., $G = \pi a^2$) for a sphere of radius a. The word "efficiency," together with the intuitive notions molded by geometrical optics, might lead us to believe that extinction efficiencies can never be greater than unity. Indeed, if geometrical optics were an utterly trustworthy guide into the world of small particles, the extinction efficiency of all particles would be identically equal to unity: all rays incident on a particle are either absorbed or deflected by reflection and refraction. However, in Nanoptics, interference effects must be taken into account, and hence, this physical picture does not simply hold. The efficiencies will be used constantly throughout this Thesis, and hence, they deserve a box in this section, just as the scattering and internal Mie coefficients,

$$Q_{\text{sca}} = \frac{2}{x^2}\sum_{l=1}^{\infty}(2l+1)\left(|a_l|^2 + |b_l|^2\right), \tag{44a}$$

$$Q_{\text{ext}} = \frac{2}{x^2}\sum_{l=1}^{\infty}(2l+1)\,\Re\{a_l + b_l\}, \tag{44b}$$

where $Q_{\text{abs}} = Q_{\text{ext}} - Q_{\text{sca}}$.
The aim of maximizing the scattering at the first Kerker condition has been addressed in previous works [121,122]. By using numerical methods, it was found that a particular refractive index material (m = 2.45) was the best candidate to fulfill the so-called optimum forward light scattering condition in the dipolar regime [121,122]. However, by imposing the first Kerker condition in the dipolar regime through the nodes notation, $S_1'(\text{m}x) = 0$, it is straightforward to notice that the electric and magnetic scattering Mie coefficients do not depend on m. Indeed, they become $a_1 = b_1 = S_1'(x)/C_1'(x)$. As a result, we will show that the scattering efficiency presents an infinite number of optimum forward light scattering conditions for a fixed x size parameter that maximizes Q_{sca}. A throughout study of this striking phenomenon can be found in Chapter 7, where these concepts are deeply studied.

2.5 Diferential cross-section and g-parameter

So far, we have introduced the concepts of the extinction, scattering, and absorption cross sections. These are measurable quantities in a laboratory

and account for the energy removed from the incident light-wave due to the presence of a target. However, these cross sections do not give any insight into the directionality of light; e.g., in an experiment, one could measure the same scattering efficiency at the first and second Kerker conditions. At these, light lies entirely in the forward and backward semi-plane, respectively. As a result, we need an extra magnitude to take into account.
The directionality of the scattered light in the far-field limit, which is one of the key ingredients in this Thesis, is governed by the differential cross-section [38],

$$\frac{\mathrm{d}\sigma_{\mathrm{sca}}}{\mathrm{d}\Omega} = \lim_{kr\to\infty} r^2 \frac{\langle \mathbf{S}_{\mathrm{sca}} \rangle \cdot \hat{\mathbf{r}}}{|\langle \mathbf{S}_{\mathrm{i}} \rangle|}, \qquad \text{with} \qquad \int_{\Omega} \frac{\mathrm{d}\sigma_{\mathrm{sca}}}{\mathrm{d}\Omega} \mathrm{d}\Omega = \sigma_{\mathrm{sca}}. \tag{45}$$

Equation (45) gives then some insight into the far-field energy pattern of the scattered wave. This angular distribution depends on the object's optical response. As a result, it may result convenient to anticipate this scattering pattern from an other physical magnitude that contains the optical properties of the scatterer. As a matter of fact, this is given by the asymmetry parameter (g-parameter), which can be straightforwardly computed from Eq.(45) as

$$g = \langle \cos\theta \rangle = \frac{\int \frac{\mathrm{d}\sigma_{\mathrm{sca}}}{\mathrm{d}\Omega} \cos\theta \, \mathrm{d}\Omega}{\sigma_{\mathrm{sca}}}. \tag{46}$$

For a particle that scatters light isotropically (i.e., the same in all directions), g vanishes. If the particle scatters more light toward the forward direction ($\theta = 0$), g is positive. Contrary, g is negative if the scattering is directed more toward the backward direction ($\theta = \pi$). For a homogeneous sphere, it can be shown that after some cumbersome but trivial algebra, the g-parameter becomes [38]

$$g = \frac{4}{x^2 Q_{\mathrm{sca}}} \left[\sum_l \frac{l\,(l+2)}{l+1} \Re\{a_l a_{l+1}^* + b_l b_{l+1}^*\} + \sum_l \frac{2l+1}{l\,(l+1)} \Re\{a_l b_l^*\} \right]. \tag{47}$$

From Eq. (47) we can distinguish two terms: one that involves an interference between l and $l+1$ terms (e.g. dipolar and quadrupolar), and other that only mixes the electric and magnetic Mie coefficients of the same multipolar order l. Since in this Thesis we will mainly focus on the dipolar regime ($l = 1$) the first term can be neglected. In this scenario, the g-parameter becomes

$$\boxed{g = \frac{\mathrm{Re}\,\{a_1 b_1^*\}}{|a_1|^2 + |b_1|^2}.} \tag{48a}$$

From this equation, it is straightforward that the maximum value of the g-parameter is given by the first Kerker condition, i.e., $g = 0.5 \Longleftrightarrow a_1 = b_1$. As we show in Chapter 4, there is unexplored physics behind this phenomenon. As a matter of fact, in Chapter 4, we demonstrate an intriguing equivalence between helicity after scattering and the g-parameter.

2.6 Summary

In this chapter, we summarise the fundamental tools used in the following chapters. We have introduced, among others, Maxwell equations, electric and Mie coefficients, scattering, extinction, and absorbing efficiencies, and g-parameter. The reader will shortly test that within the boxed expressions in this Chapter, we can explore a huge amount of information that had not been previously discussed to the best of my knowledge. Nevertheless and as previously commented, detailed discussions of the electromagnetic theory can be found in general text-books [9, 35, 38, 118].

CHAPTER 3

Enhanced spin-orbit optical mirages from dual nanoparticles

3.1 Introduction

In addition to energy and linear momentum, a light wave carries AM [41–43] that can be split into spin angular momentum (SAM) and orbital angular momentum (OAM) contributions [45, 123–125]. The interplay between these components is commonly referred to as spin-orbit interactions (SOI) of light and has attracted a great deal of interest in the past years [47, 124, 126, 127]. An interesting analogy between the SOI in light and the spin Hall effect (SHE) in electronic systems can be drawn [128, 129]. In the latter, electrons with different spins (up and down) are deflected asymmetrically by scattering off impurities due to the SOI. This well-known phenomenon drives to a transverse spin current that, in turn, induces a measurable spin accumulation at the sample edges. One of the microscopic origins of the SHE is the so-called side-jump mechanism [1], in which a spin-dependent displacement of the center of mass of the electronic wave packet occurs as a result of the SOI effect [130, 131]. Similarly, an apparent transversal shift of a target particle induced by light scattering can be derived by an AM exchange in the context of SOI of light. Hereafter, this effect is referred to as *optical mirage* and has been observed in several scenarios, for example, in beams impinging on a dielectric surface [48, 50] or when considering a target with spherical symmetry described by a single electric (or

magnetic) polarizability [2]. In the latter case, the apparent displacement of the pure electric (or magnetic) dipolar particle localization does not depend on the optical properties, but on the scattering angle, with opposite displacements for incident left and right circularly polarized photons (well-defined handedness), as occurs with the spin of electrons after scattering. The apparent shift (Δ) is maximized at the plane perpendicular to the direction of the incoming wave taking a value of $\Delta = \lambda/\pi$ [2] and thus, for circularly polarized light, is always below the incident wavelength. Remarkably, it has been recently shown that this subwavelength limit can be surpassed by illuminating with elliptically polarized light for small numerical apertures [51]. In the same vein, for larger multipolar spheres and certain combinations of radius and refractive index, resonant apparent shifts, reaching tens of wavelengths in magnitude, were numerically found at some specific angles [30]. These results were interpreted due to a full transfer from SAM to OAM at those directions [30]. At those, the scattered light was presumed to be linearly polarized (being the SAM identically to zero).

In this Chapter, we demonstrate that by considering a high refractive index (HRI) spherical particle, sustaining both an electric and magnetic dipolar response, this subwavelength maximum limit can be drastically surpassed when the spherical particle is excited by circularly polarized light (well-defined EM helicity $\sigma = \pm 1$). In other words, a large macroscopic apparent shift ($\Delta \gg \lambda$), even greater than those reported previously [30, 51], arises in the backscattering region. The scattering system together with the so-called helicity basis is briefly introduced in Sec. 3.2. Specifically, we show in Sec. 3.3 that this optical mirage is intimately related to the generation of a spiraling power flow and can be explained in terms of an AM exchange per photon between the SAM and OAM contributions in a SOI of light context. In contrast with an earlier work [30], we exhibit in Sec. 3.4 that, for HRI dipolar spheres, the optical mirage reaches its maximum value at angles where the spin of the photons is sign reversed, i.e., at directions at which the light is not linearly polarized. Based on the EM helicity preservation, we straightforwardly demonstrate that the maximum AM exchange occurs when the system is dual, i.e., when the electric and magnetic dipolar moments are equal, at the so-called first Kerker condition [23, 29]. At this first Kerker condition, the scattered light preserves the incoming EM helicity per photon in all directions with a vanishing intensity in the backscattering direction. As we show, this zero optical backscattering condition gives rise to a huge optical mirage associated with the appearance of a (2σ charge) topological optical vortex [127, 132, 133]. In Sec. 3.5, we present the main conclusions which are derived from this Chapter.

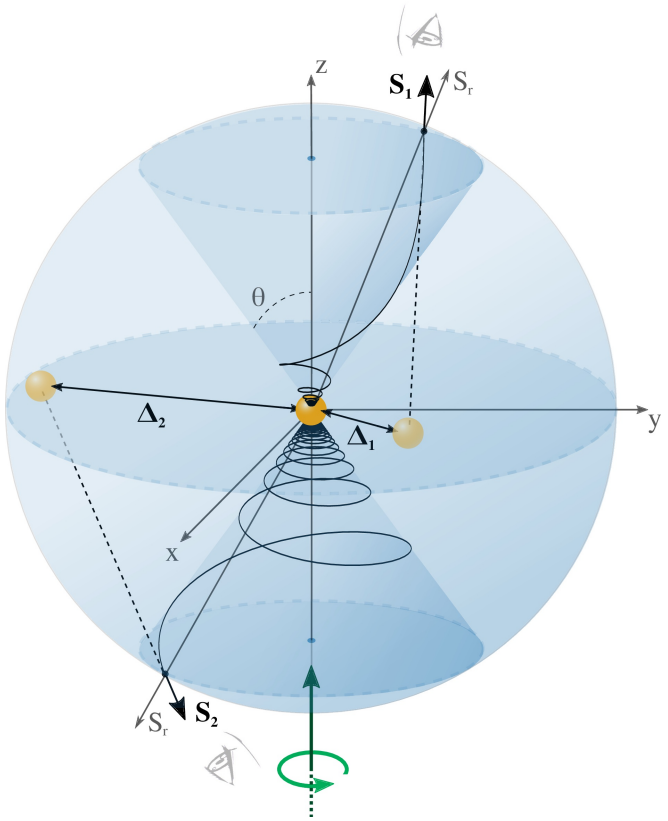

Figure 3.1 – Schematic representation of the optical mirage vector when considering a clockwise circularly polarized incoming wave (green straight arrow lying on the z-axis). The observer, represented by an eye, perceives a non-radial scattered Poynting vector $(\mathbf{S}_1, \mathbf{S}_2)$ that leads to an apparent shift $(\boldsymbol{\Delta}_1, \boldsymbol{\Delta}_2)$ of the dipole localization, both lying on the xy-plane.

3.2 System and methods

We consider a non-absorbing dielectric sphere of radius a and refractive index m_{p} embedded in an otherwise homogeneous medium with constant and real refractive index m_{h}. The geometry of the scattering system is sketched in Fig. 3.1, where we consider a circularly polarized PW with wavenumber $k = m_{\mathrm{h}} k_0 = m_h 2\pi/\lambda_0$ (being λ_0 the light wavelength in vacuum) and EM helicity per photon $\sigma = \pm 1$ (we associate left polarized light with a positive EM helicity per photon, namely, $\sigma = +1$) incident along the z-axis.

Instead of using the traditional multipole Mie expansion to describe the light which is scattered by the sphere [38], we shall find it useful to work in a basis of multipoles, $\mathbf{\Psi}^{\sigma}_{lm}$, which were introduced in Chapter 2, particularly, in Sec 2.2. Let us recall that these are eigenfunctions of the helicity operator $\mathbf{\Lambda}$, the total AM in the incident direction, J_z, and the square of the total AM, J^2, [4, 54]. In this basis, the incident field (circularly polarized PW) can be written as:

$$\frac{\mathbf{E}^{\sigma}_{\mathrm{i}}}{E_0} = \frac{\hat{\boldsymbol{x}} + \sigma \mathrm{i}\hat{\boldsymbol{y}}}{\sqrt{2}} e^{\mathrm{i}kz} = \sum_{l=0}^{\infty} \sum_{m=-l}^{+l} \sum_{\sigma'=\pm 1} C^{\sigma\sigma'}_{lm} \mathbf{\Psi}^{\sigma'}_{lm}, \tag{49}$$

$$kZ\mathbf{H}^{\sigma}_{\mathrm{i}} = -\mathrm{i}\boldsymbol{\nabla} \times \mathbf{E}^{\sigma}_{\mathrm{i}}, \tag{50}$$

$$C^{\sigma\sigma'}_{lm} = \sigma \mathrm{i}^{l} \sqrt{4\pi(2l+1)} \delta_{m\sigma} \delta_{\sigma\sigma'}, \tag{51}$$

where $1/Z = \epsilon_0 c m_h$ (being ϵ_0 and c the vacuum permittivity and speed of light, respectively). Such circularly polarized PW, with EM helicity per photon σ, carries a $j_z = m = \sigma$ unit of total AM per photon parallel to the propagation direction [118]. In a SOI of light description, this unit of total AM is entirely given by the spin contribution since a PW by definition does not carry OAM; namely, $j_z = s_z$ with $\langle L_z \rangle = 0$. In the same basis, the scattered field is given by

$$\frac{\mathbf{E}^{\sigma}_{\mathrm{sca}}}{E_0} = \sum_{l=0}^{\infty} \sum_{m=-l}^{+l} \sum_{\sigma'=\pm 1} D^{\sigma\sigma'}_{lm} \mathbf{\Phi}^{\sigma'}_{lm}, \tag{52}$$

$$D^{\sigma\sigma'}_{lm} = -\mathrm{i}^{l} \sqrt{4\pi(2l+1)} \frac{\sigma a_l + \sigma' b_l}{2} \delta_{m\sigma}. \tag{53}$$

Here a_l and b_l are the standard electric and magnetic Mie scattering coefficients, whose explicit expressions can be found in Chapter 2, specifically in Sec. 2.3. Since a sphere presents axial symmetry around the z-axis, *the j_z of the incident beam is preserved* and then, the scattered wave can only involve $m = \sigma$. Consequently, $\mathbf{E}^{\sigma}_{\mathrm{sca}}$ is an eigenfunction of the z-component of the total (dimensionless) AM operator, $\mathbf{J} = \mathbf{L} + \mathbf{S}$, with eigenvalue $j_z = m = \sigma$,

$$\sigma = \frac{{\mathbf{E}^{\sigma}_{\mathrm{sca}}}^{*} \cdot (L_z + S_z)\, \mathbf{E}^{\sigma}_{\mathrm{sca}}}{\left|\mathbf{E}^{\sigma}_{\mathrm{sca}}\right|^2} = \ell_z(\mathbf{r}) + s_z(\mathbf{r}), \tag{54}$$

$$s_z(\mathbf{r}) = \frac{-\mathrm{i}\left\{{\mathbf{E}^{\sigma}_{\mathrm{sca}}}^{*} \times \mathbf{E}^{\sigma}_{\mathrm{sca}}\right\} \cdot \hat{\boldsymbol{e}}_z}{\left|\mathbf{E}^{\sigma}_{\mathrm{sca}}\right|^2}, \tag{55}$$

$$\ell_z(\mathbf{r}) = \frac{{\mathbf{E}^{\sigma}_{\mathrm{sca}}}^{*} \cdot L_z \mathbf{E}^{\sigma}_{\mathrm{sca}}}{\left|\mathbf{E}^{\sigma}_{\mathrm{sca}}\right|^2} = \frac{-\mathrm{i}}{\left|\mathbf{E}^{\sigma}_{\mathrm{sca}}\right|^2} \left\{ {\mathbf{E}^{\sigma}_{\mathrm{sca}}}^{*} \cdot \frac{\partial \mathbf{E}^{\sigma}_{\mathrm{sca}}}{\partial \varphi} \right\}. \tag{56}$$

Equation (54) shows that the sum of the (dimensionless) OAM, $\ell_z(\mathbf{r})$, and SAM, $s_z(\mathbf{r})$, *per photon* is constant and equal to the incoming AM per photon. Note that this sum is valid even in the near field region and it would be valid even in the presence of absorption, as it is discussed in Chapter 4.

3.3 Emergence of the optical mirage from the Spiralling Poynting vector

Let us now consider the scattering from a HRI subwavelength sphere in a spectral range such that the optical response can be fully described by its first electric and magnetic dipolar Mie coefficients a_1 and b_1, i.e. by its electric and magnetic polarizabilities $\alpha_{\rm E} = {\rm i}a_1(6\pi/k^3)$ and $\alpha_{\rm M} = {\rm i}b_1(6\pi/k^3)$ [14]. We find useful to split the scattered field into the sum of two components with opposite EM helicity,

$$\frac{\mathbf{E}^{\sigma}_{\rm sca}}{E_0} = -\frac{k^3}{\sqrt{12\pi}}\left\{(\sigma\alpha_{\rm E}+\alpha_{\rm m})\mathbf{\Psi}^{+}_{1\sigma} + (\sigma\alpha_{\rm E}-\alpha_{\rm m})\mathbf{\Psi}^{-}_{1\sigma}\right\} = \mathbf{E}^{\sigma+} + \mathbf{E}^{\sigma-}, \quad (57)$$

$$\mathbf{E}^{\sigma\sigma'} \sim E^{\sigma\sigma'}e^{{\rm i}\sigma\varphi}\left(\hat{\boldsymbol{e}}_{\sigma'} + {\rm i}\sigma\frac{\sqrt{2}}{kr}\frac{\sigma\cos\theta-\sigma'}{\sin\theta}\hat{\boldsymbol{e}}_r + ...\right), \quad (58)$$

where the last identity corresponds to the medium-far-field expansion with

$$\frac{E^{\sigma\sigma'}}{E_0} = \frac{e^{ikr}}{4\pi kr}k^3\left(\frac{\sigma\alpha_{\rm E}+\sigma'\alpha_{\rm m}}{2}\right)(\sigma\cos\theta+\sigma'), \quad (59)$$

$$\hat{\boldsymbol{e}}_{\sigma'} = \frac{1}{\sqrt{2}}(\hat{\boldsymbol{e}}_\theta + {\rm i}\sigma'\hat{\boldsymbol{e}}_\varphi). \quad (60)$$

The scattered fields by HRI dielectric nanoparticles present several peculiar properties arising from the interference between the electric and magnetic dipolar radiation and have been largely discussed both theoretical [13,14] and experimentally [16, 65–67]. Most of these properties are encoded in the FF energy-radiation pattern, namely, in the differential scattering cross section, which in the helicity basis reads as

$$\frac{{\rm d}\sigma_{\rm sca}}{{\rm d}\Omega} = \lim_{kr\to\infty} r^2\frac{\mathbf{S}^{\sigma}_{\rm sca}\cdot\hat{\boldsymbol{e}}_r}{|\mathbf{S}_{\rm i}|} = r^2\frac{|E^{\sigma+}|^2+|E^{\sigma-}|^2}{|E_0|^2}, \quad (61)$$

where $\mathbf{S}^{\sigma}_{\rm sca} = \langle\mathbf{S}^{\sigma}_{\rm sca}\rangle = {\rm Re}\left\{\mathbf{E}^{\sigma}_{\rm sca}{}^{*}\times\mathbf{H}^{\sigma}_{\rm sca}\right\}/2$ is the time averaged Poynting vector[9]. In the electric *and magnetic*[10] dipolar regime the diferential scattering cross section is given for the scattering of an homogeneous sphere by [23],

$$\frac{{\rm d}\sigma_{\rm scat}}{{\rm d}\Omega} = \frac{k^4}{(4\pi)^2}\left(|\alpha_{\rm E}|^2+|\alpha_{\rm m}|^2\right)\left(\frac{1+\cos^2\theta}{2}+2g\cos\theta\right), \quad (62)$$

[9] In the FF there is no information regarding the polarization of the incoming wave. Note that this makes completely sense given the fact that the cross-sections, calculated from the FF expression of the total Poynting vector, cannot depend on polarization effects.

[10] We refer to as "magnetic" whereas we want to highlight that the dipolar object is not a Rayleight scatterer, namely, the electric dipolar regime is clearly insufficient to describe the optical response of the object.

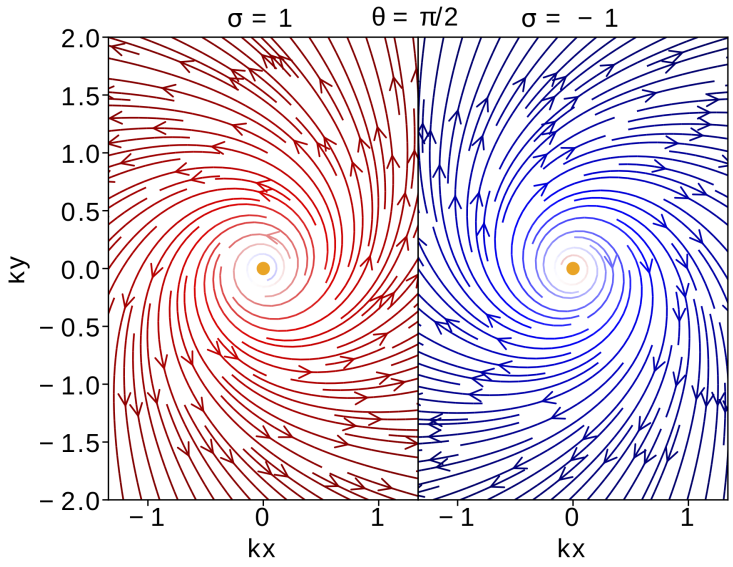

Figure 3.2 – Poynting vector streamlines with counterclockwise (clockwise) rotation for $\sigma = 1$ ($\sigma = -1$) when viewed from the perpendicular direction, $\theta = \pi/2$. This figure is valid for any dipolar response, i.e., arbitrary values of the electric or/and magnetic polarizabilities α_{E} and α_{M}. The orange circle represents the dipolar particle.

where

$$g = \frac{\mathrm{Re}\left\{a_1 b_1^*\right\}}{|a_1|^2 + |b_1|^2}, \tag{63}$$

is g-parameter, which has been previously defined in Chapter 2, particularly, in Sec. (2.5). Although in the strict FF limit the streamflow lines of the Poynting vector lie along the radial direction, tracing them to their source, they do indeed spiral towards the origin at shorter distances, in analogy with the light scattered by an electric dipole excited by circularly polarized light [2, 30, 134, 135]. Consequently, as sketched in Fig. 3.1, the Poynting vector[11], $\mathbf{S}^{\sigma}_{\mathrm{sca}}$, makes an angle with the line of sight, which drives to an apparent shift (optical mirage) $\boldsymbol{\Delta}$ in the perceived position of the spherical dipolar particle, with

$$\boldsymbol{\Delta} = \lim_{kr\to\infty}\left(\frac{\hat{\boldsymbol{e}}_r \times (\mathbf{r} \times \mathbf{S}^{\sigma}_{\mathrm{sca}})}{|\mathbf{S}^{\sigma}_{\mathrm{sca}}|}\right) = \lim_{kr\to\infty}\left(\frac{2\mathrm{i}}{k\,|\mathbf{E}^{\sigma}_{\mathrm{sca}}|^2}\frac{{\mathbf{E}^{\sigma}_{\mathrm{sca}}}^*}{\sin\theta}\cdot\frac{\partial \mathbf{E}^{\sigma}_{\mathrm{sca}}}{\partial\varphi}\right)\hat{\boldsymbol{e}}_{\varphi}. \tag{64}$$

[11] Note that the Poynting vector emerging from an electric and magnetic dipolar sphere can be seen in Appendix A.2. Particularly, the scattered Poynting vector when considering a well-defined EM helicity PW (as it is the case) is explicitly shown in Appendix A.3.

Taking into account both Eqs. (54)-(56), the optical mirage can be written as

$$\frac{\mathbf{\Delta}}{(\lambda/\pi)} = -\frac{\ell_z(\theta)}{\sin\theta}\hat{\boldsymbol{e}}_\varphi = \frac{s_z(\theta)-\sigma}{\sin\theta}\hat{\boldsymbol{e}}_\varphi = -\sigma\left[\frac{\sin\theta\,(1+2g\cos\theta)}{1+\cos^2\theta+4g\cos\theta}\right]\hat{\boldsymbol{e}}_\varphi. \quad (65)$$

In absence of a magnetic dipolar optical response, which mathematically is equivalent to set $g = 0$ in Eq. (65), one recovers the previously reported results for electric dipoles [2, 30], which were interpreted as a result of transfer from SAM to OAM [30, 31]. According to those previous works, this AM transfer is expected to be maximum at those directions at which the scattered light is linearly polarized, being the SAM of scattered photons identically zero[12]. For a pure electric (or magnetic) dipole excited by circularly polarized light, the maximum AM transfer would occur in the plane perpendicular to the incoming light ($\theta = \pi/2$) being the maximum displacement equal to $\Delta = \lambda/\pi$, and thus, it is always subwavelength. In striking contrast to the purely electric (or magnetic) case when excited with a circularly polarized field, the field scattered by electric and magnetic dipoles presents a very different polarization structure [136]: the scattered radiation on the plane perpendicular to the incoming light ($\theta = \pi/2$) is no longer linearly polarized. Notably, this change does not affect the streamlines of the Poynting vector on this particular plane (as shown in Fig. 3.2), giving rise to the same subwavelength optical mirage. However, out of this plane, the optical mirage presents a non-trivial behavior strongly dependent on both θ and the incident wavelength λ.

Figures 3.3 and 3.4 summarize the anomalous behaviour of the optical mirage $\Delta(\lambda, \theta)$ for silicon nanospheres in the infrared (similar behavior is obtained in other spectral ranges as long as the scattering cross section can be described by only the first two dipolar multipoles, see Fig. 3.3a). As can be seen in Fig. 3.4, for $\theta = \pi/2$, the apparent shift is always subwavelength λ/π for all incident frequencies, mimicking the case arising from a pure electric (or magnetic) dipolar sphere. When the g-parameter is negative ($\lambda_{g1} < \lambda < \lambda_{g2}$) the maximum optical mirage occurs for $\theta < \pi/2$ and it is always subwavelength, being slightly larger than the one for $\theta = \pi/2$. However, for $g > 0$ the optical mirage can be much larger than λ/π. Particularly, when the electric and magnetic polarizabilities are identical ($\lambda = \lambda_{K1}$), i.e., at the first Kerker condition [23], it diverges as $\theta \to \pi$. Notice that the singularity is naturally resolved since, at the first Kerker condition, there is exactly zero backscattered intensity [65, 66]. Interestingly, this can be easily understood from symmetric arguments nicely brought to the physical scene in Ref. [4] and briefly summarized in Chapter 1: at backscattering, $\Lambda = (\mathbf{J}\cdot\mathbf{p})/|\mathbf{p}| = -J_z = -\sigma$. However, when the system is dual, the EM helicity is preserved after scattering, namely, $\Lambda = J_z = \sigma$.

[12] As we show in the next Chapter, the wave's polarization after scattering cannot be generally linked with the SAM. This polarization's information is carried by the degree of circular polarization (DoCP).

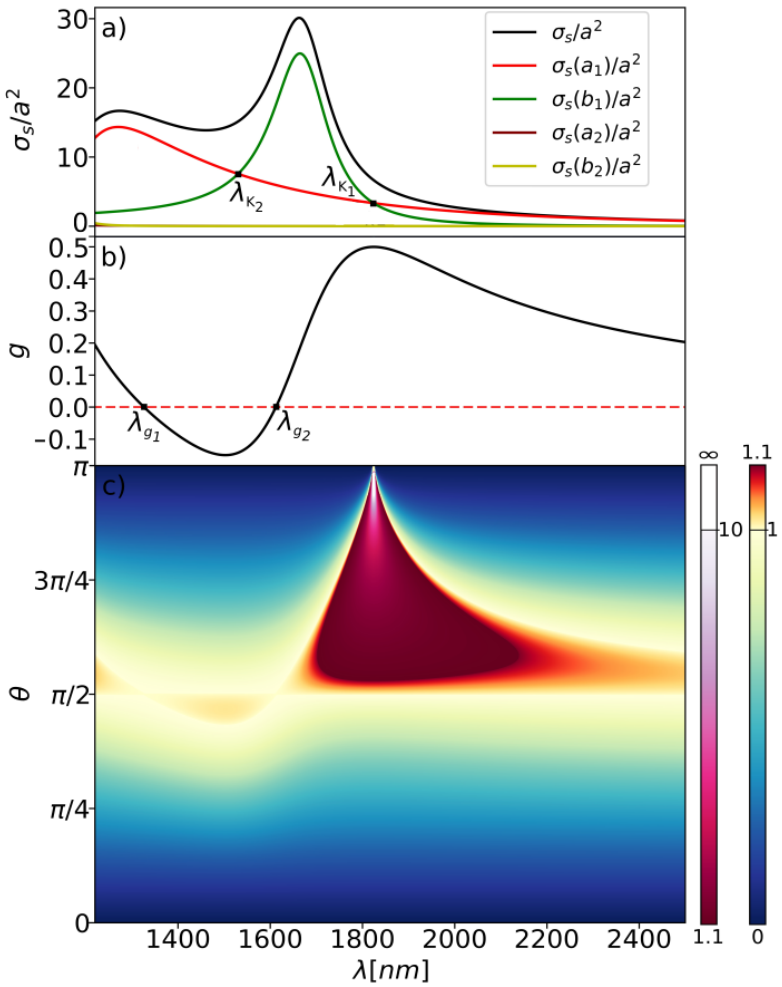

Figure 3.3 – (a) Scattering cross sections $\sigma_{\text{sca}} = \sigma_{\text{s}}$ for a 230 nm Si nanosphere versus the incident wavelength. The special wavelengths $\lambda_{\text{K}_1} = 1825$ nm and $\lambda_{\text{K}_2} = 1520$ nm correspond to the first Kerker condition and GSKC [23], respectively. (b) g-parameter versus the incident wavelength. This is identical to zero at $\lambda_{\text{g}_1} = 1326$ nm and $\lambda_{\text{g}_2} = 1612$ nm (and negative in between). The maximum value is obtained at the first Kerker condition, namely, λ_{K_1}. (c) Colormap of the normalized optical mirage, $\Delta/(\lambda/\pi)$, versus the scattering angle and the incident wavelength. The maximum optical mirage's enhancement for λ_{K_1} at backscattering ($\theta = \pi$) is clearly observed.

Evidently, both phenomena cannot be satisfied simultaneously. As a result, such light wave cannot exist at the backscattering direction.

3.4 Optical mirage near the first Kerker condition

We can now examine the peculiar behaviour of $\mathbf{\Delta}$ near the first Kerker condition. When the electric and magnetic dipolar responses are identical, i.e. $\alpha_{\mathrm{E}} = \alpha_{\mathrm{M}}$, in the electric and magnetic dipolar regime, the EM helicity is preserved after after scattering [3, 91]. In this scenario, the g-parameter is maximized, $g = 1/2$, according to Eq. (63), (see Fig. 3.3b) which gives rise to

$$\frac{\mathbf{\Delta}\pi}{\lambda_{\mathrm{K}_1}} = -\sigma \tan\left(\frac{\theta}{2}\right)\hat{\boldsymbol{e}}_{\varphi}. \tag{66}$$

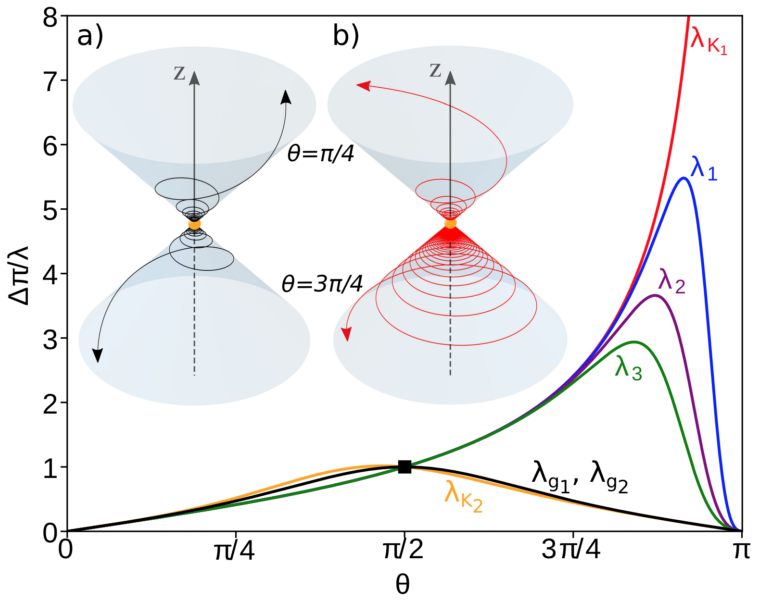

Figure 3.4 – Optical mirage colormap (Fig. 3.3) cuts versus the scattering angle θ for different values of the incident wavelength, belonging to regions with $g < 0$ (λ_{K_2}), $g = 0$ ($\lambda_{\mathrm{g}_1}, \lambda_{\mathrm{g}_2}$) and $g > 0$ (λ_1, λ_2 and λ_3, respectively decreased 5, 10 and 15 nm with respect to λ_{K_1}, and λ_{K_1} itself). At $\theta = \pi/2$, $\Delta = \lambda/\pi$ is observed to be a universal value . Both subplots show examples of trajectories of the Poynting vector at forward and backscattering, being similar for λ_{g_1} and λ_{g_2} (a) and considerably different for λ_{K_1} (b).

From Eq. (66), various interesting limiting cases can be identified: firstly, in the forward direction, the optical mirage and l_z are strictly zero since $\mathbf{S}_\varphi = 0$. This can alternatively be concluded through the system's existing symmetries: as the scatterer is dual, the system must conserve the incoming field's EM helicity, which in the forward direction corresponds to the spin density. Thus, the circular incident polarization (EM helicity) is preserved in the forward direction and must carry all the AM per photon (leaving $\ell_z = 0$). Secondly, in the direction perpendicular to the incident wavevector ($\theta = \pi/2$), the interference between the electric and magnetic dipolar contribution vanishes. As a consequence, $s_z = 0$ and $\ell_z = \sigma$ and, in analogy with pure electric (or magnetic) dipoles, we obtain a subwavelength apparent shift, $\Delta = \sigma\lambda/\pi$, although in this case the scattered light is circularly polarized. The most striking effect arises at an observation angle near backscattering $\theta \lesssim \pi$ where, as discussed above, the optical mirage diverges.

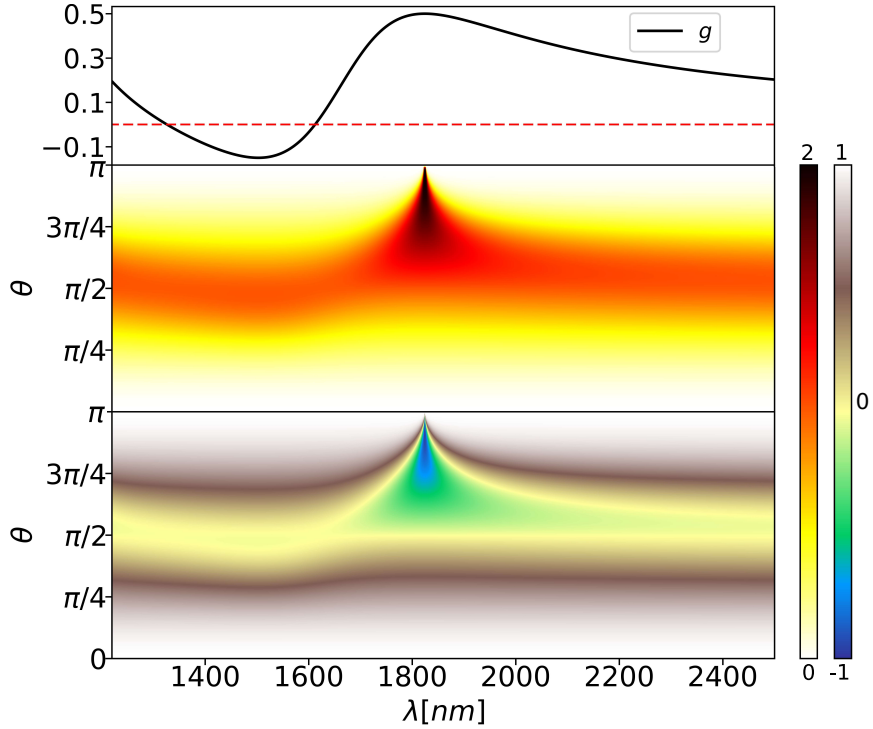

Figure 3.5 – (a) g-parameter vs the incident wavelength for a 230 nm Si sphere. (b) OAM distribution. (c) SAM distribution. At the first Kerker condition ($\lambda \approx 1824$ nm) the maximum AM exchange arises, i.e., $\ell_z = 2$ and $s_z = -1$.

This divergence is naturally solved since the Poynting vector becomes strictly zero in the backscattering direction, evidencing an optical vortex's appearance in that direction. As a matter of fact, near backscattering $\ell_z(\lesssim \theta) \to 2\sigma$, while the spin reverses sign $s_z(\theta \lesssim \pi) \to -\sigma$ (but still maintaining constant EM helicity), which confirms the existence of a vortex with $\ell_z = 2\sigma$ emerging from a nanoparticle. This phenomenon is as a nanoscale analog of the light backscattered from a perfect reflecting cone [137]. The AM exchange for a 230 nm Si particle versus the incident wavelength and the scattering angle is shown in Fig. 3.5. From this plot, we can infer all the abovementioned intriguing phenomena in the vicinity of the first Kerker condition.

3.5 Conclusions

We have shown that light scattering from a HRI nanoparticle can lead to apparent macroscopic displacements of the particle position (optical mirages). Notably, these are much larger than the incident wavelength and those that have been reported so far. Interestingly, we derived an explicit expression that relates the optical mirage and the z-component of the OAM per photon, ℓ_z. As a result of the interference between the fields scattered by the electric and magnetic dipoles, we found that ℓ_z presents a non-trivial dependence on the scattering angle, which, in contrast with previous work [30], leads to optical mirage maxima at angles where the spin of the photons is sign-reversed. Remarkably, for dual nanospheres, i.e., at the first Kerker condition, we predict a huge enhancement of the apparent shift related to the emergence of an optical vortex in the backscattering direction.

CHAPTER 4

Asymmetry, helicity and SOI of light scattered from subwavelength particles

4.1 Introduction

In Chapter 3, we have shown that the scattered light by a 230 nm Si sphere in the telecom spectral range [14] can lead to a considerable enhancement of the optical mirage at the backscattering direction [5]. As a matter of fact, the optical mirage diverges when the EM helicity is preserved after scattering. As we have shown, this phenomenon occurs when the first Kerker condition is satisfied, namely, when the first electric and magnetic Mie coefficients polarizabilities are strictly identical. In a SOI of light description, this divergent value can be derived from a full AM exchange between the spin and orbit components: at the first Kerker condition, when the EM helicity is conserved, the SAM density is sign reversed at backscattering (with $\ell_z = 2\sigma$), inducing an optical vortex in this direction. As a direct consequence, this Si sphere seems to be scattering very far from the actual source. These findings may give ground for the conjecture that any optical property related to the electric and magnetic polarizabilities, such as particle size, refractive index contrast, or absorptive effects may modify the scattered EM helicity density or the AM transfer between the spin and orbit components, and hence, the optical mirage.

In this Chapter, we show that the remarkable angular dependence of these optical mirages and those of the intensity, EM helicity, SAM, and OAM densities are all strikingly linked and entirely determined by the dimensionless g-parameter in the dipolar regime, being independent of the specific optical properties of the scatterer (including absorptive effects). Notably, we demonstrate in Sec. 4.2 that the g-parameter is precisely half of the EM helicity density in the FF limit, or equivalently, the degree of circular polarization (DoCP), at the perpendicular direction to the incoming plane wave. This intriguing phenomenon points to the maximization of the g-parameter as a straightforward detector of the EM duality restoration in the dipolar regime[13]. As a result, the g-parameter, which typically appears in the context of optical forces [22, 138], light transport phenomena [87] and radiation pressure effects [139], can be used as well as a signature of dual spheres. Note that these findings open the possibility to infer the whole angular properties of the scattered fields (OAM, SAM, optical mirage and intensity) by a single far-field polarization measurement at the perpendicular direction to the incoming wave ($\theta = \pi/2$). Nonetheless, for completeness, we write down in Sec. 4.3 both the OAM and SAM densities to explicitly demonstrate that, in striking contrast to the DoCP case, the expected value of the OAM and SAM densities are constant and identical to half of the incoming EM helicity per photon. Interestingly, the result of these calculations matches with the seminal work carried out by Marston and Crichton [124]. Finally, we explicitly illustrate in Sec. 4.4 that generally, the maximum optical mirage and the maximum AM exchange takes place at different scattering angles for a given optical response. Moreover, none of these maxima values match when the scattered light is linearly polarized, in striking contrast to when considering a pure electric (or magnetic) dipolar scatter [2, 30] and as briefly mentioned in the previous Chapter. The main conclusions of this Chapter can be found in Sec. 4.5.

4.2 DoCP in the electric and magnetic dipolar regime

Let us consider an arbitrary HRI nanoparticle in the electric and magnetic dipolar regime. By applying the helicity operator for monochromatic waves, $\mathbf{\Lambda} = (1/k)\nabla\times$, to the scattered electric field in the FF limit (see Eq. (57)), we arrive to

$$\text{DoCP} = \Lambda_\theta = \frac{\mathbf{E}^\sigma_{\text{sca}}{}^* \cdot (\mathbf{\Lambda}\mathbf{E}^\sigma_{\text{sca}})}{\mathbf{E}^\sigma_{\text{sca}}{}^* \cdot \mathbf{E}^\sigma_{\text{sca}}} = \frac{|\mathbf{E}^{\sigma+}|^2 - |\mathbf{E}^{\sigma-}|^2}{|\mathbf{E}^{\sigma+}|^2 + |\mathbf{E}^{\sigma-}|^2} = \frac{V}{I}, \tag{67}$$

[13] Rigorously speaking, the restoration of EM duality can only be achieved for magnetic materials when $\epsilon = \mu$. Nonetheless, we will relax this constraint throughout the present Thesis as dielectric nanospheres at the first Kerker condition behave as dual scatterers.

where

$$V = 4\sigma G_0 \left(\left(|\alpha_{\rm E}|^2 + \alpha_{\rm M}|^2 \right) \cos\theta + {\rm Re}\{\alpha_{\rm E}\alpha_{\rm M}^*\} \left(1 + \cos^2\theta\right) \right), \quad (68)$$

$$I = 2G_0 \left(\left(|\alpha_{\rm E}|^2 + \alpha_{\rm M}|^2 \right) \left(1 + \cos^2\theta\right) + 4{\rm Re}\{\alpha_{\rm E}\alpha_{\rm M}^*\} \cos\theta \right), \quad (69)$$

being

$$|\boldsymbol{E}^{\sigma\sigma'}|^2 = G_0 \left(|\alpha_{\rm E}|^2 + \alpha_{\rm M}|^2 + 2\sigma\sigma' \Re e\{\alpha_{\rm E}\alpha_{\rm M}^*\} \right) \left(1 + \cos^2\theta + 2\sigma\sigma' \cos\theta \right). \quad (70)$$

Here $G_0 = |E_0|^2 k^4 / 64\pi^2 r^2$, where E_0 is the incoming electric field's amplitude, $k = 2\pi/\lambda_0$, r is the sphere's radius of observation, $\alpha_{\rm E}$ and $\alpha_{\rm M}$ are the dipolar electric and magnetic polarizabilities, respectively, and θ is the scattering angle. The DoCP, which measures the helicity of the scattered electric field in the far-field limit, namely, the normalized amount of photons carrying opposite helicities at a given θ, is only expressed in terms of V and I. These denote two Stokes parameters which have been extensively analysed in the work by Crichton and Marston[14] [124]. In terms of the g-parameter in the electric and magnetic dipolar regime [87], it can be checked that the DoCP reads as,

$$\Lambda_\theta = \frac{2\sigma \left(\left(1 + \cos^2\theta\right) g + \cos\theta \right)}{1 + \cos^2\theta + 4g\cos\theta}, \quad (71)$$

while its expected value, $\langle\Lambda\rangle$, is given by

$$\langle\Lambda\rangle \equiv \frac{\int \left\{ |\mathbf{E}^{\sigma+}|^2 - |\mathbf{E}^{\sigma-}|^2 \right\} d\Omega}{\int \left\{ |\mathbf{E}^{\sigma+}|^2 + |\mathbf{E}^{\sigma-}|^2 \right\} d\Omega} = 2\sigma g. \quad (72)$$

According to Eq. (71), we can infer that the angular dependence of the DoCP depends on the g-parameter while $\langle\Lambda\rangle$ is, by a factor of 2σ, the g-parameter in the dipolar regime. In Fig. 4.1, we show the DoCP pattern vs. both scattering angle θ and g-parameter for an incoming circularly polarized PW with well-defined EM helicity per photon ($\sigma = +1$). As can be inferred from the plot, the DoCP values are restricted to $-1 < \Lambda \leq 1$, being maximized at the first Kerker condition ($\alpha_{\rm E} = \alpha_{\rm M}$), when the scattering system preserves the EM duality. In addition, we find that the polarization of the scattered light is linear ($\Lambda_{\theta_0} = 0$) when the condition $g = -\cos\theta_0/(1 + \cos^2\theta_0)$ is fulfilled, corresponding to the dashed line in Fig. 4.1. As can be seen, it matches with $\theta_0 = \pi/2$ only for $g = 0$, which corresponds with the pure electric (or magnetic) dipolar case. The relatively simple measurement of the polarization degree at a right-angle scattering configuration provides useful insight into small particles' scattering properties. In particular, the spectral evolution of the DoCP was shown to be

[14] In this work, they show that the DoCP is a measurable physical quantity as it can be unambiguously expressed in terms of Stokes parameters.

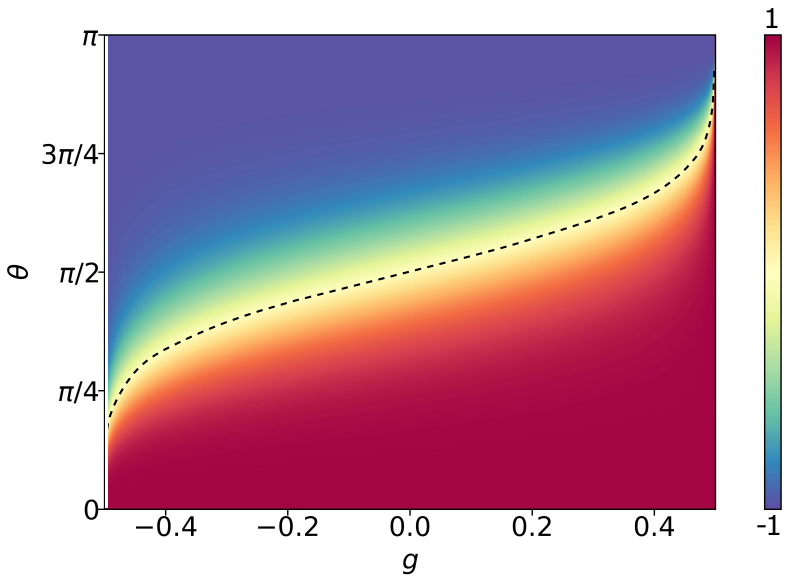

Figure 4.1 – Color map of the DoCP vs the scattering angle θ and the g-parameter. The white vertical line indicates that this set of DoCP values are forbidden due to causality, i.e., $g > -1/2$ (in absence of optical gain) [84]. The first Kerker condition, satisfied for $g = 1/2$, gives raise to the conservation of the DoCP regardless of the scattering angle (intense red-color), being this identical to the incoming EM helicity per photon ($\sigma = +1$). The dashed line illustrates the curve where the scattered light is linearly polarized, $\Lambda_\theta = 0$.

a simple and accurate way to identify electric and magnetic behaviors of the scattered fields [140, 141]. Interestingly, we find that the DoCP, measured at the perpendicular direction to the incoming wave, $\theta = \pi/2$, follows a biunivocal relation with the g-parameter,

$$\Lambda_{\frac{\pi}{2}} = \langle \Lambda \rangle = 2\sigma g. \tag{73}$$

This means that by measuring the DoCP at 90^o degrees, we can directly extract the g-parameter. From this measurement, one can straightforwardly retrieve optical parameters such as the particle size or the index contrast since the g-parameter function of these parameters[15] [38]. The abovementioned is schematically depicted in Fig. 4.2, where a specific example ($g = -0.4$) is depicted.

[15]Note that the abovementioned holds since the g-parameter is a function of the electric and magnetic Mie coefficients.

4.3 Relation between the helicity density and the SOI of light: Role of optical absorption

Once we have a complete description of the angular dependence of the EM helicity density in the FF limit, or in other words, the DoCP, in the electric and magnetic dipolar regime, it is interesting to analyse its relation with the AM exchanges and the optical mirage. Following Crichton and Marston [124], we notice that the z-component of the SAM per scattered photon, $s_z(\theta)$, is a measurable quantity simply related to the DoCP of the scattered light in the FF limit by,

$$s_z = \Lambda_\theta \cos\theta = \frac{2\sigma \cos\theta \left(\left(1+\cos^2\theta\right) g + \cos\theta\right)}{1+\cos^2\theta + 4g\cos\theta}, \tag{74}$$

where Λ_θ is given by Eq. (71).

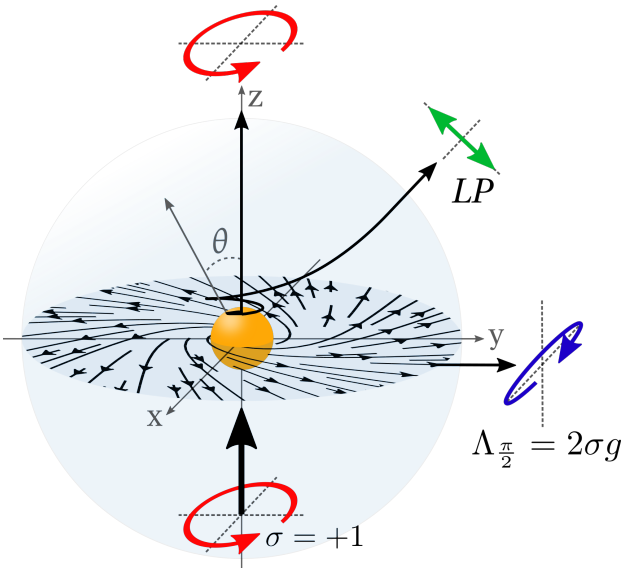

Figure 4.2 – Sketch of the system: PW with well defined EM helicity per photon, preserved in forward scattering, $\sigma = +1$, impinging on a example sphere with $g = -0.4$. The scattered light is shown via the conical trajectories of the Poynting vector. At $\theta = \pi/2$, the single measurement of the DoCP gives the value of the scatterer's g-parameter. Red and blue lines illustrate both the counterclockwise and clockwise polarizations, while the linear polarization (LP) is illustrated in green.

Additionally and as discussed in Chapter 3, due to the axial symmetry of the scatterer, the z-component of the *total* AM of the incoming photons $j_z = \sigma$ is preserved after scattering. Then, the z-component of the OAM per scatterd photon, $\ell_z(\theta)$, can also be related to the DoCP by

$$\ell_z(\theta) \equiv j_z - s_z(\theta) = \sigma - \Lambda_\theta \cos\theta = \sigma \frac{\sin^2\theta\,(1 + 2g\cos\theta)}{1 + \cos^2\theta + 4g\cos\theta}, \tag{75}$$

which allow us to link the optical mirage's apparent shift [5], Δ, with Λ_θ as

$$\frac{\Delta\pi}{\lambda} = \frac{\ell_z(\theta)}{\sin\theta} = \frac{\sigma - \Lambda_\theta\cos\theta}{\sin\theta}. \tag{76}$$

It is important to emphasize that, for electric magnetic dipolar scatterers, the SAM and OAM densities, given by Eqs (74)-(75) are general results, implying that all the optical properties of the nanoparticle, including absorption losses, are encoded in the g-parameter. The presence of absorption losses modifies the relative weight between real and imaginary parts of the electric and magnetic polarizabilities modifying the scattering asymmetry and, consequently, inducing changes in the SOI of the scattered light.
In contrast with the SAM and OAM densities, the expected (angle averaged) values of SAM and OAM do not share this behaviour since,

$$\langle S_z\rangle = \frac{\int_\Omega 2\sigma\cos\theta\left(\left(1+\cos^2\theta\right)g + \cos\theta\right)d\Omega}{\int_\Omega\left(1+\cos^2\theta+4g\cos\theta\right)d\Omega} = \frac{\sigma}{2}, \tag{77}$$

$$\langle L_z\rangle = \sigma\frac{\int_\Omega \sin^2\theta\,(1+2g\cos\theta)\,d\Omega}{\int_\Omega\left(1+\cos^2\theta+4g\cos\theta\right)d\Omega} = \frac{\sigma}{2}, \tag{78}$$

with

$$\langle S_z\rangle + \langle L_z\rangle = \langle J_z\rangle = \sigma. \tag{79}$$

These results agree with those obtained by Crichton and Marston in Ref. [124]. Although the absorption, along with any optical effects contained in the g-parameter, does not contribute to the expectation values of both OAM and SAM contributions in the electric and magnetic dipolar regime, intriguing effects associated with the SOI of light may appear in absorbing targets.
Figure 4.3 summarizes the re-distribution of the AM into OAM and SAM contributions per photon for a 55 nm Si sphere in the visible spectral range. This is calculated from Eqs (74)-(75) when impinging with a circularly polarized PW with well-defined EM helicity per photon ($\sigma = 1$). Figure 4.3(a) illustrates the g-parameter as a function of the incident wavelength, λ. As is depicted, the maximum value, $g = 1/2$, is not reached due to the fact that the absorption precludes the emergence of the first Kerker condition[16], $\alpha_{\mathrm{E}} \neq \alpha_{\mathrm{M}}$.

[16] A rigorous mathematical demonstration is given for the first time in Chapter 5.

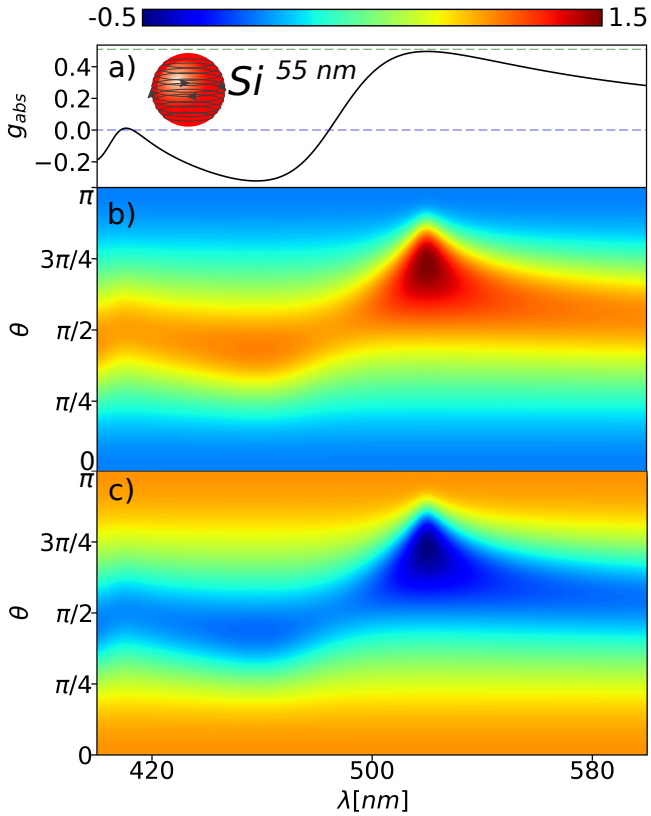

Figure 4.3 – (a) g-parameter as a function of the incident wavelength, λ, in the visible spectral range, for a 55 nm Si sphere in the electric and magnetic dipolar regime. (b)-(c) Distributions of OAM and SAM per photon, respectively, as a function of the scattering angle, and λ.

Nevertheless, as it tends to be preserved, $\Lambda_\theta \lesssim 1 \Longleftrightarrow g \lesssim 0.5$, the OAM per photon (Fig. 4.3(b)), reaches values that exceed the incident AM per photon in the incident direction, $\ell_z > j_z$. This phenomenon, previously referred to as "supermomentum" for absorptionless spheres [47, 49, 51], emerges as a simple consequence of the conservation of the AM per photon: according to Eq. (74), $-1 < s_z < 1$, and since the AM per photon must be conserved after scattering, the OAM per photon can acquire larger values than the incident AM per photon, since $\ell_z + s_z = 1$. It is important to notice that the roll of loss via absorption effects inhibits the full AM-exchange ($\ell_z^{\max} = 2$) since the EM helicity cannot be preserved, $\Lambda_\theta \lesssim 1$. This can be checked in the attached color map, where $\ell_z^{\max} = 1.5$.

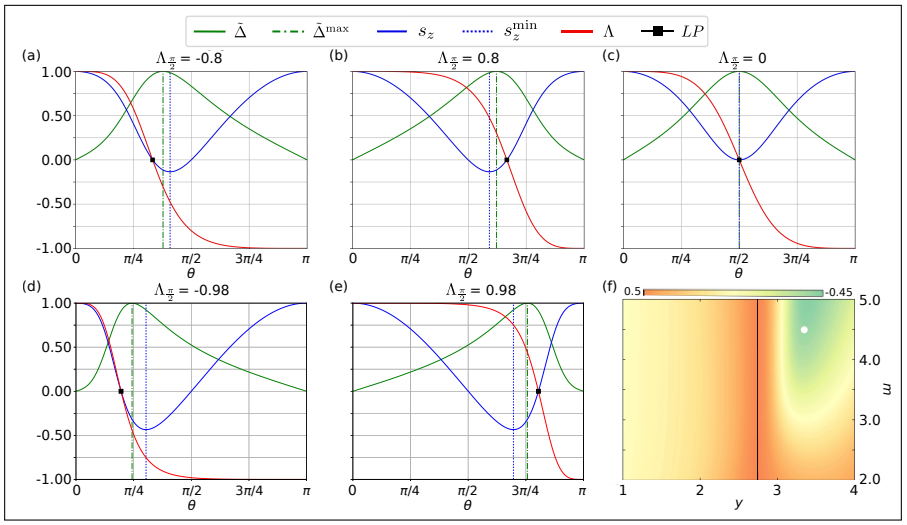

Figure 4.4 – Normalized optical mirage $\tilde{\Delta} = \Delta/\tilde{\Delta}^{\max}$, spin density ($s_z$) and DoCP ($\Lambda$) vs the scattering angle θ for an incoming circularly polarized PW of EM helicity per photon, $\sigma = +1$. The green vertical dashed-dotted lines represent the angles corresponding to the maximum of optical mirage, $\tilde{\Delta}^{\max}$. Blue dotted lines correspond to the angles at which spin-to-orbit angular momentum transfer is maximum (or minimum value of the z-component of SAM per scattered photon, $s_z^{\min}$). The black squares indicate $\Lambda_\theta = 0$, namely, the (FF) observation angles at which light is linearly polarized (LP). (a) and (b) correspond to $\Lambda_{\pi/2} = -0.8$ and $\Lambda_{\pi/2} = +0.8$ (i.e. $g = -0.4$ and $g = +0.4$), respectively. As it can be seen, for $g \neq 0$, $\tilde{\Delta}^{\max}$, $s_z^{\min}$ and LP are localized in three different scattering angles, In contrast with the $g = 0$ case (c) where they all collapse at right scattering angles $\theta = \pi/2$. (d) and (e) show the different angular dependence as the g-parameter approaches the second ($\Lambda_{\pi/2} = -0.98 \gtrsim -1$) and first ($\Lambda_{\pi/2} = 0.98 \lesssim 1$) Kerker conditions, respectively. (f) reproduces the g-parameter for isotropic spheres as a function of their refractive index m and size parameter $y = mka$ in the electric and magnetic dipolar regime (after Ref. [87]). Black vertical line indicates the first Kerker condition, where $\alpha_{\mathrm{E}} = \alpha_{\mathrm{M}}$. The solid white point highlights $g = -0.4$ which corresponds to both a high refractive index (HRI) dielectric sphere or to a small perfectly conducting sphere [118]. Both subwavelength particles will give rise to exactly the same spin-orbit coupling effects.

4.4 Discussion of optical mirage, SAM, OAM and EM helicity densities vs the scattering angle

Equations 62, 71, 74, 75 and 76 reflect the remarkable result that intensity, DoCP, SAM and OAM of scattered photons and the *optical mirage* ($\mathrm{d}\sigma_{\mathrm{scatt}}/\mathrm{d}\Omega$, Λ_θ, s_z, ℓ_z and Δ) are all linked and fully determined, by the dimensionless g-parameter, being independent of the specific optical properties of the scatterer. This finding is the most important result of the present work: within a single measurement of the DoCP at $\pi/2$ via polarization filters in the FF, we can extract the g-parameter and infer the angular dependence of all the above-mentioned scattering quantities. Moreover, within a single measurement, one could extract the average of the particle sizes of a colloidal suspension or the refractive index of single spheres since the g-parameter is a function of these optical properties.
Figure 4.4 illustrates the AM exchange and the *optical mirage* dependence with the FF observation angle θ for an incoming PW with an EM helicity per photon $\sigma = +1$ and total z-component of the total AM per photon $j_z = \sigma$. Figures 4.4 (a) and 4.4 (b) summarize the results for $g = -0.4$ and $g = 0.4$, respectively. In contrast with pure electric (or pure magnetic) dipolar particles with symmetric scattering ($g = 0$, Fig. 4.4 (c)), the maximum AM exchange (corresponding to the minimum of s_z) and the maximum *optical mirage*, $\tilde{\Delta} = \Delta/\Delta_{\max}$, take place at different scattering angles but in an angular region in which the z-component of the SAM is negative (i.e. where the photons are not linearly polarized) while the z-component of the OAM is larger than that of the total AM ($\ell_z = j_z - s_z > j_z = 1$). The equivalent effect happens for $\sigma = -1$. The angular gaps between the minimum of the z-component of the SAM (maximum AM exchange), the maximum of the optical mirage effect and the angle at which light is linearly polarized first increase when the g-parameter tends to the second or first Kerker conditions, $|g| \approx 0.5$, as it can be seen in Figs. 4.4(d) and 4.4(e). However, in the limit of dual scatterers ($g = +0.5$) $s_z \to \cos\theta$ and $\Lambda_\theta \to +1$, and the extrema collapse again at the singular back scattering angle $\theta = \pi$. At this condition, there is a divergent optical mirage at back scattering associated to the appearance of an optical vortex with $s_z = -1$ and $\ell_z = 2$ [5]. In contrast, in absence of gain, the Optical Theorem imposes that the limit of $g = -0.5$ is unreachable [84] which inhibits the complete (flipping) transformation from $s_z = \sigma$ to $s_z = -\sigma$, although a huge enhancement of the optical mirage is predictable getting close to this condition. Based on the aforementioned, in analogy with dual spheres, we can predict that an anti-dual sphere -that could be made with a material with gain- [4], with $g = -0.5$, would generate a perfect optical vortex in the forward direction with a divergent optical mirage.

4.5 Conclusions

In this Chapter we have shown that the scattered intensity of light, DoCP after scattering, SOI of light densities (SAM and OAM), and the optical mirage are entirely determined by the dimensionless g-parameter in the electric and magnetic dipolar regime. As a result, nanospheres with completely different optical properties (such as size, refractive index) but sharing an identical g parameter value will lead to the same angular dependencies of the intensity, DoCP, SAM to OAM exchanges, and optical mirage apparent shifts. Since the g-parameter can be obtained from a far-field measurement of the DoCP, our results predict the possibility of determining all angular dependences of the scattering coefficients from a single polarization measurement, and therefore we believe that our work open new perspectives in Optics and Photonics, including antennas engineering, metamaterials, nanophotonics, and optical imaging.

CHAPTER 5

Kerker conditions in lossless, absorption, and optical gain regimes

5.1 Introduction

In this Chapter, we analytically demonstrate in Sec. 5.2 that either losses or optical gain inhibit the first Kerker condition for homogeneous dielectric Mie spheres with $\mu = 1$. As a result, we show that the g-parameter cannot be maximized in the electric and magnetic dipolar regime, as numerically shown in Chapter 4. The abovementioned unveils a hidden connection between energy conservation and the first Kerker condition, regardless of the particle's size, incident wavelength, and incoming polarization. Interestingly, our proof does not depend on the multipole order or the incoming wave's nature; therefore, it is a fundamental property of the Mie coefficients. We show in Sec. 5.3 that neither the EM helicity can be preserved after scattering for lossy spheres. As a result, the zero optical backscattering condition can be neither be perfectly fulfilled in the dipolar regime under PW illumination. In particular, for a Germanium (Ge) sphere in the dipolar regime, we quantify the gradual drift from the ideal zero optical backscattering condition as the absorption rate is increased. Moreover, we show in Sec. 5.4 that optical gain is a compulsory requirement to satisfy the zero forward light scattering condition.

5.2 A fundamental property of the Mie theory

Mie theory [9] gives an exact solution of Maxwell's equations for a spherical particle in a non-dispersive homogeneous medium under PW illumination. It allows writing the extinction, scattering, and absorbing efficiencies of the particle as

$$Q_{\text{ext}} = \frac{2}{x^2}\sum_{l=1}^{\infty}(2l+1)\,\text{Re}\{a_l + b_l\} = \sum_{l=1}^{\infty}\left(Q_{\text{ext}}^{a_l} + Q_{\text{ext}}^{b_l}\right), \tag{80}$$

$$Q_{\text{sca}} = \frac{2}{x^2}\sum_{l=1}^{\infty}(2l+1)\left(|a_l|^2 + |b_l|^2\right) = \sum_{l=1}^{\infty}\left(Q_{\text{sca}}^{a_l} + Q_{\text{sca}}^{b_l}\right), \tag{81}$$

where $Q_{\text{abs}} = Q_{\text{ext}} - Q_{\text{sca}}$.
The efficiencies are dimensionless magnitudes given by the ratio between the cross-section and the geometrical area, $Q = \sigma/\pi R^2$, where R is the radius of the sphere. Here, $x = kR$ is the size parameter, $k = \text{m}_\text{h}k_0 = \text{m}_\text{h}\,(2\pi)/\lambda_0$, λ_0 being the wavelength in vacuum and $\text{m} = \text{m}_\text{p}/\text{m}_\text{h}$ is the contrast index, where m_p is the refractive index of the particle and m_h is the refractive index of the external medium. The Mie coefficients, a_l and b_l, can be expressed in terms of the scattering phase-shifts [9] by,

$$a_l = \sin\alpha_l e^{-\text{i}\alpha_l} \qquad\qquad b_l = \sin\beta_l e^{-\text{i}\beta_l} \tag{82}$$

where

$$\tan\alpha_l = -\frac{S_l'(\text{m}x)S_l(x) - \text{m}S_l(\text{m}x)S_l'(x)}{S_l'(\text{m}x)C_l(x) - \text{m}S_l(\text{m}x)C_l'(x)}, \tag{83}$$

and

$$\tan\beta_l = -\frac{\text{m}S_l'(\text{m}x)S_l(x) - S_l(\text{m}x)S_l'(x)}{\text{m}S_l'(\text{m}x)C_l(x) - S_l(\text{m}x)C_l'(x)}. \tag{84}$$

Here $S_l(z) = \sqrt{\frac{\pi z}{2}}J_{l+\frac{1}{2}}(z)$ and $C_l(z) = \sqrt{\frac{\pi z}{2}}N_{l+\frac{1}{2}}(z)$ are the Riccati-Bessel functions, where $J_{l+\frac{1}{2}}(z)$ and $N_{l+\frac{1}{2}}(z)$ are the Bessel and Neumann functions, respectively.
For non-dissipative targets, where $\text{m} \in \mathbb{R}$, and according to Eq. (82), the electric and magnetic scattering phase-shifts, α_l and β_l, respectively, are real. In this lossless regime and as a result of the optical theorem [9], the scattering and extinction efficiencies are identical, i.e., $Q_{\text{ext}} = Q_{\text{sca}}$ with $Q_{\text{abs}} = 0$. According to Eqs. (83) and (84) and as briefly introduced in Chapter 2, the first Kerker condition, in which the electric and magnetic dipolar modes oscillate *in-phase* with identical amplitude, can be obtained either when $S_1(\text{m}x) = 0$ (nodes of first kind) or when $S_1'(\text{m}x) = 0$ (nodes of second kind) [9]. However, for complex values of the refractive index contrast, i.e., $\Im\{\text{m}\} \neq 0$, which corresponds either with absorption ($\Im\{\text{m}\} > 0$) or active media ($\Im\{\text{m}\} < 0$), these nodes are unreachable. To prove it, let us make use of the following Lemmas,

1. When $v > -1$ the zeros of $J_v(z)$ are all real [142],

2. When $v > -1$ and $a, b \in \mathbb{R}$, then $aJ_v(z) + bzJ'_v(z)$ has all its zeros real, except when $a/b + v < 0$ [142].

From Lemma 1, it is noticeable that the node of the first kind, $S_l(\mathrm{m}x) = 0$, is inhibited for either absorbing or optical gaining homogeneous dielectric Mie spheres with $\mu = 1$ since the zeros of the Bessel functions are all real. On the other hand, the node of second kind, given by

$$S'_l(\mathrm{m}x) = J_{l+\frac{1}{2}}(\mathrm{m}x) + 2\mathrm{m}x\ J'_{l+\frac{1}{2}}(\mathrm{m}x) = 0, \tag{85}$$

corresponds to the function of Lemma 2 with $a = 1$, $b = 2$, and $v = l + 1/2$. Therefore, Eq. (85) cannot be satisfied for $\Im\{\mathrm{m}\} \neq 0$ since the condition $a/b + v < 0$ is inaccessible for homogeneous dielectric Mie spheres with $\mu = 1$, according to Mie theory ($l \geq 1$) [9].

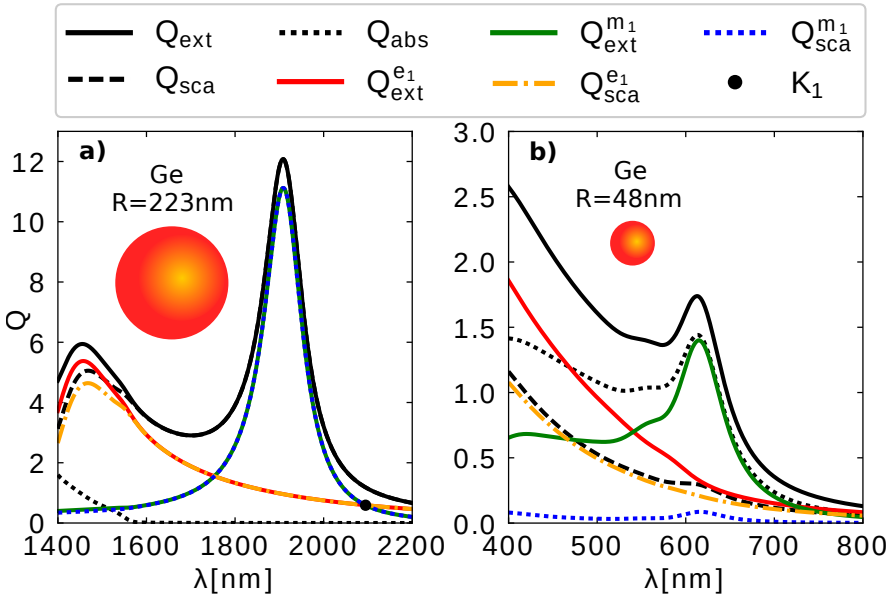

Figure 5.1 – Extinction, scattering, and absorbing efficiencies from the scattering by 223 and 48 nm Ge spheres in the telecom and visible spectral range, respectively. The electric (e) and magnetic (m) dipolar ($l = 1$) contribution is depicted for the extinction and scattering efficiencies. The first Kerker condition (K_1) arises for the non-absorbing sphere (a) while it is not met for the lossy one (b).

The immediate physical consequence of these Lemmas is straightforward: either absorption or optical gain inhibits the emergence of the first Kerker condition. It is important to note that these calculations' validity holds regardless of the particle size, incident wavelength, refractive index contrast, and the incoming light's polarization. Remarkably, this result is valid for any multipole order l. In short, we can conclude that $a_l \neq b_l \; \forall \, l$ whereas $\Im\{\mathrm{m}\} \neq 0$, making this demonstration general.
Interestingly, the breaking of the emergence of the first Kerker condition can be understood through the extinction and scattering efficiencies arising from electric and magnetic modes. Indeed, in the presence of losses or active media, the extinction and scattering efficiencies arising from an arbitrary electric multipole l cannot be identical to the magnetic counterpart emerging from the same multipole l. According to the right side of Eqs. (80) and (81), this phenomenon can be encompassed as following: if $Q^{a_l}_{\mathrm{sca}} = Q^{b_l}_{\mathrm{sca}}$ then $Q^{a_l}_{\mathrm{ext}} \neq Q^{b_l}_{\mathrm{ext}}$ for $\Im\{\mathrm{m}\} \neq 0$. These relations imply that the electric and magnetic modes cannot *simultaneously* oscillate in-phase with equal amplitude, circumstance that can occur for lossless spheres, as can be inferred from Fig. 5.1.
Figure 5.1a) illustrates the extinction, scattering, and absorbing efficiencies versus the incident wavelength for a 223 nm Ge sphere in the telecom spectral range, where losses are negligible. As can be inferred, the first Kerker condition (black circle) arises at $\lambda \approx 2100$ nm. In contrast and as previously discussed, for a 48 nm Ge sphere in the visible spectral range, where losses become considerable, the electric and magnetic modes do not *simultaneously* oscillate in-phase with equal amplitude, precluding the first Kerker condition.

5.3 Absorption inhibits the conservation of helicity

To get a more in-depth insight into these results, based on the first Kerker condition breaking, let us calculate EM helicity's expected value after scattering. The scattered fields outside the sphere, in a well-defined EM helicity decomposition [143], i.e., $\mathbf{E}_{\mathrm{sca}} = \mathbf{E}^{+}_{\mathrm{sca}} + \mathbf{E}^{-}_{\mathrm{sca}}$ with $\mathbf{\Lambda}\mathbf{E}^{\sigma}_{\mathrm{sca}} = \sigma \mathbf{E}^{\sigma}_{\mathrm{sca}}$, can be written, as illustrated in the previous Chapters, in terms of "outgoing" VSWFs, $\mathbf{\Phi}^{\sigma'}_{lm}$ (defined in [5]) as

$$\mathbf{E}^{\sigma}_{\mathrm{sca}} = E_0 \sum_{l=1}^{\infty} \sum_{m=-l}^{+l} D^{\sigma}_{lm} \mathbf{\Phi}^{\sigma}_{lm}, \tag{86}$$

$$\begin{pmatrix} D^{+}_{lm} \\ D^{-}_{lm} \end{pmatrix} = -\begin{pmatrix} [a_l + b_l] & [a_l - b_l] \\ [a_l - b_l] & [a_l + b_l] \end{pmatrix} \begin{pmatrix} C^{+}_{lm} \\ C^{-}_{lm} \end{pmatrix}, \tag{87}$$

$$Z\mathbf{H}^{\sigma}_{\mathrm{sca}} = -\mathrm{i}\mathbf{\Lambda}\mathbf{E}^{\sigma}_{\mathrm{sca}}, \tag{88}$$

where $C^{\sigma\sigma'}_{lm}$ are the coefficients of the incoming wave.

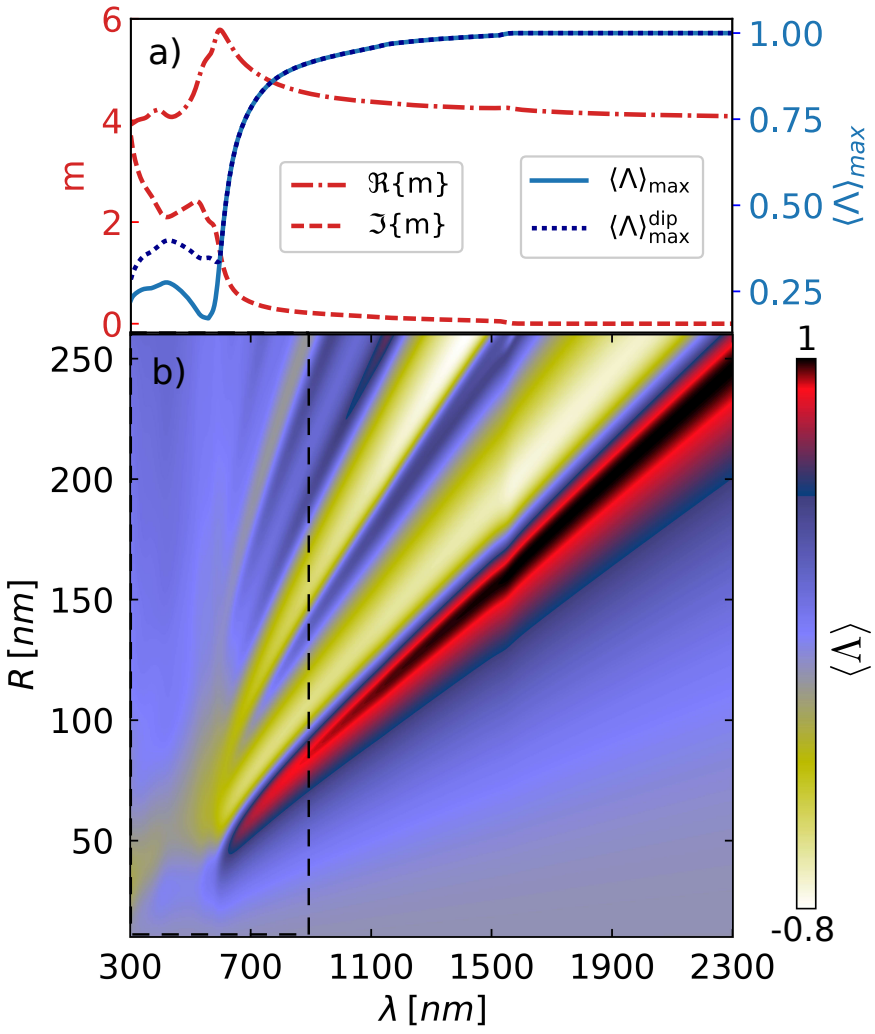

Figure 5.2 – (a) Real (dash-dotted red) and imaginary part (dashed-red) of the refractive index contrast (m) vs the incident wavelength (λ) for a Ge sphere. Maximum value of the expected value of the EM helicity in solid-blue, $\langle\Lambda\rangle_{max}$, for a Ge sphere vs λ under plane wave illumination with $\sigma = +1$. (b) Color map of $\langle\Lambda\rangle$ vs λ and particle's size (R) for a Ge sphere under plane wave illumination with $\sigma = +1$. The visible range is encompassed by a dashed rectangle, where $\langle\Lambda\rangle < 1$.

The expected value of the EM helicity of the scattered field is given by

$$\langle \Lambda_{\text{sca}} \rangle = \langle \Lambda \rangle = \frac{\langle \mathbf{E}^{\sigma}_{\text{sca}}{}^{*} \cdot (\mathbf{\Lambda} \mathbf{E}^{\sigma}_{\text{sca}}) \rangle}{\langle \mathbf{E}^{\sigma}_{\text{sca}}{}^{*} \cdot \mathbf{E}^{\sigma}_{\text{sca}} \rangle} = \frac{\sum_{l=1}^{\infty} \sum_{m=-l}^{+l} |D^{+}_{lm}|^2 - |D^{-}_{lm}|^2}{\sum_{l=1}^{\infty} \sum_{m=-l}^{+l} |D^{+}_{lm}|^2 + |D^{-}_{lm}|^2}. \tag{89}$$

Under illumination by a circularly polarized PW with well-defined helicity and AM ($m = \sigma = \pm 1$), $\langle \Lambda \rangle$ can be derived as [10]

$$\langle \Lambda \rangle = \frac{\int \mathbf{E}^{\sigma}_{\text{sca}}{}^{*} \cdot \mathbf{\Lambda} \mathbf{E}^{\sigma}_{\text{sca}} \, d\Omega}{\int \mathbf{E}^{\sigma}_{\text{sca}}{}^{*} \cdot \mathbf{E}^{\sigma}_{\text{sca}} \, d\Omega} = 2\sigma \left[\frac{\sum_{l=1}^{\infty} (2l+1) \, \text{Re}\{a_l b_l^{*}\}}{\sum_{l=1}^{\infty} (2l+1) \, |a_l|^2 + |b_l|^2} \right]. \tag{90}$$

From Eq. (90) it is straightforward to notice that for either losses or optical gain regimes, where the inequality $a_l \neq b_l \; \forall l$ holds, the EM helicity is not preserved, namely, $|\langle \Lambda \rangle| < 1$. Figure 5.2 summarizes most of the quantitative insights about the previous property for a Germanium (Ge) sphere. For $\Im\{\text{m}\} > 0$, corresponding to the visible spectral range (see Fig. 5.2a)), the maximum value of the EM helicity, $\langle \Lambda \rangle_{\text{max}}$, is far from being preserved, regardless of the size of the Ge sphere in the entire visible spectral range which corresponds to the dashed rectangle in Fig. 5.2b). Contrary, in the telecom spectral range, where losses are negligible (see Fig. 5.2a)), the maximum value of the EM helicity is essentially dipolar, namely, $\langle \Lambda \rangle_{\text{max}} = \langle \Lambda \rangle^{\text{dip}}_{\text{max}}$, being this preserved at the first Kerker condition. This conservation can be inferred from $\langle \Lambda \rangle_{\text{max}} \approx 1$ in Fig. 5.2a), which corresponds to the intense black region arising in Fig. 5.2b)). To get insights into the relevance of the first Kerker condition breaking due to absorption effects in the scattering radiation pattern, let us consider the normalized-differential scattering cross-section, introduced in Chapter 2, particularly in Sec. 2.5.

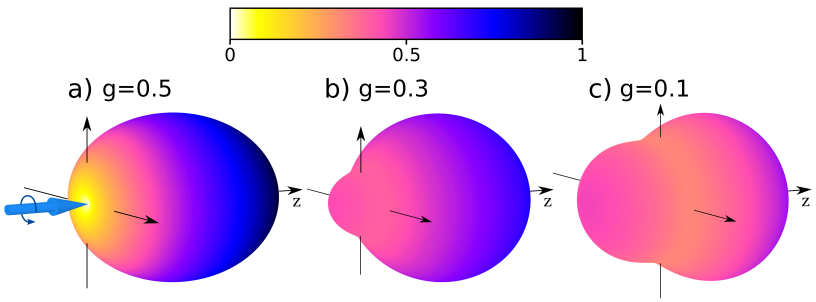

Figure 5.3 – Normalized scattering patterns by Ge spheres calculated from Eq. (91) in the telecom spectral regime (a) [$\lambda = 2100$ nm and $R = 223$ nm] and visible spectral range (b) [$\lambda = 632$ nm and $R = 48$ nm] and (c) [$\lambda = 575$ nm and $R = 35$ nm]. The g-parameter is given by $g = 0.5, 0.3, 0.1$, respectively, in the dipolar regime.

In the electric and magnetic dipolar regime [6], it can be shown that this magnitude reads as[17]

$$\frac{1}{\sigma_{\text{sca}}}\frac{\mathrm{d}\sigma_{\text{sca}}}{\mathrm{d}\Omega} = \frac{3}{8\pi}\left(\frac{1+\cos^2\theta}{2} + 2g\cos\theta\right), \qquad \text{with} \qquad \langle\Lambda\rangle = 2\sigma g, \tag{91}$$

where g is the asymmetry parameter in the dipolar regime [87].
From the right side of Eq. (91), it is noticeable that at the first Kerker condition, when the EM helicity is preserved, the g-parameter is maximized in the dipolar regime, i.e., $g = 0.5$. In this scenario, it can be inferred from the left part of Eq. (91) that there is no light radiation in the backscattering direction ($\theta = \pi$) [65–67]. However, in the presence of losses or optical gain, the zero optical backscattering condition cannot emerge in the dipolar regime due to the first Kerker condition breaking that imposes both $g < 0.5$ and $|\Lambda| < 1$.
As an illustrative example, we show in Fig. 5.3 the gradual loss of the zero optical backscattering condition (see Fig. 5.3a)), as the absorption rate is increased for a Ge sphere (see Fig. 5.3b) and Fig. 5.3c)). Consciously, Fig. 5.3a) illustrates the first Kerker condition depicted in Fig. 5.1a)) while Fig. 5.3b)) represents the maximum value of g (not the first Kerker condition) for Fig. 5.2b)). As can be inferred, the zero optical backscattering condition is lost for lossy spheres.

5.4 Optical Gain and second Kerker condition

Finally, let us briefly analyse the second Kerker condition, given by $a_1 = -b_1$. Let us recall that at this dipolar optical response, the EM helicity flips its value from $\langle\Lambda\rangle = +\sigma$ to $\langle\Lambda\rangle = -\sigma$, according to Eq. (90), and the g-parameter is minimized, $g = -0.5$, leading to the zero optical scattering condition in the forward direction (see Eq. (91)). According to Eq. (82), the second Kerker condition implies both

$$\sin 2\alpha_1 = -\sin 2\beta_1 \qquad \text{and} \qquad \sin^2\alpha_1 = -\sin^2\beta_1. \tag{92}$$

It is straightforward to notice that lossless spheres, where $\Im\{\mathrm{m}\} = 0$, cannot satisfy the second Kerker condition since in that scenario $\alpha_l, \beta_l \in \mathbb{R}$ and then, the right side of Eq. (92) is unreachable. In contrast, it can be achieved for active media, i.e., $\Im\{\mathrm{m}\} < 0$ as we can infer from Fig. 5.4.
Figure 5.4 illustrates the g-parameter for a Ge-like sphere ($m = 4$) versus the size parameter, $x = kR$, and the imaginary part of the refractive index contrast, $\Im\{\mathrm{m}\}$, under a plane wave with well-defined helicity ($\sigma = +1$). In this regime, the optical response is almost entirely dipolar and, as a result, the

[17] This magnitude can be found in Chapter 3, specifically in Sec. 3.3.

g-parameter is the same magnitude as the expected value of the EM helicity, $\langle\Lambda\rangle = 2g$, according to the right side of Eq. (91). As previously mentioned, the first Kerker condition ($a_1 = b_1$) arises in a lossless regime ($\Im\{\mathrm{m}\} = 0$) at $x \sim 0.675$. This specific size parameter corresponds to the first Kerker condition appearing on Fig. 5.1a) and Fig. 5.3a). As expected, the first Kerker condition does not emerge for $\Im\{\mathrm{m}\} \neq 0$. On the other hand, the second Kerker condition does not appear for $\Im\{\mathrm{m}\} = 0$, according to Eq. (92). In fact, it arises if and only if optical gain is being pumped onto the system, e.g., in the particular case of the Ge-like sphere, it emerges for $\Im\{\mathrm{m}\} \sim -0.3$ and $x \sim 0.825$, as can be reckoned from Fig. 5.4.

Let us now recall that in the far field the EM helicity density and the SAM and OAM densities can be related as $s_z = \Lambda_\theta \cos\theta$ and $\ell_z = \sigma - \Lambda_\theta \cos\theta$ [54]. These expressions imply that in the presence of losses or optical gain, the emerging optical vortex along the backscattering direction with topological charge $\ell_z = 2\sigma$ is broken [144]. As a consequence, the optical mirage, given by the simple relation $|\Delta_\theta| = \ell_z / \sin\theta$ [5], does not fully diverge in the backscattering direction.

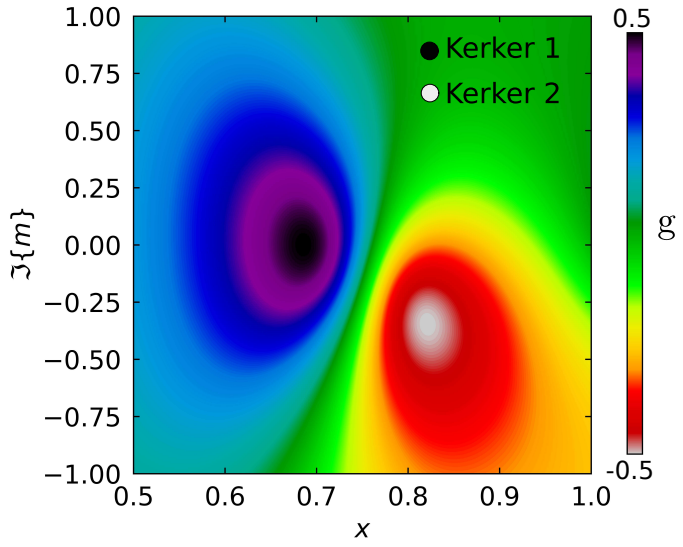

Figure 5.4 – g-parameter vs the imaginary part of the refractive index contrast, $\Im\{\mathrm{m}\}$ and the $x = ka$ size parameter under well-defined EM helicity ($\sigma = +1$) plane wave illumination. In this range, the optical response is purely of dipolar nature. The first and second Kerker conditions are depicted by black and white circles, respectively.

This phenomenon can be then summarized as

$$\Im\{m\} \neq 0 \qquad \Longleftrightarrow \qquad \ell_z < 2\sigma \qquad \Longleftrightarrow \qquad |\Delta_\pi| < \infty. \tag{93}$$

5.5 Conclusions

We have rigorously demonstrated that either losses or optical gain inhibit the first Kerker condition's appearance for dielectric spheres. As a direct consequence of our analysis, we have shown that the EM duality restoration, identified through the conservation of the EM helicity, cannot be achieved in the presence of losses. Furthermore, we have studied the gradual loss of the zero optical backscattering condition for a Ge sphere as the absorption is increased. Furthermore, we have determined the conditions under which the second Kerker condition emerges and, therefore, the zero forward optical scattering condition is met. The abovementioned statements can be summarized as follows: for the imaginary part of the contrast index $\Im\{\mathrm{m}\} \neq 0$, while the second Kerker condition is achievable, the first Kerker condition is inhibited. In this scenario, the zero optical forward light scattering can be achieved in the presence of optical gain. In contrast, for $\Im\{\mathrm{m}\} = 0$, the first Kerker condition is obtainable while the second Kerker condition is unreachable. In this case, only the zero optical backscattering condition is reachable. Our straightforward but fundamental analysis unveils an intriguing connection between the Kerker conditions and energy conservation, opening new insights into the Mie theory.

CHAPTER 6

Optimal backward light scattering by dipolar particles

6.1 Introduction

In Chapter 5, particularly in Sec. 5.4, we have demonstrated that optical gain ($\Im\{\mathrm{m}\} < 0$) is a compulsory requirement to satisfy the zero light-scattering condition in the forward direction. We have explicitly shown that the second Kerker condition, given by $a_1 = -b_1$, can be satisfied in this scenario. However, in the absence of optical gain, the second Kerker condition is precluded by the optical theorem. As an alternative definition, we can consider the generalized second Kerker condition (GSKC) [23], $\alpha_1 = -\beta_1$, corresponding to crossed electric and magnetic dipoles of equal amplitude oscillating in *anti-phase*. Strong suppression of forwarding scattering was already experimentally observed in the microwave regime at this condition [65], in agreement with the near-zero-forward intensity condition for Rayleigh particles [23, 84]. Controlling the directionality of light is an important issue in light transport and scattering in nanostructured complex media [68, 87–95], is also relevant in the discussion of the so-called anapole modes [27, 69, 101], as well as in the context of optical forces [22, 25, 139, 145, 146]. In most of the works mentioned above, the equivalence between the GSKC and the near zero-forward condition was presupposed even though it was only formally demonstrated in the Rayleigh limit, where the particle's scattering cross sections are very small.

This Chapter demonstrates that the GSKC for dipolar particles can be formally derived as the optimal combination of electric and magnetic dipolar responses leading to maximum backward scattered intensities *for a fixed scattering cross section* in the absence of optical gain. The optimal backward scattering takes place at $\alpha_1 = -\beta_1$ (i.e., the GSKC), but, interestingly, it does not lead to the near-zero optical forward condition for strong scattering regimes. Our results reveal that, in the dipolar regime, the GSKC straightforwardly returns the minimum g-parameter for a fixed scattering cross-section in the absence of optical gain. However, the g-parameter is not always negative at the GSKC. As a result, the differential scattering cross-section or, in other words, the re-distribution of energy in the FF limit, ranges all possible scattering angle diagrams, in striking contrast to the current state of the art. In particular, our results provide a consistent explanation of the intriguing exception for zero-forward scattering predicted for small, $\epsilon = \mu = -2$, magnetic particles [83]: when the scattering cross-section approaches its maximum value (when the electric and magnetic dipolar resonances are excited simultaneously), the differential scattering cross-section resembles the one given by the first Kerker condition, in opposition to the physical insight given thus far.

6.2 Role of the GSKC in the g-parameter

The EM fields scattered by HRI dielectric nanoparticles present unique properties from the interference between the electric and magnetic multipoles. As introduced in Chapter 2 and as discussed in the previous chapters, most of them are embedded in the g-parameter. For electric and magnetic dipolar spheres, it is easy to show that the g-parameter and the scattering cross section read in terms of the electric and magnetic scattering phase-shifts as [8]

$$g = \frac{\sin\alpha_1 \sin\beta_1 \cos\left(\alpha_1 - \beta_1\right)}{\sin^2\alpha_1 + \sin^2\beta_1}, \tag{94}$$

$$\sigma_{\text{sca}} = \frac{6\pi}{k^2}\left(\sin^2\alpha_1 + \sin^2\beta_1\right). \tag{95}$$

The GSKC was proposed by Nieto-Vesperinas *et al.*: $\alpha_1 = -\beta_1$ [23]. So far, this was thought to be the optimized condition that gives rise to a negative g-parameter, which in turn might reduce the scattered light in the forward direction [147]. Surprisingly, it is straightforward to notice via Eq. (94) that the GSKC ($\alpha_1 = -\beta_1$) does not (generally) lead to a negative g-parameter,

$$g = \frac{1}{2}\left[\frac{k^2}{6\pi}\sigma_{\text{sca}}^{K_2} - 1\right], \tag{96}$$

where $\sigma_{\text{sca}}^{K_2} = (12\pi/k^2)\sin^2\alpha_1$, according to Eq. (95).

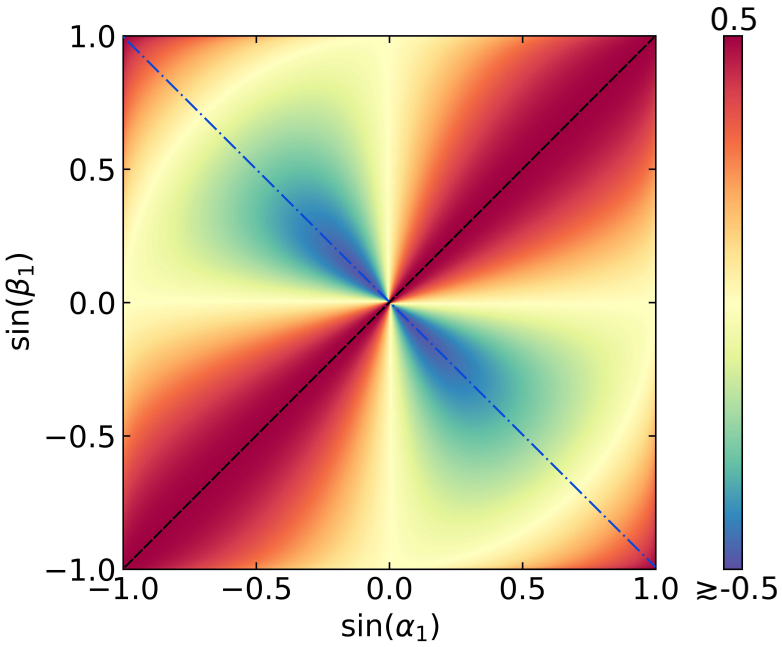

Figure 6.1 – g-parameter as a function of the dipolar electric and magnetic scattering phase-shifts, α_1 and β_1, respectively. The first Kerker condition ($\alpha_1 = \beta_1$) is depicted by a black dashed line. The GSKC ($\alpha_1 = -\beta_1$) is illustrated by a blue dash-dotted line.

This is the first significant result of the present Chapter. As can be seen from Eqs. (95) and (96), only a relatively weak scattering leads to negative values of the g-parameter. The threshold, i.e., $g = 0$, is given by $\pm\alpha_1 = \mp\beta_1 = \pi/4$. Interestingly, this value corresponds to the scattering cross section that arises from a pure dipolar electric (or magnetic) resonant particle, $\sigma_{\text{sca}}^{\text{res}} = 6\pi/k^2$. This phenomenology can be inferred from Fig. 6.1, where the g-parameter is illustrated as a function of the dipolar electric and magnetic scattering phase-shifts. Notice that Fig. 6.1 covers all possible optical responses in the dipolar regime as they run over all possible values of the first electric and magnetic Mie coefficients, according to Eq. (82). As predicted, the first Kerker condition ($\alpha_1 = \beta_1$) gives rise to the maximum value of the g-parameter, $g = 0.5$. Besides, this is completely independent of the scattering cross-section, σ_{sca}, which would correspond to circles in the figure, according to Eq. (95). Interestingly, it can be inferred that the GSKC, $\alpha_1 = -\beta_1$, minimizes the g-parameter for a fixed scattering cross-section. However, this is not sufficient to state that this condition always leads to negative values of the g-parameter.

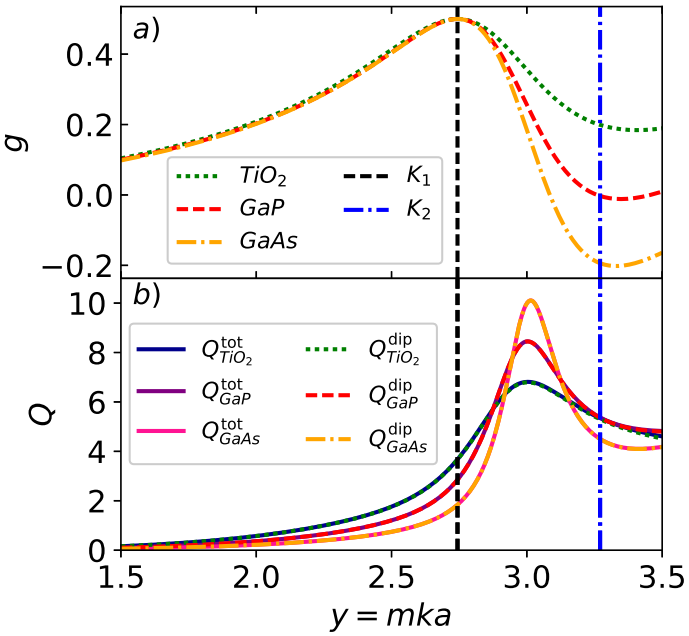

Figure 6.2 – (a) g-parameter as a function of the $y = \text{mka}$ size parameter. The black dashed and blue dash-dotted lines specify the first Kerker and the GSKCs, respectively. (b) Scattering efficiencies arising from both a dipolar and a fully multipolar optical response.

As an illustrative example that confirms the previous statement, the g-parameter is considered for three spheres of different materials, Titanium Oxide-like (TiO_2, m = 2.6), Gallium Phosphide-like (GaP, m = 3.1) and Gallium Arsenide-like (GaAs, m = 3.6) in air, as can be seen in Fig. 6.2a). Refractive index data for these materials were taken from [148]. This figure shows that, at the first Kerker condition, $\alpha_1 = \beta_1$, the maximum value of the asymmetry is always reached (dashed vertical black line). On the other hand, at the GSKC, $\alpha_1 = -\beta_1$, which corresponds to the dash-dotted vertical blue line, the g-parameter is not always negative. The g-parameter is positive for the TiO_2-like sphere, almost zero for the GaP-like sphere case while it becomes negative for the GaAs-like sphere. According to Eq. (96), this change of sign depends strongly on the strength of the scattering cross-section. For completeness, the scattering efficiency, $Q = \sigma_{\text{sca}}/\pi a^2$, is depicted in Fig. 6.2b) assuming both a dipolar response ($l = 1$) and the full Mie multipolar expansion. As can be inferred, the optical responses are purely dipolar, even for relatively strong scattering regimes.

6.3 The nearly-zero forward light scattering condition

Once we have discussed the role of the GSCK into the sign of the g-parameter, let us now analyze the relevance of the GSKC in the nearly-zero optical forward scattering condition,

$$\frac{\mathrm{d}\sigma_{\mathrm{sca}}}{\mathrm{d}\Omega} = \frac{3}{8\pi}\sigma_{\mathrm{sca}}^{K_2}\left(\frac{1+\cos^2\theta}{2} + \left[\frac{k^2}{6\pi}\sigma_{\mathrm{sca}}^{K_2} - 1\right]\cos\theta\right). \tag{97}$$

At the GSKC, $\alpha_1 = -\beta_1$, the scattering cross section, $\sigma_{\mathrm{sca}}^{K_2}$, governs the intensity of the far-field pattern of the differential scattering cross section. As a consequence, the GSKC is not sufficient (not even necessary) to obtain the typical pear-like structure, in striking contrast to previous analysis [138, 149]. In fact, it is clear that near the electric and magnetic dipole resonances, in which $g \lesssim 0.5 \Longleftrightarrow \sigma_{\mathrm{sca}}^{K_2} \lesssim 12\pi/k^2$, the radiation pattern of the differential scattering cross section reminds to the one arising when the first Kerker condition is satisfied. In this particular case, there is no net radiation at backscattering. On the other hand, when $\sigma_{\mathrm{sca}}^{K_2} = \sigma_{\mathrm{sca}}^{\mathrm{res}} = 6\pi/k^2$, condition that leads to $g = 0$, according to Eq. (96), the differential scattering cross section is identical to the one given by a pure electric (or magnetic) dipole. Finally, when $\sigma_{\mathrm{sca}}^{K_2} < \sigma_{\mathrm{sca}}^{\mathrm{res}}$, which implies a negative g-parameter, the target scatters mostly in the backward direction.

This phenomenology is further confirmed in Fig. 6.3, where the FF radiation pattern of the (integral normalized) differential scattering cross-section is considered, at the GSKC, for the materials illustrated in Fig. 6.2: TiO_2-like, GaP-like, and GaAs-like spheres. As expected, when $g > 0$, the scattering pattern almost entirely lies in the forward direction, according to Fig. 6.3a.

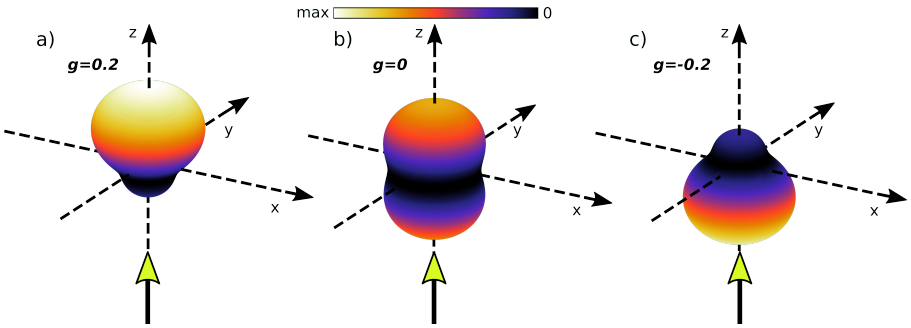

Figure 6.3 – (Integral-normalized) differential scattering cross section, $(\mathrm{d}\sigma_{\mathrm{sca}}(\theta)/\mathrm{d}\Omega)/\sigma_{\mathrm{sca}}^{K_2}$, for different optical responses at the generalized second Kerker conditon, i.e $g = 0.2$ (TiO_2-like sphere), $g = 0$ (GaP-like sphere), $g = -0.2$ (GaAs-like sphere), according to Fig. 6.2.

This corresponds to the energy radiation pattern in the FF limit of the $Ti0_2$-like sphere at the GSKC, where $g = 0.2$ (see dotted green line Fig. 6.2). At $g = 0$, which arises from the GaP-like sphere at the GSKC, according to the dashed red line in Fig. 6.2, the energy radiation pattern in the FF limit is symmetrical, as it can be seen in Fig. 6.3b. This is identical to the one that arises from a pure electric (or magnetic) dipole. Finally, when $g < 0$, the target preferentially scatters in the backward direction, as it can be inferred in Fig. 6.3c. This phenomenon corresponds to the energy radiation pattern in the FF limit of the GaAs-like sphere at the GSKC, where $g = -0.2$, according to the dash-dotted yellow line of Fig. 6.2. Note that this last case was the "expected" from previous assumptions. Our analysis is straightforward to derive that the nearly-zero optical forward scattering condition is only achievable through a negative g-parameter.
In order to get deeper physical insight into the relevance of the GSKC, it is interesting to derive the explicit expression of the differential scattering cross section evaluated at the forward direction, as shown in Fig. 6.4. Under these conditions,

$$\begin{matrix}\alpha_1 = -\beta_1, \\ \theta = 0,\end{matrix} \qquad \Longrightarrow \qquad \frac{\mathrm{d}\sigma_{\mathrm{sca}}}{\mathrm{d}\Omega} = \frac{k^2}{16\pi}\left(\sigma_{\mathrm{sca}}^{K_2}\right)^2 .$$

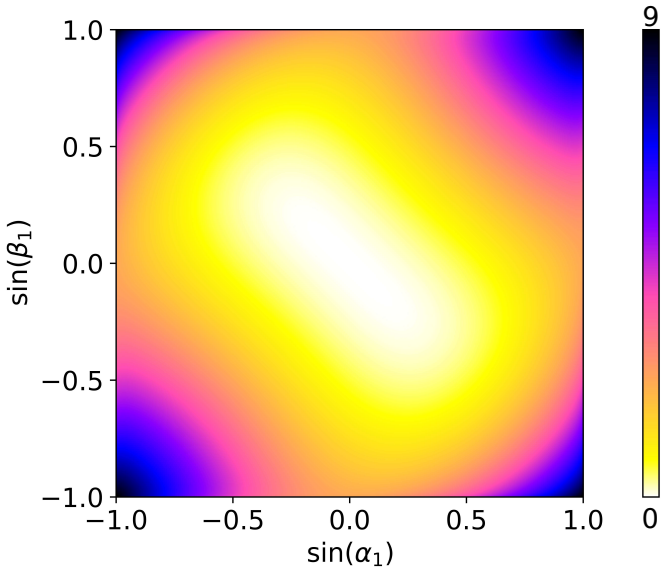

Figure 6.4 – Dimensionless differential scattering cross section, $k^2\mathrm{d}\sigma_{\mathrm{sca}}/\mathrm{d}\Omega$, evaluated at the forward direction, $\theta = 0$.

This equation shows that at the GSKC, in the forward direction ($\theta = 0$), the differential scattering cross section scales quadratically with the scattering cross section. As a direct result, for a relatively large scattering cross section, the target may scatter preferentially in the forward direction ($\theta = 0$), leading to a counterintuitive result, as the nearly-zero optical forward intensity condition for light is far from being obtained. In fact, near the electric and magnetic dipolar resonances, where $\pm\alpha_1, \mp\beta_1 \approx \pi/2 \Longleftrightarrow g \lesssim 0.5$, the intensity in the forward direction ($\theta = 0$) is close to be maximized. Therefore, both Figs. 6.1 and 6.4 can be understood together as the actual implication of the GSKC: Only when the scattering cross section is smaller than that for a pure resonant particle, $\sigma_{\text{sca}}^{K_2} < \sigma_{\text{sca}}^{\text{res}}$, a negative g-parameter can be obtained. In this regime and only in this regime, the nearly-zero optical forward scattering can be achieved.

6.4 Conclusions

We have shown that the GSKC can be derived as the optimal condition that minimizes the g-parameter for a fixed scattering cross-section in the absence of optical gain. We have found that the GSKC does not necessarily give rise to a negative g-parameter. In fact, under this condition, we have exposed that the g-parameter ranges from positive to negative values, crossing $g = 0$ when the scattering cross-section is identical to the one arising from a pure electric (or magnetic) resonant target. Consequently, we have demonstrated that the far-field scattering pattern of the differential scattering cross-section runs over all its possible polar diagrams. Notably, near the electric and magnetic dipole resonances, we have explicitly exposed that this resembles the one given at the first Kerker condition, where there is no net radiation in the backscattering direction. To have a more in-depth insight, we have then confirmed this behavior by showing that the energy radiation pattern in the far-field limit, or, in other words, the differential scattering cross-section at the GSKC in the forward direction, scales quadratically with the scattering cross-section. Consequently, for strong scattering regimes, the target preferably scatters in the forward direction, striking contrast with the current understanding.
These findings are of considerable importance in different contexts where minimization of the g-parameter can be most relevant. This includes theory and experimental work on optical forces (where the radiation pressure cross-section strongly depends on the g-parameter) [150–152], light transport, and radiative transfer phenomena since the minimization of g can significantly reduce the transport mean free path [153].

CHAPTER 7

Unveiling dipolar regimes of large dielectric Mie spheres from helicity preserving

7.1 Introduction

The so-called *optimum forward light scattering* was found at the first Kerker condition for a given contrast index nano-sphere with m ~ 2.45 [121,122]. This optimization consists of maximizing the light-scattering at the first Kerker condition in the electric and magnetic dipolar regime[18]. Nonetheless, the ideal mapping from the scattering by dual magnetic spheres ($\epsilon = \mu$) onto the scattering by larger dual dielectric spheres ($\mu = 1$) can only be achieved *in a multipolar scattering process*[19] when the electric and magnetic Mie coefficients are strictly identical, i.e., $a_l = b_l \; \forall l$. This (non-magnetic) generalized EM duality condition has not been proved to be unattainable, although it has been extensively conjectured [3, 4, 154, 155].

[18] From the results derived in Chapter 5; it is straightforward to notice that lossy spheres cannot be candidates to fulfill the optimum forward light scattering condition since the first Kerker condition is not reached, namely, $a_l \neq b_l$ for $\Im\{\mathrm{m}\} \neq 0$.

[19] We denote multipolar scattering process whereas several multipoles contribute to the optical response of the object, e.g., dipolar plus quadrupolar orders.

In this Chapter, we rigorously demonstrate in Sec. 7.2 that the ideal mapping from $\epsilon = \mu$ onto the scattering by homogeneous dielectric spheres with $\mu = 1$ is precluded due to a fundamental property of the Bessel functions. The proof is general since it does not depend on the contrast index, multipole order, incoming polarization, and x size parameter. As a result, the absence of backscattered light and EM helicity conservation can not be ideally obtained in a multipolar scattering process for the scattering of homogeneous dielectric spheres with $\mu = 1$. Nevertheless and as a direct consequence from our proof, we show in Sec. 7.3 that the almost entirely conservation of the EM helicity after scattering implies the existence of pure-multipolar spectral regions, particularly dipolar spectral regimes. Remarkably, for HRI spheres, these dipolar regimes arise for large dielectric homogeneous spheres, well-beyond its presumed interval. We show in Sec. 7.4 that the optimum forward light scattering condition, predicted for a given refractive index contrast of $m = 2.45$ [121,122], arises quasi-periodically at a fixed size parameter in these unexplored dipolar regimes, in striking contrast to previous assumptions [121, 122]. The main conclusions of this Chapter can be found in Sec. 7.5.

7.2 Another fundamental property of the Mie theory

When $a_l = b_l \; \forall l$ the particle behaves as a dual sphere, preserving the EM helicity of the EM field [154]. In terms of the Bessel functions, this non-magnetic generalized duality condition can be derived from the master equation,

$$aJ_{l+\frac{1}{2}}(\mathrm{m}x) + b\mathrm{m}xJ'_{l+\frac{1}{2}}(\mathrm{m}x) = 0. \tag{98}$$

Notice that when $a = 1$ and $b = 0$ the node of the first kind emerges, i.e., $S_l(\mathrm{m}x) = 0 \Longleftrightarrow a_l = b_l = S_l(x)/\xi_l(x)$. On the other hand, when $a = 1$ and $b = 2$, the node of the second kind arises, i.e., $S'_l(\mathrm{m}x) = 0 \Longleftrightarrow a_l = b_l = S'_l(x)/\xi'_l(x)$. In this section, we firstly unveil a fundamental property of a non-magnetic dielectric homogeneous Mie sphere with $\mu = 1$ that has been broadly conjectured [3, 4, 154, 155] but not yet demonstrated: The EM helicity cannot be conserved in a multipolar scattering process. In order to prove it, let us make use of the following Lemma,

1. When $v > -1$ and $a, b \in \mathbb{R}$ such as $a^2 + b^2 \neq 0$ then no function of the type $aJ_v(z) + bzJ'_v(z) = 0$ can have a repeated zero other than $z = 0$.

Note that Lemma. 1 generalizes a well-known result based on the interlacing nature of the zeros of the Bessel functions for different v-order values [156,157]. Since the trivial solution $\mathrm{m}x = 0$ implies no particle, then Eq. (98) can not be formally satisfied $\forall l$.

On physical grounds this phenomenon implies that, when $a_l(\mathrm{m}, x) = b_l(\mathrm{m}, x)$, then no other pair of electric and magnetic Mie coefficients can be identical, $a_j(\mathrm{m}, x) \neq b_j(\mathrm{m}, x)\ \forall j \neq l$. Note that this phenomenon occurs regardless of the incoming polarization, multiple order, size parameter and contrast index, making this demonstration general. There we have revealed a fundamental property of the so-called Mie theory [12]. As an illustrative example, the multipole first Kerker conditions, given by both the nodes of first and second kind, i.e. $S_l(\mathrm{m}x) = 0$ and $S_l'(\mathrm{m}x) = 0$, respectively, for $l = 1, 2, 3$, are shown in Fig. 7.1. As a result of Lemma 1, these trajectories do not cross each other neither overlap showing that the EM helicity after scattering can not be preserved in a multipolar scattering process. Nevertheless it can be conserved in *pure-multipolar* spectral regions with well-defined square of the total AM, $\mathbf{J}^2$, and its z-component, $\mathbf{J}_z$, particularly, in dipolar spectral regimes under PW illumination, as we will shorty see.

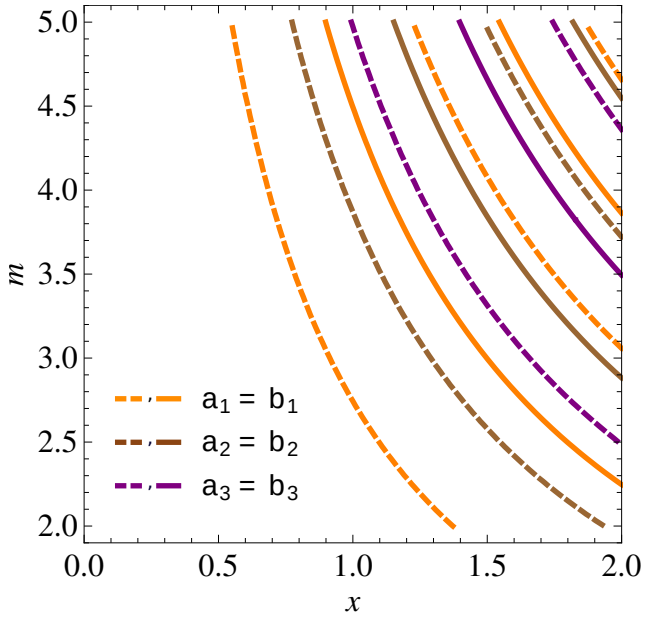

Figure 7.1 – Multipole Kerker conditions arising from the nodes of first and second kind $S_l(\mathrm{m}x) = 0$ and $S_l'(\mathrm{m}x) = 0$, respectively, for $l = 1, 2, 3$, versus the contrast index m and the x size parameter. The nodes of first kind are illustrated by dashed lines while the nodes of second kind are represented by solid lines. Either of them leads to $a_l = b_l$. The nodal trajectories neither cross nor overlap, proving that the EM helicity can not be preserved in a multipolar scattering process.

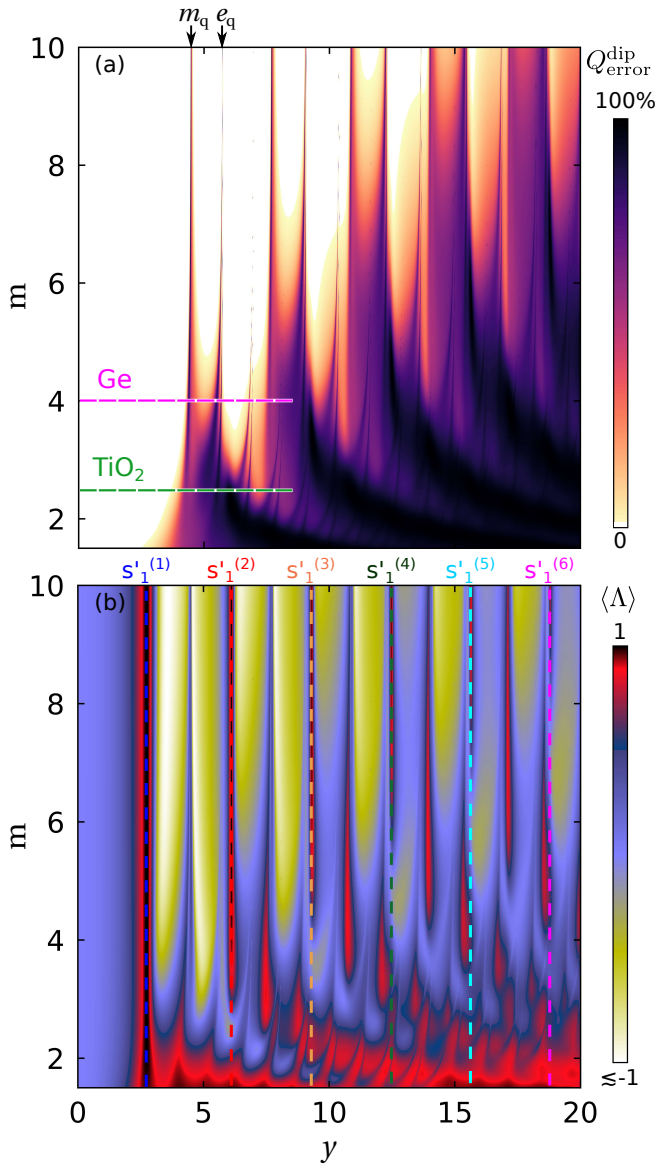

Figure 7.2 – (a) Percentage error of assuming a dipolar response, i.e., $Q^{dip}_{error} = |Q^{dip}_{sca}/Q_{sca} - 1|\%$ vs the $y = mx$ size parameter and refractive index contrast m. The dipolar spectral regime corresponds to white regions. (b) Expected value of the EM helicity after scattering by a dielectric Mie sphere.

7.3 Dipolar spectral regimes from the conservation of the EM helicity

To confirm it, let us make use of the expected value of the scattered EM helicity (see Eq. (90)). When the sphere is illuminated by a circularly polarized PW with helicity σ, or by a cylindrically symmetric beam (eigenvector of the helicity, $\mathbf{\Lambda}$ and z-component of the AM, J_z, with eigenvalues m and σ), the scattered field is, in general, a combination of multipolar modes with fixed m,

$$\langle \Lambda \rangle = \sigma \frac{1-T}{1+T}, \qquad \text{where} \qquad T = \frac{\sum_{l=|m|}^{\infty} \left| C_{lm}^{+} \right|^2 |a_l - b_l|^2}{\sum_{l=|m|}^{\infty} \left| C_{lm}^{+} \right|^2 |a_l + b_l|^2}, \tag{99}$$

is the helicity transfer function [154].
When T goes to zero, the particle response is said to be dual [154], and the scattered EM helicity is the same as the EM helicity of the incoming beam. However, as we have previously demonstrated, the EM helicity is not preserved in a multipolar scattering process. Nevertheless, the EM helicity can be reasonably preserved in pure-multipolar spectral regions, particularly, in dipolar spectral regimes under PW illumination, as can be inferred from Fig. 7.2. Firstly, we identify dipolar regions (white colors) from Figure 7.2a, where the percentage error of assuming a dipolar response, i.e., $Q_{\text{error}}^{\text{dip}} = |Q_{\text{sca}}^{\text{dip}}/Q_{\text{sca}} - 1|\%$, versus the $y = \text{m}x$ size parameter and index contrast m is depicted. Notice that $Q_{\text{sca}}^{\text{dip}}$ corresponds to Eq. (81) but retaining only $l = 1$ (dipolar contribution). Surprisingly, several dipolar spectral regimes are found far beyond its presumed spectral interval (beyond the magnetic (m_{q}) and electric quadrupole (e_{q}) resonances) for HRI spheres with $m \geq 3.5$. Secondly, we show in Figure 7.2b the expected value of the EM helicity after scattering, $\langle \Lambda \rangle$, under well-defined EM helicity plane wave illumination, $\sigma = +1$ (see Eq. (99)). As can be inferred from the attached color-bar, $\langle \Lambda \rangle \approx 1$ when the $s_1^{\prime(q)}$ vertical trajectories, corresponding to the q-th zeros of $S_1'(\text{m}x) = 0$[20], pass through a dipolar spectral region. In contrast, $\langle \Lambda \rangle$ is not conserved in a multipolar scattering process as a result of Lemma 1 since if $a_l = b_l$ then $a_j \neq b_j \; \forall \, j \neq l$.
In order to get a deeper insight into the appearing of these dipolar spectral regimes, in Fig. 7.3 we analyze the dipolar contribution (blue dashed line) to the total scattering efficiency (black solid line) for two different dielectric-like spheres [148]: Titanium Oxide (TiO_2) with m = 2.5 and Germanium (Ge) with m = 4. While in the case of TiO_2 the dipolar regime (blue background in Fig. 7.3a) just emerges in the limit of small particle [14, 16], the scattering efficiency arising from the Ge sphere presents an unexpected dipolar regime

[20] We denote the q-th positive zeros of $S_l(\text{m}x) = 0$ and $S_l'(\text{m}x) = 0$ as $s_l^{(q)}$ and $s_l^{\prime(q)}$, respectively.

beyond the point-dipole approximation in the interval given by $5.75 < y < 6.25$ (narrow blue background in Fig. 7.3b), far beyond the m_q and e_q resonances. Let us recall that, at this dipolar regime, the EM helicity is preserved at $s_1'^{(2)}$ for the Ge sphere. This phenomenon implies that the zero optical backscattering condition can be fulfilled for dipolar HRI microspheres.

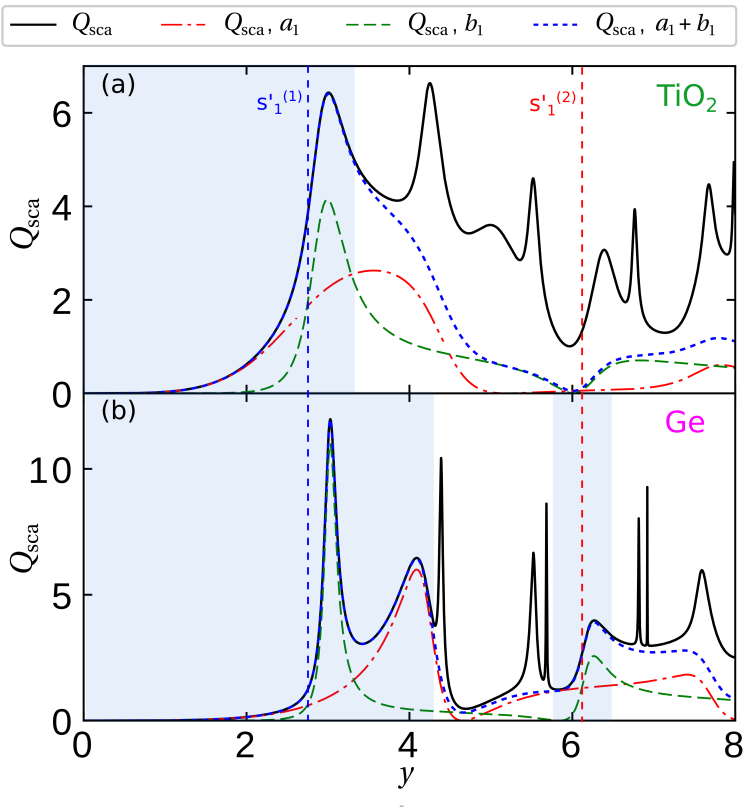

Figure 7.3 – Scattering efficiency from: (a) TiO_2-like sphere with m = 2.5 and (b) Ge-like sphere with m = 4. Blue regions illustrate the regimes that are essentially described by a dipolar response. The fist and second multipolar Kerker conditions are willfully depicted in order to show that just $s_1'^{(1)}$ and $s_1'^{(2)}$ lead to EM helicity preserving for HRI spheres (m > 3.5), according to Fig. 7.2.

7.4 Optimum forward light scattering condition

The aim to obtain a minimum backscattering together with maximized total and forward scattering has been tackled for spherical and spheroidal nanoparticles [121, 122]. In the latter works, it was found that a diamond-like sphere (m $\sim$ 2.45) [148] is the best candidate fulfilling the optimum forward light scattering condition in the dipolar spectral regime, below the $m_{\rm q}$ and $e_{\rm q}$ resonances. The problem consists on maximizing the scattering efficiency (see Eq. (81)) at the first Kerker condition given by $S_1'(\mathrm{m}x) = 0 \Longleftrightarrow a_1 = b_1$. This maximization is mathematically expressed as,

$$\max\left[Q_{\rm scat}\right] = 12\max\left|\frac{S_1'(x)}{x\xi_1'(x)}\right|^2 \sim 3.75, \qquad \text{with} \qquad x_{\rm max} \sim 1.12. \tag{100}$$

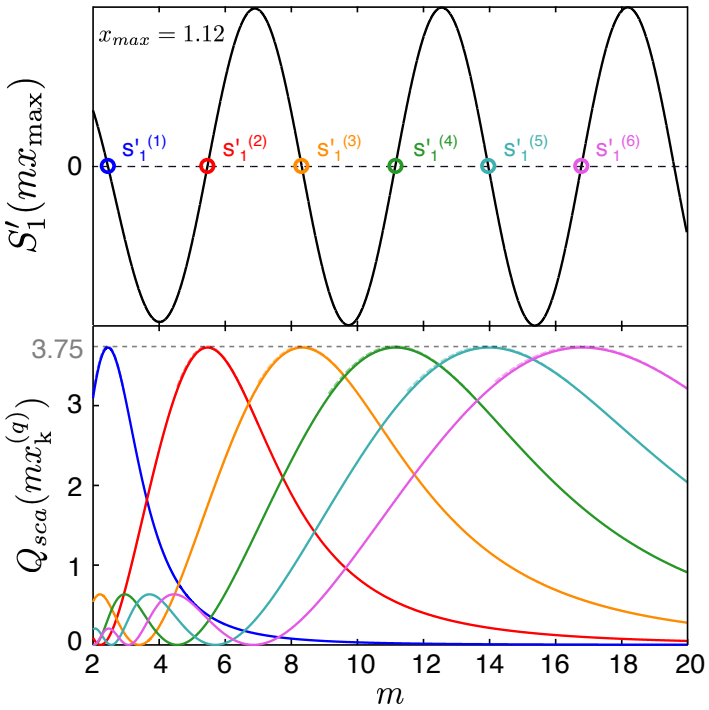

Figure 7.4 – (a) Node of the second kind, $S_1'(\mathrm{m}x_{\rm max})$, where $x_{\rm max} \sim 1.12$, as a function of the contrast index m. The q-th positive zero of this function, depicted by circles, satisfies the optimum forward light scattering condition. (b) Scattering efficiency, $Q_{\rm sca}$, evaluated at the $x_{\rm k}^{(q)}$, i.e., the size parameter that leads to the first Kerker condition given by $s_1'^{\,q}$, as a function of m.

This calculation is not surprising: The scattering efficiency depends on the x size parameter, and its maximum value is bounded. From the dipolar node of second kind namely, $S_1'(\mathrm{m}x_{\max}) = 0$, it is straightforward to derive the material(s) that satisfy the optimum forward light scattering condition, as it can be inferred from Fig. 7.4. Interestingly, for the asymptotic limit given by $\mathrm{m} \gg x, l$ the dipolar node of the second kind reads as $S_1'(\mathrm{m}x) \sim -\sin(\mathrm{m}x)$ and then the optimum forward light scattering condition is not a transcendental but an analytical solution given by the simple form $\mathrm{m} = q\pi/x_{\max}$. For completeness, we illustrate the differential scattering cross-section, arising from two materials with $\mathrm{m} \approx 2.45$ and $\mathrm{m} \approx 5.47$ satisfying the optimum forward light scattering condition, in Fig. 7.5a and Fig. 7.5b, respectively. As previously discussed, the scattering radiation pattern is identical since the optimum forward light scattering condition arises at a fixed x size parameter ($x_{\max} \approx 1.12$) for an infinite number of materials, contrary to previous interpretations [121, 122]. Finally, let us discuss one aspect of interest about the dipolar regimes arising beyond

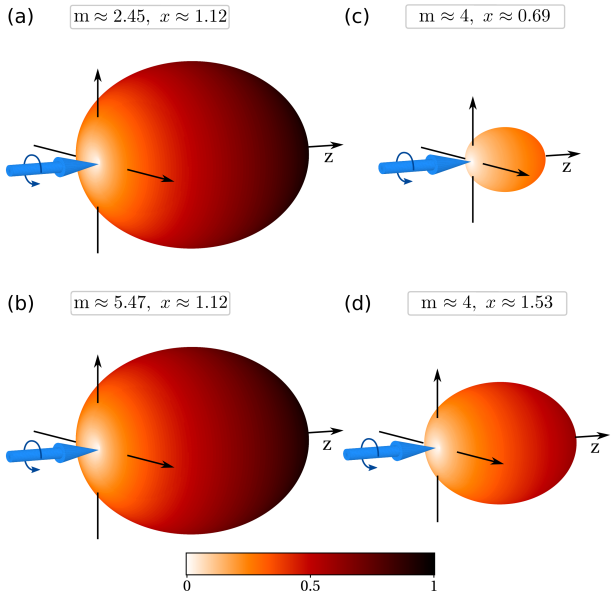

Figure 7.5 – Scattering radiation patterns arising from dual materials in the dipolar spectral regime, normalized by the maximum value at the optimum forward light scattering condition: (a)-(b) two dual materials satisfying the optimum forward light scattering condition; (c)-(d) two dual Ge spheres with index contrast $\mathrm{m} \approx 4$ below and above the quadrupole resonances, respectively.

the m_{q} and e_{q} resonances: The scattering radiation pattern arising from HRI dual spheres such as Ge exceeds the one emerging from the same index contrast in the limit of small particle, as can be inferred from Fig. 7.5c and Fig. 7.5d. This phenomenon could drive future experiments based on the EM duality restoration: EM helicity conservation and absence of backscattered light for HRI spheres in the dipolar spectral regime arising well-beyond the limit of a small particle.

7.5 Conclusions

We have unveiled a fundamental property of the Mie scattering of a dielectric sphere. Namely, that when $a_l = b_l$, no other pair of electric and magnetic Mie coefficients can be identical, $a_j \neq b_j \; \forall \, j \neq l$. This finding precludes the ideal EM duality restoration (or ideal helicity conservation) in scattering processes where several multipoles contribute to the optical response of an object [155]. The proof is general since it is solely based on a fundamental mathematical property of the Bessel functions and, thus, remains valid regardless of the particle size, refractive index contrast, incident wavelength, and multipole order. Nevertheless, we have shown that the EM helicity conservation can be used as a probe of pure-multipolar spectral regimes, particularly dipolar nature, which arises from its presumed spectral region. This intriguing finding shows that the dipolar behavior is not necessarily limited to small particles, where the point-dipole approximation works correctly [158]. From our results, it is straightforward to note that electric and magnetic dipolar optical forces [24, 73, 159, 160], radiation pressure [161, 162], light transport phenomena [8, 87], and the novel concept of anapole modes [27], originally derived for small nanoparticles, can be extended to larger HRI dipolar spheres. Moreover, the novel dipolar regions where the EM helicity is preserved can be used to enhance the sensitivity of circular dichroism spectroscopy of chiral particles [163, 164]. This finding could drive to experiments beyond the actual physical picture, mostly restricted to small HRI materials that present a relatively weak scattering efficiency at the first Kerker condition [165, 166]. Finally, we have proved that the optimum forward light scattering condition, derived initially for a specific nanoparticle, is satisfied for an infinite number of materials at a fixed x size parameter, in contrast to previous interpretations [121, 122]. We believe that our results open new perspectives in studying the light scattered by dielectric Mie spheres, including new possible applications of HRI particles as building blocks in all-dielectric optics and photonic devices.

CHAPTER 8

Conclusions and outlook

8.1 Conclusions

This Thesis has been written to provide a closed but thorough theoretical description of the electromagnetic interaction between light and matter in the emerging field of Nanophotonics. Mainly, I have focused on the electromagnetic interaction between a PW with the most symmetric object existent in nature: an homogeneous sphere. Although Gustav Mie solved this scattering problem at the beginning of XX century [12], I have been able to explore some overlooked aspects in the previous Chapters.
The main findings of this Thesis can be summarized into the following items:

- **Enhanced errors in optical localization due to the first Kerker condition**. It is customary challenging to infer the existing errors in optical localization from nanostructures. In Chapter 3, it is demonstrated that the subwavelength displacement from a pure electric dipole under plane wave illumination can be drastically surpassed by making use of a HRI Si sphere sustaining both an electric and magnetic dipolar response. This optical error commonly referred to as optical mirages, diverges in backscattering at the first Kerker condition, i.e., when the electric and magnetic dipolar response is identical. As demonstrated in Chapter 3, this phenomenon can be understood employing a new theoretical and practical framework for the study of light-matter interactions: helicity, total angular momentum, and the use of symmetries.

- **Bringing together the concepts of helicity and asymmetry in light scattering from small particles**. Electromagnetic helicity, the nonparaxial generalization of the notion of polarization, and the asymmetry parameter, which governs the scattered light's directionality, were unseemly uncorrelated magnitudes. In Chapter 4, it is shown that both helicity and the g-parameter are strikingly linked in the electric and magnetic dipolar regime. Consequently, the whole scattering pattern, given by the sign of the g, can be indirectly inferred from a relatively simple measurement of the polarization in the far-field limit. This result opens new insights into several physics branches such as optical forces, particularly laser tractor beams, optical anapoles, and light transport phenomena.

- **An overlooked fundamental property of the Mie coefficients**. The first Kerker condition had been historically presented in terms of the electric and magnetic Mie coefficients as $a_l = b_l$. However, this notation does not give insight into the first Kerker condition we are dealing with. To tackle this problem, and in Chapter 5, we have introduced a brand-new nodal notation that simplifies the first Kerker condition. Within this formalism, it is demonstrated that absorption inhibits the first Kerker condition for homogeneous spheres. As a result, the first Kerker condition cannot be achieved in plasmonic nanostructures nor dielectric spheres in the visible spectral range. This phenomenon precludes the conservation of the incoming helicity and the zero optical backscattering condition in the dipolar regime. In this vein, it is also shown that the zero optical condition in the forward direction can only be achieved utilizing optical pumping, namely, optical gain.

- **Revisiting the so-called second Kerker condition and the nearly-zero forward scattering**. The perfect zero forward light scattering condition, first introduced by Kerker, Wang, and Miles [29], has been historically revisited due to its incompatibility with the optical theorem. As a result, an energy-viable optical condition, referred to as the Generalized second Kerker condition (GSKC), was proposed as a plausible alternative for HRI nanostructres [23]. Thus, the link with both GSKC and nearly-zero forward light scattering has been taken for granted in all previous works as it was thought to mimic the light scattering effects of those presented in Ref. [29]. However, it is shown in Chapter 6, the GSKC does not generally give rise to the nearly-zero forward light scattering condition. It ranges all possible light-scattering scenarios in the dipolar regime. This result invites the optical community to revisit some of their conclusions regarding scattered light's directionality at the GSKC.

- **Optimizing the zero optical backscattering condition in brand-new dipolar spectral regimes**. The absence of backscattered light has been observed in several HRI nanostructures at the first Kerker condition. However, the scattering efficiency at the first Kerker condition is several orders of magnitude below the electric or magnetic resonances. In Chapter 7, it is demonstrated that the optimum zero optical backscattering condition appears for a given x size parameter instead of for a given index contrast at brand-new dipolar spectral regimes. These appear for large dielectric spheres, such as Germanium, and, in a sense, break the continuous association of dipolar regime with small particles. Our results give new insights into understanding the absence of backscattered light and the physical scenario behind the dipolar approximation. The latter is quite handy as the analytical approach is suitable.

8.2 Outlook

We hope that the present Thesis has generated many interesting questions and opened several directions worth exploring in the future. For example, we aim to explore the relationship between the Kerker conditions and optical invisibility through the so-called optical anapoles. In the latter optical condition, the electric and magnetic scattering efficiency simultaneously vanishes while the internal energy is enhanced. As a result, these anapoles, commonly referred to as hybrid anapoles, are mathematically found by imposing the first Kerker condition with zero scattering. While hybrid anapoles are hindered for spheres under plane wave illumination, we intend to excite the hybrid anapole through a tightly-focused gaussian beam that discards higher multipolar orders in the optical response of the sphere. This tightly-focused Gaussian beam is intimately related to the concept of dipolar field, which is nothing but an ideal field that only excites electric and magnetic dipoles at the focus. A review of the concept of dipolar field can be found in Ref. [167].
Another field in which the findings of this Thesis can be directly applied is optical chirality. Particularly, we aim to explore which is the optimum building block enhancing the circular dichroism of a well-defined helicity signal. Based on the properties of the spherical harmonics, eigenstates of the total angular momentum, and helicity, we intend to derive a closed-analytical expression that directly points out which is the best candidate to enhance the circular dichroism of a signal. In contrast to previous assumptions, we expect not to be the sphere the best building block since the first Kerker condition cannot be associated with a resonant behavior.

CHAPTER A

Poynting vector from an electric and magnetic dipole

A.1 EM fields from an electric and magnetic dipole

The EM fields emitted by an electric and magnetic dipole can be written following Jackson's notation [118] as

$$\mathbf{E}_{\mathrm{e}} = \frac{1}{4\pi\epsilon_0}\left\{k^2\left(\hat{\mathbf{r}}\times\mathbf{p}\right)\times\hat{\mathbf{r}}\frac{e^{\mathrm{i}kr}}{r}+\left[3\hat{\mathbf{r}}\left(\hat{\mathbf{r}}\cdot\mathbf{p}\right)-\mathbf{p}\right]\left(\frac{1}{r^2}-\frac{\mathrm{i}k}{r}\right)\frac{e^{\mathrm{i}kr}}{r}\right\} \quad (101)$$

$$\mathbf{E}_{\mathrm{m}} = -\frac{Z_0}{4\pi}k^2\left(\hat{\mathbf{r}}\times\mathbf{m}\right)\frac{e^{\mathrm{i}kr}}{r}\left(1-\frac{1}{\mathrm{i}kr}\right), \quad (102)$$

while the magnetic field can be straightforwardly computed by $Z\mathbf{H}=-\mathrm{i}\Lambda\mathbf{E}$. Here $Z=\sqrt{\mu/\epsilon}$ is the host medium impedance, μ and ϵ being the permeability and permittivity in the host medium, $\hat{\mathbf{r}}$ is the radial unit vector and $k=\mathrm{m_h}2\pi/\lambda_0$ is the wavevector in the host medium described.

A.2 Poynting vector from an electric and magnetic dipole

The time-averaged Poynting vector is given by the simple relation

$$\mathbf{S}_{\rm scat} = \frac{1}{2}{\rm Re}\left\{\mathbf{E}\times\mathbf{H}^*\right\} = \mathbf{S}_{\rm e} + \mathbf{S}_{\rm m} + \mathbf{S}_{\rm em}. \tag{103}$$

where the subindex (em) refers to the interference between the electric and magnetic contribution. After some cumbersome but trivial algebra it can be shown the Poynting vector is given in the electric and magnetic dipolar regime by

$$\mathbf{S}_{\rm e} = \frac{ck^4}{32\pi^2\epsilon_0 r^2}\left\{\hat{\mathbf{r}}\left(|\mathbf{p}|^2 - (\hat{\mathbf{r}}\cdot\mathbf{p})\,(\hat{\mathbf{r}}\cdot\mathbf{p}^*)\right) - \frac{2}{kr}\left(1+\frac{1}{(kr)^2}\right){\rm Im}\left\{(\hat{\mathbf{r}}\cdot\mathbf{p})\,\mathbf{p}^*\right\}\right\}, \tag{104}$$

$$\mathbf{S}_{\rm m} = \frac{Zk^4}{32\pi^2 r^2}\left\{\hat{\mathbf{r}}\left(|\mathbf{m}|^2 - (\hat{\mathbf{r}}\cdot\boldsymbol{m})\,(\hat{\mathbf{r}}\cdot\boldsymbol{m}^*)\right) - \frac{2}{kr}\left(1+\frac{1}{(kr)^2}\right){\rm Im}\left\{(\hat{\mathbf{r}}\cdot\mathbf{m})\,\mathbf{m}^*\right\}\right\} \tag{105}$$

and

$$\begin{aligned}\mathbf{S}_{\rm em} = \frac{Zck^4}{32\pi^2 r^2}\Bigg\{&\left(2+\frac{3}{(kr)^4}\right)\left[\hat{\mathbf{r}}\cdot{\rm Re}\left\{\mathbf{p}\times\mathbf{m}^*\right\}\right]\hat{\mathbf{r}} - \frac{2}{(kr)^4}{\rm Re}\left\{\mathbf{p}\times\mathbf{m}^*\right\}\\ &+\left(\frac{2}{kr}\right){\rm Im}\left\{(\hat{\mathbf{r}}\times\mathbf{p})\,(\hat{\mathbf{r}}\cdot\mathbf{m}^*) + (\hat{\mathbf{r}}\times\mathbf{m}^*)\,(\hat{\mathbf{r}}\cdot\mathbf{p})\right\}\Bigg\}.\end{aligned} \tag{106}$$

A.3 Poynting vector from circularly polarized plane waves

Let us consider an homogeneous spherical target, located in the origin of coordinates $\mathbf{r}=0$, sustaining both an electric and magnetic dipole, illuminated by a well-defined helicity (circularly polarized) PW,

$$\mathbf{E}_{\rm i} = E_0 e^{{\rm i}kz}\hat{\boldsymbol{\xi}}_\sigma, \qquad Z\mathbf{H}_{\rm i} = {\rm i}\sigma E_0 e^{{\rm i}kz}\hat{\boldsymbol{\xi}}_\sigma, \tag{107}$$

with

$$\hat{\boldsymbol{\xi}}_\sigma \;=\; \frac{\hat{\boldsymbol{x}}+{\rm i}\sigma\hat{\boldsymbol{y}}}{\sqrt{2}} = \frac{e^{{\rm i}\sigma\varphi}}{\sqrt{2}}\left(\sin\theta\hat{\mathbf{r}} + \cos\theta\hat{\boldsymbol{\theta}} + {\rm i}\sigma\hat{\boldsymbol{\varphi}}\right). \tag{108}$$

Here $\sigma=\pm1$ is the incoming helicity, E_0 is the amplitude of the electric field, θ the scattering angle, i.e. $z = r\cos\theta$ and $[\hat{\boldsymbol{e}}_{\rm r}, \hat{\boldsymbol{e}}_\theta, \hat{\boldsymbol{e}}_\varphi]$ the typical spherical (unitary) basis. In this description, the induced electric and magnetic dipoles become

$$\mathbf{p} = \epsilon_0\alpha_{\rm E}\mathbf{E}_{\rm i}(\mathbf{r}=0) \qquad \text{and} \qquad \mathbf{m} = \alpha_{\rm M}\mathbf{H}_{\rm i}(\mathbf{r}=0). \tag{109}$$

Here $\alpha_{\rm E} = {\rm i}a_1 k^3/(6\pi)$ and $\alpha_{\rm M} = {\rm i}b_1 k^3/(6\pi)$ denote the electric and magnetic polarizabilities, being a_1 and b_1 the so-called Mie coefficients [9]. The Poynting vector can be easily computed from Eqs. (104)-(105)-(106) when considering the induced dipoles as appear in Eq. (109). Neglecting the near-field terms, we arrive to

$$\mathbf{S}_{\rm e} = \frac{2G_0|\alpha_{\rm E}|^2}{r^2}\left\{\hat{\mathbf{r}}\left(1-\frac{\sin^2\theta}{2}\right)+\frac{\sigma}{kr}\sin\theta\hat{\boldsymbol{\varphi}}\right\} \tag{110}$$

$$\mathbf{S}_{\rm m} = \frac{2G_0|\alpha_{\rm M}|^2}{r^2}\left\{\hat{\mathbf{r}}\left(1-\frac{\sin^2\theta}{2}\right)+\frac{\sigma}{kr}\sin\theta\hat{\boldsymbol{\varphi}}\right\} \tag{111}$$

$$\mathbf{S}_{\rm em} = \frac{4G_0}{r^2}{\rm Re}\left\{\alpha_{\rm E}\alpha_{\rm M}^*\right\}\cos\theta\left\{\hat{\mathbf{r}}+\frac{\sigma}{kr}\sin\theta\hat{\boldsymbol{\varphi}}\right\}, \tag{112}$$

where $G_0 = c\epsilon_0|E_0|^2k^4/64\pi^2$.

A.4 Poynting vector from linearly polarized plane waves

Let us consider an homogeneous spherical target, located in the origin of coordinates $\mathbf{r}=0$, sustaining both an electric and magnetic dipole, illuminated by a linearly polarized PW,

$$\mathbf{E}_{\rm i} = E_0 e^{{\rm i}kz}\hat{\boldsymbol{x}}, \qquad Z\mathbf{H}_{\rm i} = E_0 e^{{\rm i}kz}\hat{\boldsymbol{y}}. \tag{113}$$

The Poynting vector can be easily computed from Eqs. (104)-(105)-(106) when considering linearly polarized dipoles induced by Eq. (113). Neglecting the near-field terms, we arrive to

$$\mathbf{S}_{\rm e} = \frac{2G_0}{r^2}|\alpha_{\rm E}|^2\left(1-\cos^2\varphi\sin^2\theta\right)\hat{\mathbf{r}}, \tag{114}$$

$$\mathbf{S}_{\rm m} = \frac{2G_0}{r^2}|\alpha_{\rm M}|^2\left(1-\sin^2\varphi\sin^2\theta\right)\hat{\mathbf{r}}. \tag{115}$$

The interference between the electric and magnetic dipoles given by

$$\mathbf{S}_{\rm em} = \frac{4G_0}{r^2}\Big({\rm Re}\left\{\alpha_{\rm E}\alpha_{\rm M}^*\right\}\cos\theta\hat{\mathbf{r}} \tag{116}$$

$$- \frac{1}{kr}{\rm Im}\left\{\alpha_{\rm E}\alpha_{\rm M}^*\right\}\sin\theta\left(\cos(2\varphi)\hat{\boldsymbol{\theta}}-\cos\theta\sin(2\varphi)\hat{\boldsymbol{\varphi}}\right)\Big). \tag{117}$$

It is important to notice that generally, ${\rm Im}\left\{\alpha_E\alpha_M^*\right\} \neq 0$.

Full list of publications

Published articles included in this Thesis:

1. Jorge Olmos-Trigo, Cristina Sanz-Fernández, Aitzol García-Etxarri, Gabriel Molina-Terriza, F. Sebastián Bergeret and Juan José Sáenz. **Enhanced spin-orbit optical mirages from dual nanospheres.** Phys. Rev. A 2019, 99, 013852. January 2019.

2. Jorge Olmos-Trigo, Cristina Sanz-Fernández, F. Sebastián Bergeret, and Juan José Sáenz. **Asymmetry and spin-orbit coupling of light scattered from subwavelength particles.** Opt. Lett. 44, 1762, March 2019.

3. Jorge Olmos-Trigo, Cristina Sanz-Fernández, Diego Romero Abujetas, Aitzol García-Etxarri, Gabriel Molina-Terriza, Jose Antonio Sánchez-Gil, F. Sebastián Bergeret, and Juan José Sáenz. **Role of the absorption on the spin-orbit interactions of light with Si nano-particles**. J. Appl. Phys. 126, 033104, July 2019.

4. Jorge Olmos-Trigo, Diego Romero Abujetas, Cristina Sanz-Fernández, Jose Antonio Sánchez-Gil, and Juan José Sáenz. **Optimal backward light scattering by dipolar particles.** Phys. Rev. Research 2, 013225, February 2020.

5. Jorge Olmos-Trigo, Cristina Sanz-Fernández, Diego Romero Abujetas, Jon Lasa-Alonso, Aitzol García-Etxarri, Nuno de Sousa, Jose Antonio Sánchez-Gil, Gabriel Molina-Terriza, and Juan José Sáenz. **Kerker Conditions upon Lossless, Absorption, and Optical Gain Regimes**. Phys. Rev. Lett. 125, 073205, July 2020.

6. Jorge Olmos-Trigo, Diego Romero Abujetas, Cristina Sanz-Fernández, Xavier Zambrana-Puyalto, Jose Antonio Sánchez-Gil, and Juan José Sáenz. **Unveiling dipolar spectral regimes of large dielectric Mie spheres from helicity conservation.** Phys. Rev. Research 2, 043021, October 2020.

Published articles not included in this Thesis:

7. Jorge Olmos-Trigo and Juan José Sáenz. **Spin control of macroscopic objects.** Nature Photonics volume 12, pages 444–445, July 2018.

8. Cecilia Zaza, Ianina L. Violi, Julián Gargiulo, Germán Chiarelli, Ludmilla Schumacher, Jurij Jakobi, Jorge Olmos-Trigo, Emiliano Cortes, Matthias König, Stephan Barcikowski, Sebastian Schlücker, Juan José Sáenz, Stefan A. Maier, and Fernando D. Stefani. **Size-Selective Optical Printing of Silicon Nanoparticles through Their Dipolar Magnetic Resonance.** ACS Photonics 2019, 6, 4, 815–822, March 2019.

9. Jorge Olmos-Trigo, Marc Meléndez, Rafael Delgado-Buscalioni, and Juan José Sáenz. **Sectoral multipole focused beams.** Opt. Exp., Vol. 27, pp. 16384-16394, May 2019.

10. Diego R. Abujetas, Jorge Olmos-Trigo, Juan José Sáenz, and José A. Sánchez-Gil. **Coupled electric and magnetic dipole formulation for planar arrays of particles: Resonances and bound states in the continuum for all-dielectric metasurfaces.** Phys. Rev. B 102, 125411, September 2020.

11. Cristina Sanz-Fernández, Martín Molezuelas, Jon Lasa-Alonso, Nuno de Sousa, Xavier Zambrana-Puyalto, Jorge Olmos-Trigo. **Multiple Kerker anapoles in dielectric microspheres.** LPR, 2100035, June 2021.

List of Abbreviations

Abbreviation	Description
AM	Angular momentum
SAM	Spin angular momentum
OAM	Orbital angular momentum
SOI	Spin-Orbit interactions
GSKC	Generalized second Kerker condition
HRI	High refractive index
BC	Boundary conditions
FF	Far-field
em	Interference between the electric and magnetic dipoles
LP	Linear polarization
SHE	Spin Hall effect
DoCP	Degree of circular polarization
g-parameter	Asymmetry parameter
PW	Plane wave
VSWFs	Vector spherical wavefunctions

List of Figures

References

[1] L Berger. Side-jump mechanism for the hall effect of ferromagnets. *Phys. Rev. B*, 2(11):4559, 1970.

[2] Henk F Arnoldus, Xin Li, and Jie Shu. Subwavelength displacement of the far-field image of a radiating dipole. *Opt. Lett.*, 33(13):1446–1448, 2008.

[3] Ivan Fernandez-Corbaton, Xavier Zambrana-Puyalto, Nora Tischler, Xavier Vidal, Mathieu L Juan, and Gabriel Molina-Terriza. Electromagnetic duality symmetry and helicity conservation for the macroscopic maxwell's equations. *Phys. Rev. Lett.*, 111(6):060401, 2013.

[4] Xavier Zambrana-Puyalto, I Fernandez-Corbaton, ML Juan, Xavier Vidal, and Gabriel Molina-Terriza. Duality symmetry and kerker conditions. *Opt. Lett.*, 38(11):1857–1859, 2013.

[5] Jorge Olmos-Trigo, Cristina Sanz-Fernández, Aitzol García-Etxarri, Gabriel Molina-Terriza, F Sebastián Bergeret, and Juan José Sáenz. Enhanced spin-orbit optical mirages from dual nanospheres. *Phys. Rev. A*, 99(1):013852, 2019.

[6] Jorge Olmos-Trigo, Cristina Sanz-Fernández, F Sebastián Bergeret, and Juan José Sáenz. Asymmetry and spin-orbit coupling of light scattered from subwavelength particles. *Opt. Lett.*, 44(7):1762–1765, 2019.

[7] Jorge Olmos-Trigo, Cristina Sanz-Fernández, Diego R. Abujetas, Aitzol García-Etxarri, Gabriel Molina-Terriza, José A. Sánchez-Gil, F. Sebastián Bergeret, and Juan José Sáenz. Role of the absorption on the spin-orbit interactions of light with si nano-particles. *Journal of Applied Physics*, 126(3):033104, July 2019.

[8] Jorge Olmos-Trigo, Diego R Abujetas, Cristina Sanz-Fernández, José A Sánchez-Gil, and Juan José Sáenz. Optimal backward light scattering by dipolar particles. *Physical Review Research*, 2(1):013225, 2020.

[9] Hendrik Christoffel Hulst and Hendrik C van de Hulst. *Light scattering by small particles*. Courier Corporation, 1957.

[10] Jorge Olmos-Trigo, Cristina Sanz-Fernández, Diego R. Abujetas, Jon Lasa-Alonso, Nuno de Sousa, Aitzol García-Etxarri, José A. Sánchez-Gil, Gabriel Molina-Terriza, and Juan José Sáenz. Kerker conditions upon lossless, absorption, and optical gain regimes. *Phys. Rev. Lett.*, 125:073205, Aug 2020.

[11] Jorge Olmos-Trigo, Diego R. Abujetas, Cristina Sanz-Fernández, Nuno de Sousa, José A. Sánchez-Gil, and Juan José Sáenz. Unveiling dipolar spectral regimes of large dielectric mie spheres from helicity conservation, 2020.

[12] Gustav Mie. Beiträge zur optik trüber medien, speziell kolloidaler metallösungen. *Annalen der physik*, 330(3):377–445, 1908.

[13] Andrey B Evlyukhin, Carsten Reinhardt, Andreas Seidel, Boris S Luk'yanchuk, and Boris N Chichkov. Optical response features of si-nanoparticle arrays. *Phys. Rev. B*, 82(4):045404, 2010.

[14] Aitzol García-Etxarri, R Gómez-Medina, Luis S Froufe-Pérez, Cefe López, L Chantada, Frank Scheffold, J Aizpurua, M Nieto-Vesperinas, and Juan José Sáenz. Strong magnetic response of submicron silicon particles in the infrared. *Opt. Express*, 19(6):4815–4826, 2011.

[15] Arseniy I Kuznetsov, Andrey E Miroshnichenko, Yuan Hsing Fu, JingBo Zhang, and Boris Luk'Yanchuk. Magnetic light. *Sci. Rep.*, 2:492, 2012.

[16] Arseniy I Kuznetsov, Andrey E Miroshnichenko, Mark L Brongersma, Yuri S Kivshar, and Boris Luk'yanchuk. Optically resonant dielectric nanostructures. *Science*, 354(6314):aag2472, 2016.

[17] Stefan Alexander Maier. *Plasmonics: fundamentals and applications*. Springer Science & Business Media, 2007.

[18] Harry A Atwater. The promise of plasmonics. *Scientific American*, 296(4):56–63, 2007.

[19] Ekmel Ozbay. Plasmonics: merging photonics and electronics at nanoscale dimensions. *science*, 311(5758):189–193, 2006.

[20] Jon A Schuller, Edward S Barnard, Wenshan Cai, Young Chul Jun, Justin S White, and Mark L Brongersma. Plasmonics for extreme light concentration and manipulation. *Nature materials*, 9(3):193–204, 2010.

[21] Dmitri K Gramotnev and Sergey I Bozhevolnyi. Plasmonics beyond the diffraction limit. *Nature photonics*, 4(2):83–91, 2010.

[22] M Nieto-Vesperinas, JJ Sáenz, R Gómez-Medina, and L Chantada. Optical forces on small magnetodielectric particles. *Opt. Express*, 18(11):11428–11443, 2010.

[23] M Nieto-Vesperinas, R Gomez-Medina, and J J Saenz. Angle-suppressed scattering and optical forces on submicrometer dielectric particles. *J. Opt. Soc. Am. A*, 28(1):54–60, 2011.

[24] Onofrio M Maragò, Philip H Jones, Pietro G Gucciardi, Giovanni Volpe, and Andrea C Ferrari. Optical trapping and manipulation of nanostructures. *Nature nanotechnology*, 8(11):807, 2013.

[25] Dongliang Gao, Weiqiang Ding, Manuel Nieto-Vesperinas, Xumin Ding, Mahdy Rahman, Tianhang Zhang, ChweeTeck Lim, and Cheng-Wei Qiu. Optical manipulation from the microscale to the nanoscale: fundamentals, advances and prospects. *Light: Science & Applications*, 6(9):e17039, 2017.

[26] Andrey E Miroshnichenko, Andrey B Evlyukhin, Ye Feng Yu, Reuben M Bakker, Arkadi Chipouline, Arseniy I Kuznetsov, Boris Luk'yanchuk, Boris N Chichkov, and Yuri S Kivshar. Nonradiating anapole modes in dielectric nanoparticles. *Nature communications*, 6(1):1–8, 2015.

[27] Boris Luk'yanchuk, Ramón Paniagua-Domínguez, Arseniy I Kuznetsov, Andrey E Miroshnichenko, and Yuri S Kivshar. Hybrid anapole modes of high-index dielectric nanoparticles. *Phys. Rev. A*, 95(6):063820, 2017.

[28] Gustavo Grinblat, Yi Li, Michael P Nielsen, Rupert F Oulton, and Stefan A Maier. Efficient third harmonic generation and nonlinear subwavelength imaging at a higher-order anapole mode in a single germanium nanodisk. *ACS nano*, 11(1):953–960, 2017.

[29] Milton Kerker, D-S Wang, and CL Giles. Electromagnetic scattering by magnetic spheres. *J. Opt. Soc. Am. A*, 73(6):765–767, 1983.

[30] D Haefner, S Sukhov, and A Dogariu. Spin hall effect of light in spherical geometry. *Phys. Rev. Lett.*, 102(12):123903, 2009.

[31] Konstantin Y Bliokh, Elena A Ostrovskaya, Miguel A Alonso, Oscar G Rodríguez-Herrera, David Lara, and Chris Dainty. Spin-to-orbital angular momentum conversion in focusing, scattering, and imaging systems. *Opt. Express*, 19(27):26132–26149, 2011.

[32] Arno A Penzias and Robert Woodrow Wilson. A measurement of excess antenna temperature at 4080 mc/s. *The Astrophysical Journal*, 142:419–421, 1965.

[33] Benjamin P Abbott, Richard Abbott, TD Abbott, MR Abernathy, Fausto Acernese, Kendall Ackley, Carl Adams, Thomas Adams, Paolo Addesso, RX Adhikari, et al. Observation of gravitational waves from a binary black hole merger. *Physical review letters*, 116(6):061102, 2016.

[34] James Clerk Maxwell. Viii. a dynamical theory of the electromagnetic field. *Philosophical transactions of the Royal Society of London*, (155):459–512, 1865.

[35] Julius Adams Stratton. *Electromagnetic theory*, volume 33. John Wiley & Sons, 2007.

[36] Max Born and Emil Wolf. *Principles of optics: electromagnetic theory of propagation, interference and diffraction of light*. Elsevier, 2013.

[37] Milton Kerker. *The scattering of light and other electromagnetic radiation: physical chemistry: a series of monographs*, volume 16. Academic press, 2013.

[38] Craig F Bohren and Donald R Huffman. *Absorption and scattering of light by small particles*. John Wiley & Sons, 2008.

[39] WC Mundy, JA Roux, and AM Smith. Mie scattering by spheres in an absorbing medium. *JOSA*, 64(12):1593–1597, 1974.

[40] Arthur L Aden and Milton Kerker. Scattering of electromagnetic waves from two concentric spheres. *Journal of Applied Physics*, 22(10):1242–1246, 1951.

[41] John Henry Poynting. The wave motion of a revolving shaft, and a suggestion as to the angular momentum in a beam of circularly polarised light. *Proceedings of the Royal Society of London. Series A, Containing Papers of a Mathematical and Physical Character*, 82(557):560–567, 1909.

[42] Richard A Beth. Mechanical detection and measurement of the angular momentum of light. *Physical Review*, 50(2):115, 1936.

[43] J Humblet. Sur le moment d'impulsion d'une onde electromagnetique. *Physica*, 10(7):585–603, 1943.

[44] Les Allen, Marco W Beijersbergen, RJC Spreeuw, and JP Woerdman. Orbital angular momentum of light and the transformation of laguerre-gaussian laser modes. *Phys. Rev. A*, 45(11):8185, 1992.

[45] H He, MEJ Friese, NR Heckenberg, and H Rubinsztein-Dunlop. Direct observation of transfer of angular momentum to absorptive particles from a laser beam with a phase singularity. *Phys. Rev. Lett.*, 75(5):826, 1995.

[46] MEJ Friese, TA Nieminen, NR Heckenberg, and H Rubinsztein-Dunlop. Optical alignment and spinning of laser-trapped microscopic particles. *Nature*, 394(6691):348–350, 1998.

[47] K Yu Bliokh, FJ Rodríguez-Fortuño, Franco Nori, and Anatoly V Zayats. Spin–orbit interactions of light. *Nat. Photonics*, 9(12):796, 2015.

[48] Masaru Onoda, Shuichi Murakami, and Naoto Nagaosa. Hall effect of light. *Phys. Rev. Lett.*, 93(8):083901, 2004.

[49] Konstantin Y Bliokh, Aleksandr Y Bekshaev, and Franco Nori. Optical momentum, spin, and angular momentum in dispersive media. *Phys. Rev. Lett.*, 119(7):073901, 2017.

[50] Onur Hosten and Paul Kwiat. Observation of the spin hall effect of light via weak measurements. *Science*, 319(5864):787–790, 2008.

[51] G Araneda, S Walser, Y Colombe, DB Higginbottom, J Volz, R Blatt, and A Rauschenbeutel. Wavelength-scale errors in optical localization due to spin–orbit coupling of light. *Nature Physics*, 15(1):17, 2019.

[52] Konstantin Y Bliokh, Aleksandr Y Bekshaev, and Franco Nori. Extraordinary momentum and spin in evanescent waves. *Nat. Commun.*, 5:3300, 2014.

[53] Lorenzo Marrucci, C Manzo, and D Paparo. Optical spin-to-orbital angular momentum conversion in inhomogeneous anisotropic media. *Phys. Rev. Lett.*, 96(16):163905, 2006.

[54] Ivan Fernandez-Corbaton, Xavier Zambrana-Puyalto, and Gabriel Molina-Terriza. Helicity and angular momentum: A symmetry-based framework for the study of light-matter interactions. *Phys. Rev. A*, 86(4):042103, 2012.

[55] MG Calkin. An invariance property of the free electromagnetic field. *Am. J. Phys*, 33(11):958–960, 1965.

[56] Milton Kerker, D-S Wang, and CL Giles. Electromagnetic scattering by magnetic spheres. *J. Opt. Soc. Am. A*, 73(6):765–767, 1983.

[57] Stefan A Maier and Harry A Atwater. Plasmonics: Localization and guiding of electromagnetic energy in metal/dielectric structures. *Journal of applied physics*, 98(1):10, 2005.

[58] Hongxing Xu, Javier Aizpurua, Mikael Käll, and Peter Apell. Electromagnetic contributions to single-molecule sensitivity in surface-enhanced raman scattering. *Physical Review E*, 62(3):4318, 2000.

[59] Ruben Esteban, Andrei G Borisov, Peter Nordlander, and Javier Aizpurua. Bridging quantum and classical plasmonics with a quantum-corrected model. *Nature communications*, 3(1):1–9, 2012.

[60] Mark S Tame, KR McEnery, ŞK Özdemir, Jinhyoung Lee, Stefan A Maier, and MS Kim. Quantum plasmonics. *Nature Physics*, 9(6):329–340, 2013.

[61] Jaysen Nelayah, Mathieu Kociak, Odile Stéphan, F Javier García de Abajo, Marcel Tencé, Luc Henrard, Dario Taverna, Isabel Pastoriza-Santos, Luis M Liz-Marzán, and Christian Colliex. Mapping surface plasmons on a single metallic nanoparticle. *Nature Physics*, 3(5):348–353, 2007.

[62] Feng Hao, Yannick Sonnefraud, Pol Van Dorpe, Stefan A Maier, Naomi J Halas, and Peter Nordlander. Symmetry breaking in plasmonic nanocavities: subradiant lspr sensing and a tunable fano resonance. *Nano letters*, 8(11):3983–3988, 2008.

[63] Boris Luk'yanchuk, Nikolay I Zheludev, Stefan A Maier, Naomi J Halas, Peter Nordlander, Harald Giessen, and Chong Tow Chong. The fano resonance in plasmonic nanostructures and metamaterials. *Nature materials*, 9(9):707–715, 2010.

[64] Vincenzo Giannini, Antonio I Fernández-Domínguez, Susannah C Heck, and Stefan A Maier. Plasmonic nanoantennas: fundamentals and their use in controlling the radiative properties of nanoemitters. *Chemical reviews*, 111(6):3888–3912, 2011.

[65] Jean-Michel Geffrin, B García-Cámara, R Gómez-Medina, P Albella, L S Froufe-Pérez, Christelle Eyraud, Amelie Litman, Rodolphe Vaillon, F González, M Nieto-Vesperinas, J J Sáenz, and F Moreno. Magnetic and electric coherence in forward-and back-scattered electromagnetic waves by a single dielectric subwavelength sphere. *Nat. Commun.*, 3:1171, 2012.

[66] Steven Person, Manish Jain, Zachary Lapin, Juan Jose Sáenz, Gary Wicks, and Lukas Novotny. Demonstration of zero optical backscattering from single nanoparticles. *Nano Lett.*, 13(4):1806–1809, 2013.

[67] Yuan Hsing Fu, Arseniy I Kuznetsov, Andrey E Miroshnichenko, Ye Feng Yu, and Boris Luk'yanchuk. Directional visible light scattering by silicon nanoparticles. *Nat. Commun.*, 4:1527, 2013.

[68] Manuel Decker and Isabelle Staude. Resonant dielectric nanostructures: a low-loss platform for functional nanophotonics. *J. Opt.*, 18(10):103001, 2016.

[69] Wei Liu and Yuri S Kivshar. Generalized kerker effects in nanophotonics and meta-optics. *Opt. Express*, 26(10):13085–13105, 2018.

[70] Wei Liu, Andrey E Miroshnichenko, Rupert F Oulton, Dragomir N Neshev, Ortwin Hess, and Yuri S Kivshar. Scattering of core-shell nanowires with the interference of electric and magnetic resonances. *Opt. Lett.*, 38(14):2621–2624, 2013.

[71] Wei Liu, Jianfa Zhang, Bing Lei, Haotong Ma, Wenke Xie, and Haojun Hu. Ultra-directional forward scattering by individual core-shell nanoparticles. *Opt. Express*, 22(13):16178–16187, 2014.

[72] Hadi K Shamkhi, Kseniia V Baryshnikova, Andrey Sayanskiy, Polina Kapitanova, Pavel D Terekhov, Pavel Belov, Alina Karabchevsky, Andrey B Evlyukhin, Yuri Kivshar, and Alexander S Shalin. Transverse scattering and generalized kerker effects in all-dielectric mie-resonant metaoptics. *Phys. Rev. Lett.*, 122(19):193905, 2019.

[73] Xiaohao Xu, Manuel Nieto-Vesperinas, Cheng-Wei Qiu, Xiaoshuai Liu, Dongliang Gao, Yao Zhang, and Baojun Li. Kerker-type intensity-gradient force of light. *Laser & Photonics Reviews*, 14(4):1900265, 2020.

[74] Zhonghua Wang, Ning An, Fei Shen, Hongping Zhou, Yongxuan Sun, Zhaoneng Jiang, Yanhua Han, Yan Li, and Zhongyi Guo. Enhanced forward scattering of ellipsoidal dielectric nanoparticles. *Nanoscale Res. Lett.*, 12(1):58, 2017.

[75] AV Poshakinskiy and AN Poddubny. Optomechanical kerker effect. *Physical Review X*, 9(1):011008, 2019.

[76] Brice Rolly, Brian Stout, and Nicolas Bonod. Boosting the directivity of optical antennas with magnetic and electric dipolar resonant particles. *Opt. Express*, 20(18):20376–20386, 2012.

[77] Marc Dubois, Lisa Leroi, Zo Raolison, Redha Abdeddaim, Tryfon Antonakakis, Julien De Rosny, Alexandre Vignaud, Pierre Sabouroux, Elodie Georget, Benoit Larrat, et al. Kerker effect in ultrahigh-field magnetic resonance imaging. *Phys. Rev. X*, 8(3):031083, 2018.

[78] Martin Neugebauer, Paweł Woźniak, Ankan Bag, Gerd Leuchs, and Peter Banzer. Polarization-controlled directional scattering for nanoscopic position sensing. *Nat. Commun.*, 7:11286, 2016.

[79] Ankan Bag, Martin Neugebauer, Paweł Woźniak, Gerd Leuchs, and Peter Banzer. Transverse kerker scattering for angstrom localization of nanoparticles. *Phys. Rev. Lett.*, 121(19):193902, 2018.

[80] Sergey Nechayev, Jörg S Eismann, Martin Neugebauer, Paweł Woźniak, Ankan Bag, Gerd Leuchs, and Peter Banzer. Huygens' dipole for polarization-controlled nanoscale light routing. *arXiv preprint arXiv:1902.01231*, 2019.

[81] Cristina Sanz Fernández, Jorge Olmos Trigo, and Juan José Saenz. Multiple kerker conditions in arbitrary dielectric spheres. *arXiv preprint arXiv:1904.06687*, 2019.

[82] B García-Cámara, F Moreno, F González, and JM Saiz. Comment on "experimental evidence of zero forward scattering by magnetic spheres". *Phys. Rev. Lett.*, 98(17):179701, 2007.

[83] Braulio García-Cámara, Francisco González, Fernando Moreno, and Jose M Saiz. Exception for the zero-forward-scattering theory. *JOSA A*, 25(11):2875–2878, 2008.

[84] Andrea Alù and Nader Engheta. How does zero forward-scattering in magnetodielectric nanoparticles comply with the optical theorem? *J. Nanophotonics*, 4(1):041590, 2010.

[85] Braulio García-Cámara, R Alcaraz de La Osa, JM Saiz, F González, and F Moreno. Directionality in scattering by nanoparticles: Kerker's null-scattering conditions revisited. *Opt. Lett.*, 36(5):728–730, 2011.

[86] Braulio García-Cámara, F Moreno, F González, JM Saiz, and G Videen. Light scattering resonances in small particles with electric and magnetic properties. *JOSA A*, 25(2):327–334, 2008.

[87] R Gómez-Medina, LS Froufe-Pérez, M Yépez, Frank Scheffold, M Nieto-Vesperinas, and Juan José Sáenz. Negative scattering asymmetry parameter for dipolar particles: Unusual reduction of the transport mean free path and radiation pressure. *Phys. Rev. A*, 85(3):035802, 2012.

[88] MQ Liu, CY Zhao, and BX Wang. Polarization management based on dipolar interferences and lattice couplings. *Opt. Express*, 26(6):7235–7252, 2018.

[89] BX Wang and CY Zhao. Achieving a strongly negative scattering asymmetry factor in random media composed of dual-dipolar particles. *Phys. Rev. A*, 97(2):023836, 2018.

[90] Anders Pors, Sebastian KH Andersen, and Sergey I Bozhevolnyi. Unidirectional scattering by nanoparticles near substrates: generalized kerker conditions. *Opt. Express*, 23(22):28808–28828, 2015.

[91] Mikolaj K Schmidt, Javier Aizpurua, Xavier Zambrana-Puyalto, Xavier Vidal, Gabriel Molina-Terriza, and Juan José Sáenz. Isotropically polarized speckle patterns. *Phys. Rev. Lett.*, 114(11):113902, 2015.

[92] Roxana Rezvani Naraghi, Sergey Sukhov, and Aristide Dogariu. Directional control of scattering by all-dielectric core-shell spheres. *Opt. Lett.*, 40(4):585–588, 2015.

[93] Evgenii Evgen'evich Gorodnichev, Aleksandr Ivanovich Kuzovlev, and Dmitrii Borisovich Rogozkin. Anomalous depolarizing properties of a disordered ensemble of resonant mie particles. *JETP Lett.*, 104(3):157–162, 2016.

[94] Patrice Genevet, Federico Capasso, Francesco Aieta, Mohammadreza Khorasaninejad, and Robert Devlin. Recent advances in planar optics: from plasmonic to dielectric metasurfaces. *Optica*, 4(1):139–152, 2017.

[95] Yuri Kivshar and Andrey Miroshnichenko. Meta-optics with mie resonances. *Optics and Photonics News*, 28(1):24–31, 2017.

[96] Toshihiko Shibanuma, Pablo Albella, and Stefan A Maier. Unidirectional light scattering with high efficiency at optical frequencies based on low-loss dielectric nanoantennas. *Nanoscale*, 8(29):14184–14192, 2016.

[97] Angela I Barreda, Hassan Saleh, Amelie Litman, Francisco González, Jean-Michel Geffrin, and Fernando Moreno. Electromagnetic polarization-controlled perfect switching effect with high-refractive-index dimers and the beam-splitter configuration. *Nature communications*, 8(1):1–8, 2017.

[98] Sheng Liu, Michael B Sinclair, Sina Saravi, Gordon A Keeler, Yuanmu Yang, John Reno, Gregory M Peake, Frank Setzpfandt, Isabelle Staude, Thomas Pertsch, et al. Resonantly enhanced second-harmonic generation using iii–v semiconductor all-dielectric metasurfaces. *Nano letters*, 16(9):5426–5432, 2016.

[99] Heiko Linnenbank, Yevgen Grynko, Jens Förstner, and Stefan Linden. Second harmonic generation spectroscopy on hybrid plasmonic/dielectric nanoantennas. *Light: Science & Applications*, 5(1):e16013–e16013, 2016.

[100] Ia B Zel'Dovich. Electromagnetic interaction with parity violation. *Sov. Phys. JETP*, 6(6):1184–1186, 1958.

[101] Boris Luk'yanchuk, Ramón Paniagua-Domínguez, Arseniy I Kuznetsov, Andrey E Miroshnichenko, and Yuri S Kivshar. Suppression of scattering for small dielectric particles: anapole mode and invisibility. *Philosophical Transactions of the Royal Society A: Mathematical, Physical and Engineering Sciences*, 375(2090):20160069, 2017.

[102] Maria Timofeeva, Lukas Lang, Flavia Timpu, Claude Renaut, Alexei Bouravleuv, Igor Shtrom, George Cirlin, and Rachel Grange. Anapoles in free-standing iii–v nanodisks enhancing second-harmonic generation. *Nano letters*, 18(6):3695–3702, 2018.

[103] Ruggero Verre, Denis G Baranov, Battulga Munkhbat, Jorge Cuadra, Mikael Käll, and Timur Shegai. Transition metal dichalcogenide nanodisks as high-index dielectric mie nanoresonators. *Nature nanotechnology*, 14(7):679–683, 2019.

[104] Yuanqing Yang, Vladimir A Zenin, and Sergey I Bozhevolnyi. Anapole-assisted strong field enhancement in individual all-dielectric nanostructures. *Acs Photonics*, 5(5):1960–1966, 2018.

[105] Wei Liu, Jianfa Zhang, Bing Lei, Haojun Hu, and Andrey E Miroshnichenko. Invisible nanowires with interfering electric and toroidal dipoles. *Optics letters*, 40(10):2293–2296, 2015.

[106] Juan S Totero Gongora, Andrey E Miroshnichenko, Yuri S Kivshar, and Andrea Fratalocchi. Anapole nanolasers for mode-locking and ultrafast pulse generation. *Nature communications*, 8(1):1–9, 2017.

[107] Gustavo Grinblat, Haizhong Zhang, Michael P Nielsen, Leonid Krivitsky, Rodrigo Berté, Yi Li, Benjamin Tilmann, Emiliano Cortés, Rupert F Oulton, Arseniy I Kuznetsov, et al. Efficient ultrafast all-optical modulation in a nonlinear crystalline gallium phosphide nanodisk at the anapole excitation. *Science Advances*, 6(34):eabb3123, 2020.

[108] Tianyue Zhang, Ying Che, Kai Chen, Jian Xu, Yi Xu, Te Wen, Guowei Lu, Xiaowei Liu, Bin Wang, Xiaoxuan Xu, et al. Anapole mediated giant photothermal nonlinearity in nanostructured silicon. *Nature communications*, 11(1):1–9, 2020.

[109] Wei Liu, Jianfa Zhang, and Andrey E Miroshnichenko. Toroidal dipole-induced transparency in core–shell nanoparticles. *Laser & Photonics Reviews*, 9(5):564–570, 2015.

[110] Tianhua Feng, Yi Xu, Wei Zhang, and Andrey E Miroshnichenko. Ideal magnetic dipole scattering. *Phys. Rev. Lett.*, 118(17):173901, 2017.

[111] Lei Wei, Zheng Xi, Nandini Bhattacharya, and H Paul Urbach. Excitation of the radiationless anapole mode. *Optica*, 3(8):799–802, 2016.

[112] John A Parker, Hiroshi Sugimoto, Brighton Coe, Daniel Eggena, Minoru Fujii, Norbert F Scherer, Stephen K Gray, and Uttam Manna. Excitation of nonradiating anapoles in dielectric nanospheres. *Physical Review Letters*, 124(9):097402, 2020.

[113] Stanislav B Glybovski, Sergei A Tretyakov, Pavel A Belov, Yuri S Kivshar, and Constantin R Simovski. Metasurfaces: From microwaves to visible. *Physics reports*, 634:1–72, 2016.

[114] Isabelle Staude, Andrey E Miroshnichenko, Manuel Decker, Nche T Fofang, Sheng Liu, Edward Gonzales, Jason Dominguez, Ting Shan Luk, Dragomir N Neshev, Igal Brener, et al. Tailoring directional scattering through magnetic and electric resonances in subwavelength silicon nanodisks. *ACS nano*, 7(9):7824–7832, 2013.

[115] Ye Feng Yu, Alexander Y Zhu, Ramón Paniagua-Domínguez, Yuan Hsing Fu, Boris Luk'yanchuk, and Arseniy I Kuznetsov. High-transmission dielectric metasurface with 2π phase control at visible wavelengths. *Laser & Photonics Reviews*, 9(4):412–418, 2015.

[116] Zhijie Ma, Stephen M Hanham, Pablo Albella, Binghao Ng, Hsiao Tzu Lu, Yandong Gong, Stefan A Maier, and Minghui Hong. Terahertz all-dielectric magnetic mirror metasurfaces. *Acs Photonics*, 3(6):1010–1018, 2016.

[117] Toshihiko Shibanuma, Stefan A Maier, and Pablo Albella. Polarization control of high transmission/reflection switching by all-dielectric metasurfaces. *Applied physics letters*, 112(6):063103, 2018.

[118] J David Jackson. *Classical Electrodynamics*. John Wiley & Sons, New York, 1999.

[119] Alan Robert Edmonds. *Angular momentum in quantum mechanics*. Princeton University, 1957.

[120] Ferdinando Borghese, Paolo Denti, and Rosalba Saija. *Scattering from model nonspherical particles: theory and applications to environmental physics*. Springer Science & Business Media, 2007.

[121] Yan Zhang, Manuel Nieto-Vesperinas, and Juan José Sáenz. Dielectric spheres with maximum forward scattering and zero backscattering: a search for their material composition. *Journal of Optics*, 17(10):105612, 2015.

[122] Boris S Luk'yanchuk, Nikolai V Voshchinnikov, Ramón Paniagua-Domínguez, and Arseniy I Kuznetsov. Optimum forward light scattering by spherical and spheroidal dielectric nanoparticles with high refractive index. *ACS Photonics*, 2(7):993–999, 2015.

[123] NB Simpson, K Dholakia, L Allen, and MJ Padgett. Mechanical equivalence of spin and orbital angular momentum of light: an optical spanner. *Opt. Lett.*, 22(1):52–54, 1997.

[124] James H Crichton and Philip L Marston. The measurable distinction between the spin and orbital angular momenta of electromagnetic radiation. *Electronic Journal of Differential Equations*, 4:37–50, 2000.

[125] Leslie Allen, Stephen M Barnett, and Miles J Padgett. *Optical angular momentum*. CRC Press, 2003.

[126] VS Liberman and BY Zel'dovich. Spin-orbit interaction of a photon in an inhomogeneous medium. *Phys. Rev. A*, 46(8):5199, 1992.

[127] MV Berry, MR Jeffrey, and M Mansuripur. Orbital and spin angular momentum in conical diffraction. *J. Opt. A: Pure Appl. Opt.*, 7(11):685, 2005.

[128] MI Dyakonov and VI Perel. Current-induced spin orientation of electrons in semiconductors. *Phys. Lett. A*, 35(6):459–460, 1971.

[129] JE Hirsch. Spin hall effect. *Phys. Rev. Lett.*, 83(9):1834, 1999.

[130] Michel I Dyakonov and AV Khaetskii. Spin hall effect. In *Spin physics in semiconductors*, pages 211–243. Springer, 2008.

[131] Jairo Sinova, Sergio O Valenzuela, J Wunderlich, CH Back, and T Jungwirth. Spin hall effects. *Rev. Mod. Phys.*, 87(4):1213, 2015.

[132] Michael V Berry. Optical currents. *Journal of Optics A: Pure and Applied Optics*, 11(9):094001, 2009.

[133] MV Berry. Lateral and transverse shifts in reflected dipole radiation. *Proceedings of the Royal Society A: Mathematical, Physical and Engineering Sciences*, 467(2133):2500–2519, 2011.

[134] Henk F Arnoldus and John T Foley. The dipole vortex. *Opt. Commun.*, 231(1-6):115–128, 2004.

[135] Chaim Schwartz and Aristide Dogariu. Backscattered polarization patterns, optical vortices, and the angular momentum of light. *Opt. Lett.*, 31(8):1121–1123, 2006.

[136] Aitzol García-Etxarri and Jennifer A. Dionne. Surface-enhanced circular dichroism spectroscopy mediated by nonchiral nanoantennas. *Phys. Rev. B*, 87:235409, Jun 2013.

[137] Masud Mansuripur, Armis R Zakharian, and Ewan M Wright. Spin and orbital angular momenta of light reflected from a cone. *Phys. Rev. A*, 84(3):033813, 2011.

[138] Raquel Gomez-Medina, Braulio Garcia-Camara, Irene Suárez-Lacalle, Francisco González, Fernando Moreno, Manuel Nieto-Vesperinas, and Juan Jose Saenz. Electric and magnetic dipolar response of germanium nanospheres: interference effects, scattering anisotropy, and optical forces. *Journal of Nanophotonics*, 5(1):053512, 2011.

[139] Manuel Nieto-Vesperinas. Optical torque: Electromagnetic spin and orbital-angular-momentum conservation laws and their significance. *Phys. Rev. A*, 92(4):043843, 2015.

[140] B Setién, P Albella, JM Saiz, F González, and F Moreno. Spectral behavior of the linear polarization degree at right-angle scattering configuration for nanoparticle systems. *New J. Phys.*, 12(10):103031, 2010.

[141] Braulio García-Cámara, Francisco González, and Fernando Moreno. Linear polarization degree for detecting magnetic properties of small particles. *Opt. Lett.*, 35(23):4084–4086, 2010.

[142] George Neville Watson. *A treatise on the theory of Bessel functions*. Cambridge university press, 1995.

[143] Andrea Aiello and MV Berry. Note on the helicity decomposition of spin and orbital optical currents. *J. Opt.*, 17(6):062001, 2015.

[144] Aitzol Garcia-Etxarri. Optical polarization mobius strips on all-dielectric optical scatterers. *ACS Photonics*, 4(5):1159–1164, 2017.

[145] Juan Miguel Auñón and Manuel Nieto-Vesperinas. Optical forces from evanescent bessel beams, multiple reflections, and kerker conditions in magnetodielectric spheres and cylinders. *JOSA A*, 31(9):1984–1992, 2014.

[146] Nils Odebo Länk, Peter Johansson, and Mikael Käll. Directional scattering and multipolar contributions to optical forces on silicon nanoparticles in focused laser beams. *Opt. Express*, 26(22):29074–29085, 2018.

[147] Braulio García-Cámara, J Francisco Algorri, Alexander Cuadrado, Virginia Urruchi, José Manuel Sánchez-Pena, Rosalía Serna, and Ricardo Vergaz. All-optical nanometric switch based on the directional scattering of semiconductor nanoparticles. *The Journal of Physical Chemistry C*, 119(33):19558–19564, 2015.

[148] David E Aspnes and AA Studna. Dielectric functions and optical parameters of si, ge, gap, gaas, gasb, inp, inas, and insb from 1.5 to 6.0 ev. *Phys. Rev. B*, 27(2):985, 1983.

[149] Braulio García-Cámara, Raquel Gómez-Medina, Juan José Sáenz, and Borja Sepúlveda. Sensing with magnetic dipolar resonances in semiconductor nanospheres. *Opt. Express*, 21(20):23007–23020, 2013.

[150] Tongtong Zhu, Yuzhi Shi, Weiqiang Ding, Din Ping Tsai, Tun Cao, Ai Qun Liu, Manuel Nieto-Vesperinas, Juan José Sáenz, Pin Chieh Wu, and Cheng-Wei Qiu. Extraordinary multipole modes and ultra-enhanced optical lateral force by chirality. *Physical review letters*, 125(4):043901, 2020.

[151] Hang Li, Yongyin Cao, Lei-Ming Zhou, Xiaohao Xu, Tongtong Zhu, Yuzhi Shi, Cheng-Wei Qiu, and Weiqiang Ding. Optical pulling forces and their applications. *Advances in Optics and Photonics*, 12(2):288–366, 2020.

[152] Hang Li, Yongyin Cao, Bojian Shi, Tongtong Zhu, Yong Geng, Rui Feng, Lin Wang, Fangkui Sun, Yuzhi Shi, Mohammad Ali Miri, et al. Momentum-topology-induced optical pulling force. *Physical review letters*, 124(14):143901, 2020.

[153] Paris Varytis and Kurt Busch. Negative asymmetry parameter in plasmonic core-shell nanoparticles. *Optics Express*, 28(2):1714–1721, 2020.

[154] Xavier Zambrana-Puyalto, Xavier Vidal, Mathieu L Juan, and Gabriel Molina-Terriza. Dual and anti-dual modes in dielectric spheres. *Opt. Express*, 21(15):17520–17530, 2013.

[155] M Ismail Abdelrahman, Carsten Rockstuhl, and Ivan Fernandez-Corbaton. Broadband suppression of backscattering at optical frequencies using low permittivity dielectric spheres. *Scientific reports*, 7(1):1–8, 2017.

[156] Milton Abramowitz and Irene A Stegun. *Handbook of mathematical functions: with formulas, graphs, and mathematical tables*, volume 55. Courier Corporation, 1965.

[157] Árpád Baricz and Róbert Szász. The radius of convexity of normalized bessel functions of the first kind. *Analysis and Applications*, 12(05):485–509, 2014.

[158] Patrick C Chaumet and Manuel Nieto-Vesperinas. Time-averaged total force on a dipolar sphere in an electromagnetic field. *Optics letters*, 25(15):1065–1067, 2000.

[159] Silvia Albaladejo, Manuel I Marqués, Marine Laroche, and Juan José Sáenz. Scattering forces from the curl of the spin angular momentum of a light field. *Phys. Rev. Lett.*, 102(11):113602, 2009.

[160] Andrey Novitsky, Cheng-Wei Qiu, and Haifeng Wang. Single gradientless light beam drags particles as tractor beams. *Physical review letters*, 107(20):203601, 2011.

[161] Philip H Jones, Onofrio M Maragò, and Giovanni Volpe. *Optical tweezers: Principles and applications*. Cambridge University Press, 2015.

[162] Aleksandr Y Bekshaev, Konstantin Y Bliokh, and Franco Nori. Transverse spin and momentum in two-wave interference. *Physical Review X*, 5(1):011039, 2015.

[163] M Decker, MW Klein, M Wegener, and S Linden. Circular dichroism of planar chiral magnetic metamaterials. *Optics letters*, 32(7):856–858, 2007.

[164] Martin Schäferling, Daniel Dregely, Mario Hentschel, and Harald Giessen. Tailoring enhanced optical chirality: design principles for chiral plasmonic nanostructures. *Physical Review X*, 2(3):031010, 2012.

[165] Ivan Fernandez-Corbaton, Martin Fruhnert, and Carsten Rockstuhl. Dual and chiral objects for optical activity in general scattering directions. *ACS Photonics*, 2(3):376–384, 2015.

[166] Michelle L Solomon, Jack Hu, Mark Lawrence, Aitzol García-Etxarri, and Jennifer A Dionne. Enantiospecific optical enhancement of chiral sensing and separation with dielectric metasurfaces. *ACS Photonics*, 6(1):43–49, 2018.

[167] J. Olmos-Trigo, M. Meléndez, R. Delgado-Buscalioni, and J. J. Sáenz. Sectoral multipole focused beams. *Opt. Express*, 27(11):16384–16394, May 2019.